University of Groningen

Automated Beam Line Tuning at the AGOR Accelerator Facility

Author:
O.G. Tjepkema
First Examiner:
Dr. S. Brandenburg
Second examiner:
Prof. dr. ir. B. Jayawardhana

Date:
July 12, 2021

Contents

1 Introduction

1.1 Motivation and Research Goals

The AGOR cyclotron at KVI-CART is able to accelerate all stable ions over a wide energy range. After the extraction of the ions from the cyclotron they need to be transported to the rooms in which the experiments take place. This guidance system comprises many magnet elements and beam profile monitors. In order to guarantee that minimal beam losses occur during transport and to achieve a sufficiently small beam profile size at the experimental sites, each of these magnet elements must be set correctly.

Currently, the tuning of the magnets is done manually. The initial settings are calculated by means of ion-optical calculations after which fine-tuning is done by the operators. Due to the large number of magnets in the system, this is a very time-consuming process. Furthermore, due to the different strategies used by different operators the reproducibility of the beam properties at the experimental sites is also limited.

The tuning procedure requires the adjustment of many parameters. The effect of these parameters can be calculated via mathematical relations derived from the physics of ion transport. By using these relations during tuning, the number of required iterations before the optimal parameters are achieved will be reduced, and convergence to a global minimum is more likely. However, it would be difficult to impossible for the operator to make full use of these mathematical equations without a calculation tool because of the large number of computations that are required. Therefore it would be advantageous to automate the process, which will improve both tuning speed and reproducibility.

The goal of this thesis is to develop and test an algorithm for beam tuning based on a linear ion-optics model. The actual system is not linear since magnets generally contain higher-order terms, however by utilizing symmetries in the beamline and by keeping the beam centroid deviations as well as the beam size sufficiently small it is possible to neglect the effects of these higher-order terms.

To control the beam it is necessary to know its properties along the length of the beamline. For this purpose beam profile monitors (BPM) are set up at fixed locations in the system. These are only able to measure the profile of the beam. To also measure the angle of the beam the quadrupole variation method is used.

When the initial beam conditions are known, the beam can be aligned and focused. This will be divided into two steps. In the first step, the beam centroid is aligned with the reference trajectory using the steering and bending magnets in the system.

In the second step, the quadrupole magnets will be adjusted such that minimum beam sizes are achieved at desired locations in the beamline. By design of the beamline, these locations generally coincide with the locations of the beam profile monitors. By minimizing the beam sizes at these locations the best agreement between the actual and designed beam properties is achieved.

To validate the algorithms they will first be tested using simulations based on linear optics. Afterward, they will be tested experimentally at the AGOR cyclotron to investigate the effects of the nonlinear terms and misalignment of beam elements on convergence and accuracy of the algorithm.

1.2 Research Questions

The introduction above gives the motivation and required steps for the beamline algorithm. These can be summarized into the main research question (**MQ**) and a set of sub-questions (**SQ**)

MQ: How to create an algorithm for alignment and focusing of the beam coming from the cyclotron?

SQ1 How to measure the initial conditions of the beam?

SQ1.1 How to extract the beam centroid values from the beamprofile measurements which measure the entire beam?

SQ1.2 What values of quadrupole strengths should be used to sample beam positions?

SQ1.3 What is the effect of statistical errors of the measurements on the behaviour of the control system?

SQ2 How to perform the required corrections to the beam?

SQ2.1 What is the size of correction needed based on the position and angle deviation of the beam?

SQ2.1 How do positional alignment errors of the magnets in the beamline affect the accuracy and precision of the algorithm?

2 Theory

In this section the basic theory behind ion optics and the first order approximation is explained. The material is primarily drawn from the textbook *Physik der Teilchenbeschleuniger und Ionenoptik* by F. Hinterberger [1].

2.1 Forces Used in Particle Acceleration and Bending

The main governing force in ion optics is the Lorentz force

$$\boldsymbol{F} = q\left(\boldsymbol{E} + \boldsymbol{v} \times \boldsymbol{B}\right) \tag{1}$$

where $\boldsymbol{F}$ is the force experienced by a charged particle, q is the charge of the particle, v is the velocity of the particle, and $\boldsymbol{E}$ and $\boldsymbol{B}$ are the electric field and magnetic field at the particle location respectively.

From this equation, it can be seen that only the electric field can be used to accelerate the ions. The force caused by the magnetic field $\boldsymbol{B}$ is always perpendicular to the velocity, due to the cross product, which means that it can only be used to change the direction of the ions. Another important consequence of the $\boldsymbol{B}$ being related to the velocity is that a magnetic field is much more suited to steer high-energy beams than an electric field. To illustrate this, two equations are given for a particle that follows a circular trajectory in an electric or magnetic field. For an electric field the following equation holds

$$E_{\perp}\rho = \frac{\gamma m v^2}{q} = \frac{pv}{q} \tag{2}$$

where $E_{\perp}$ is the electric field component perpendicular to the particle velocity, ρ is the radius of curvature of the particle, m is the particle rest mass, γ is the relativistic Lorentz parameters and $p = \gamma m v$ is the relativistic particle momentum. The quantity $E_{\perp}\rho$ is called the electric rigidity and is a measure of how difficult it is to deflect the particle using an electric field.

A similar quantity can be defined for the magnetic field

$$B_{\perp}\rho = \frac{p}{q} \tag{3}$$

where $B_{\perp}$ is the magnetic field component perpendicular to the particle velocity. The quantity $B\rho$ is called the magnetic rigidity.

Often beam impulse is given in units of GeV/c, while electric and magnetic fields are given in SI-units, the following relation can be used to convert the quantities

$$1\,[e\mathrm{Tm}] = 0.299\,792\,458\,[\mathrm{GeV}/c] \tag{4}$$

Table 1 shows a numeric example of bending ions using magnetic and electric fields. For the beam which has a large impulse and velocity, a magnetic field of 1 T is needed, which can physically be

achieved. However the required electric field is 91.19 MV/m, which is not feasible. The maximum electric field that can be achieved in vacuum using polished metals is approximately 10 MV/m. In the case of a low impulse and velocity beam both the magnetic and electric field can be used, as seen in the table.

Table 1: Numerical example showing the effect of deflecting a proton beam using a magnetic and electric field. The protons are bend with a radius of $\rho = 1\,\mathrm{m}$

Beam Impulse (MeV/c)	Particle velocity (c)	Magnetic Rigidity (Tm)	Required Magnetic Field (T)	Electric Rigidity (MV)	Required Electric Field (MV/m)
299.8	0.304	1	1	91.19	91.19
29.98	0.0319	0.1	0.1	0.9564	0.9564

2.2 Magnet Elements

In the section, a physical description is given of the magnets that are used to control the beam. These magnets all consist out of three main components, which are the copper coils, a magnetic yoke, and the pole shoes. Current is fed through the copper coils which produce a magnetic field according to Maxwell's equations. The magnetic yoke provides mechanical structure to the magnet and provides a path of return for the magnetic field lines. The produced magnetic field enters and leaves the vacuum or air space in the magnet via the pole shoes. The shape of these pole shoes determines the shape of the magnetic field in the vacuum and consequently determines the guiding properties of the magnet. A formal derivation of the pole shoe shapes and accompanying magnetic fields can be found in [2].

2.2.1 Dipole Magnet

A dipole magnet is used to bend the beam, when bending a beam in the horizontal plane a homogeneous magnetic field that only has a vertical component should be produced by the magnet. This is achieved by making the pole shoes parallel to each other and parallel to the bending plane of the reference particle. The bending direction can be switched by changing the polarity of the current through the magnet, which in turn reverses the magnetic field. Four popular designs for a dipole magnet can be seen in Figure 1. The C-magnet has the advantage that it is open on one side, which means that installing and removing diagnostic equipment is easier. However, its magnetic field will be slightly asymmetric because the magnetic yoke is larger on one side which amplifies the magnetic field there. Furthermore, since the poles exert a force on each other [3] and the bending stiffness of the design is low, the yoke needs to be thicker than for other designs. The H-magnet has higher symmetry, however, it is less compact and requires a larger yoke. The window frame magnet also has high symmetry and is more compact, however, the coils have to be curved at the entrance and exit of the magnet to allow the ion beam to pass through. It is also possible to wrap the coils around the vertical parts of the yoke to simplify the design. This will however reduce the quality of the magnetic field.

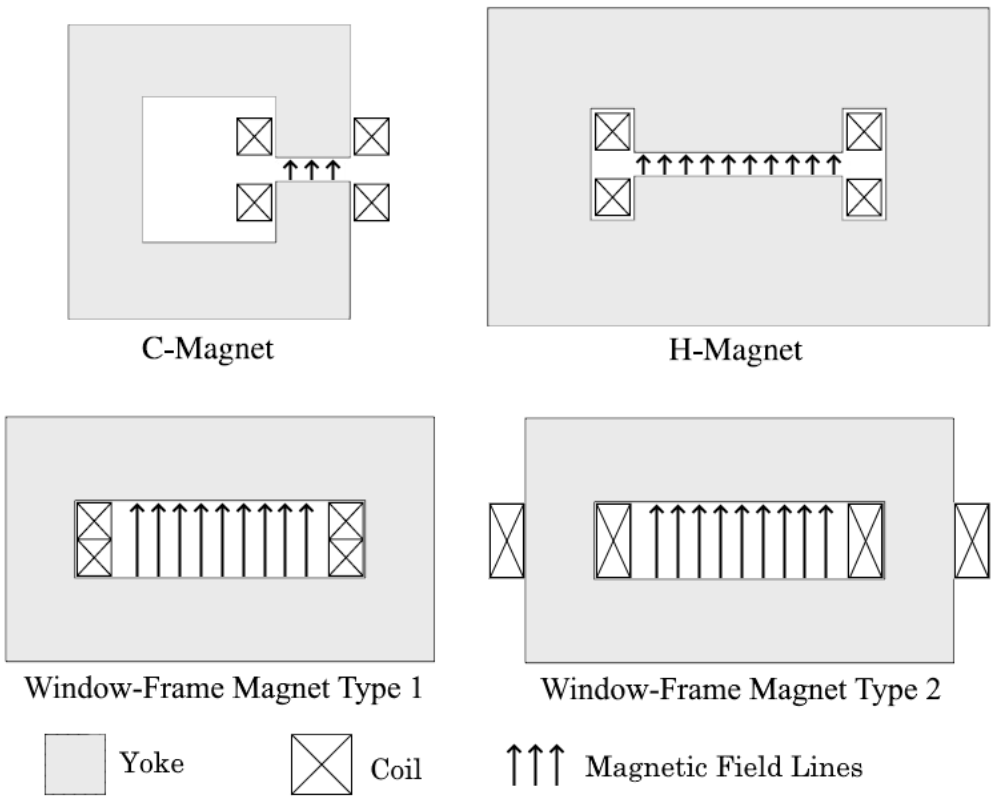

Figure 1: Cross section of three different types of dipole magnets. Image adapted from [1].

The relation between the magnetic flux density and current supplied to the magnet can be seen in Figure 2. The graph flattens off at a high value of the magnetic flux density because of saturation effects of the iron yoke. There is also a small hysteresis effect present as indicated by the zoomed-in region. The beamline design is such that the magnets always operate inside the linear region of the graph, furthermore, the hysteresis effect is sufficiently small such that it can be neglected. The linear part can be described by the following equation

$$B = \mu_0 \frac{nI}{g} - \mu_0 \frac{l_{Fe}}{g} H_{Fe} \approx \mu_0 \frac{nI}{g} \tag{5}$$

where μ_0 is the permeability of free space, n is the number of coil windings, I is the current through the coils, g the gap size, l_{Fe} the path-length of the magnetic field through the magnetic yoke and H_{Fe} the magnetic field strength along this path. The last approximation can be made because the permeability of iron μ_{Fe} is much higher than that of a vacuum $H = B/\mu_0 \gg H_{Fe} = B/\mu_{Fe}$.

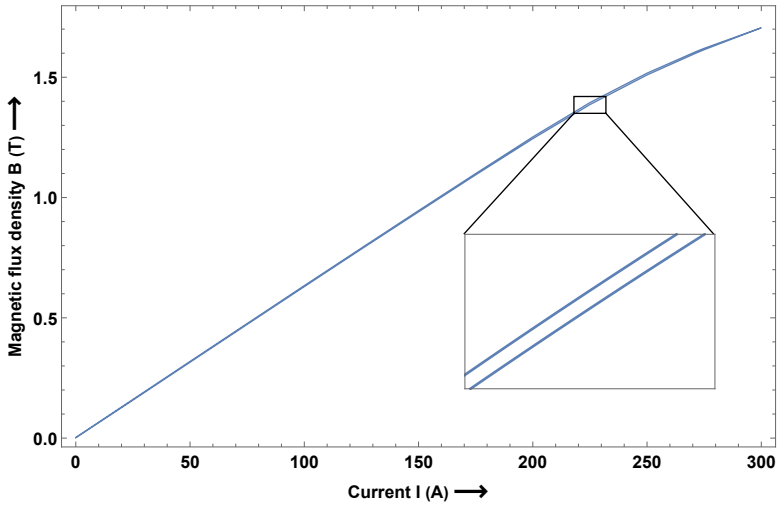

Figure 2: B-I curve for one of the bending magnets which is used in the beamline.

2.2.2 Quadrupole Magnet

An image of a basic quadrupole magnet can be seen in Figure 3. It has four poles, each is surrounded by a copper coil. The magnitude of the current flowing through each coil is the same, however to produce the north and south poles, the current in coils surrounding opposite poles has opposite sign. The function of a quadrupole magnet is to focus the beam, to achieve this it produces the following magnetic field

$$|B_x| = \frac{B_0}{a} y, \qquad |B_y| = \frac{B_0}{a} x \tag{6}$$

where B_0 is the magnitude of the field at the tip of the pole shoes, a is the radius of the circle tangent to all pole shoes, and x and y are the coordinates as described in Figure 3. Because the field increases linearly with the distance from the central trajectory particles which have large positional deviations will experience a larger force, which causes focusing. However, because of the shape of the field lines, the quadrupole magnet can only focus in one direction and causes de-focusing in the other direction. The quadrupole drawn in Figure 3 focuses positive ions moving into the paper in the x-direction and defocuses in the y direction. By reversing the polarity of the supplied current the focusing and de-focusing directions can be switched.

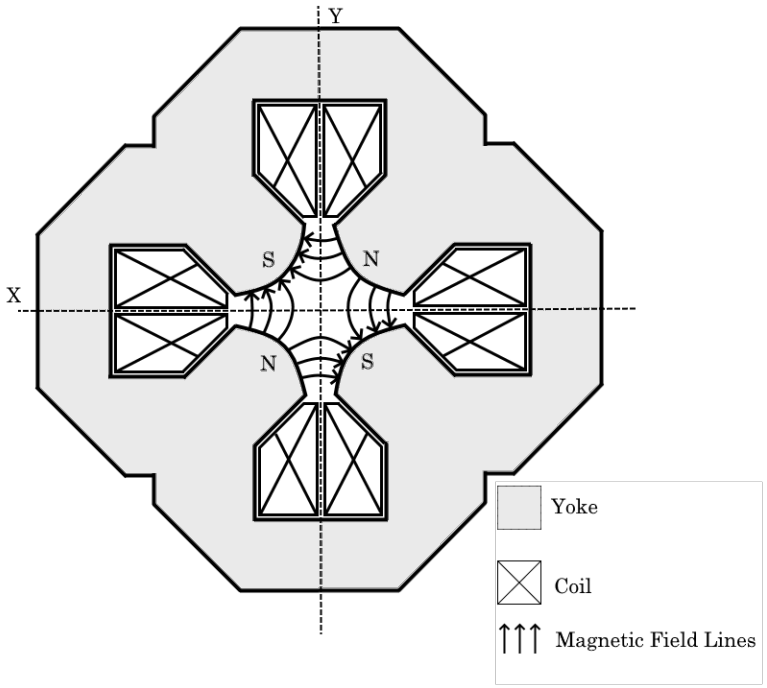

Figure 3: Cross section of a quadrupole magnet. Image adapted from [2].

The relation between the magnetic field gradient and the current supplied to the magnet can be seen in Figure 4. Similar to the dipole magnets, the graph flattens off for high values of the field gradient, because of the saturation effects in the iron yoke. Also, a small hysteresis effect is observed. If this small effect is neglected, the magnetic field gradient of a quadrupole is approximately given by

$$\frac{B_0}{a} = \frac{2\mu_0}{a^2}(nI - H_{Fe}l_{Fe}) \approx 2\mu_0\frac{nI}{a^2} \tag{7}$$

the approximation can again be made because the permeability of the iron core μ_{Fe} is much larger than that of a vacuum, which means that $B_0/\mu_0 \gg H_{Fe} = B_0/\mu_{Fe}$.

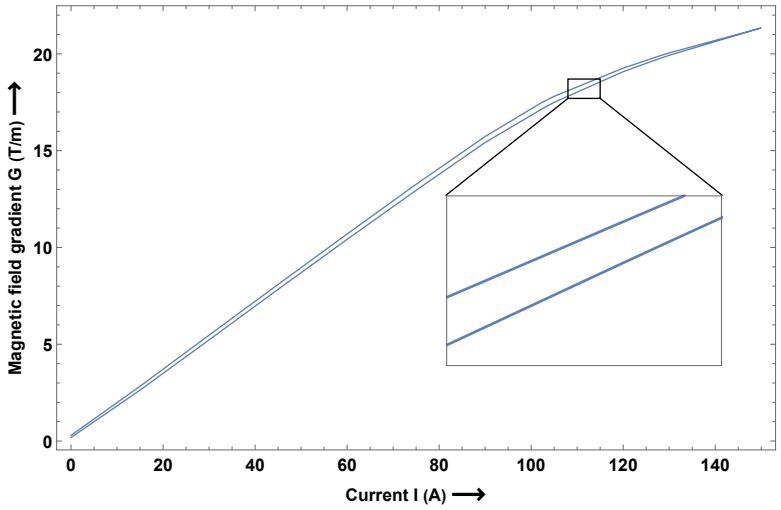

Figure 4: Gradient vs current curve for one of the quadrupole magnets that is used in the beamline

2.2.3 Effective Length of a Magnet

The magnetic field produced by a magnet extends beyond the faces of the magnet, a plot of the magnetic field versus the distance travelled can be seen in Figure 5. This field distribution is often simplified by replacing it by a rectangle with an effective length L_eff and height B_0, which has the same surface area as the original distribution. The effective length for a dipole can then be calculated as

$$L_{eff} = \frac{1}{B_0} \int_{-\infty}^{\infty} B(s)ds \tag{8}$$

where B is the magnetic flux density of the dipole, the effective length of a quadrupole can be determined by

$$L_eff = \frac{1}{g_0} \int_{-\infty}^{\infty} g(s)ds \tag{9}$$

where g is the magnetic field gradient of the quadrupole

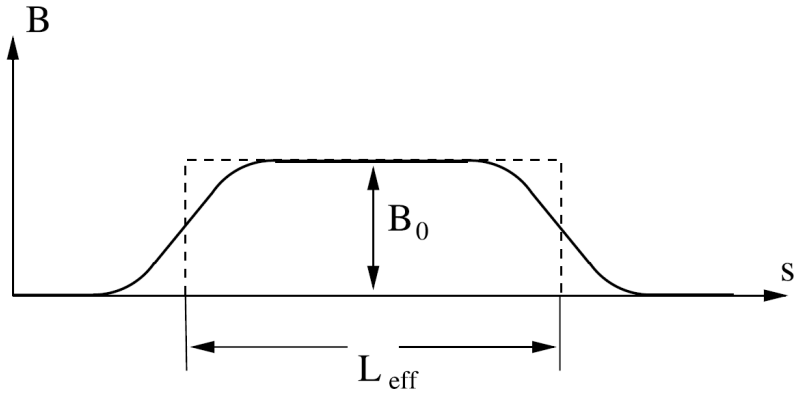

Figure 5: Illustration of the effective length of a magnet, the field approximation using a rectangle is indicated by the dotted line.

2.3 Coordinate System

To simplify the mathematics and provide more insight into the underlying physics, the coordinate system is defined with respect to a reference particle following the designed central trajectory of the beam. This choice of coordinate system will later facilitate the derivation of the first order approximation of the beam description, under the assumptions that the deviations of the transverse positions and angles of the particles with respect to the reference trajectory are small. An image of such a coordinate system is given in Figure 6. The transverse components of the position of the particles are given by the x and y coordinates. These are defined to lie in a plane perpendicular to the vector which is tangent to the central trajectory and whose origin coincides with the central particle location.

The x-axis is defined to lie in the plane of the reference orbit of a particle in a dipole magnet. The direction of x, when looking along the beam direction, is to the left. The y-axis is defined to be perpendicular to x and points such that a right-handed coordinate system is formed. Other conventions are also possible, another common one found in literature is where the x-axis points to the right and the y and z axes are switched. However all these conventions will ultimately lead to the same results, therefore either can be used based on preference.

Generally, the x and y-axis are referred to as the radial and axial directions respectively. The intersect of the x-y plane with the central particle trajectory is given by the s coordinate. In this way, the position of a described particle can be described as

$$\boldsymbol{r}(s) = \boldsymbol{r}_0(s) + x(s)\boldsymbol{u}_x(s) + y(s)\boldsymbol{u}_y(s) \tag{10}$$

In the case where the reference particle moves in a straight line, it is possible to attach a Cartesian coordinate system to it, with the z-axis tangential to the $\boldsymbol{u}_s$ vector. In such a frame a line element can be described as.

$$\mathrm{d}\boldsymbol{r} = \boldsymbol{u}_x \mathrm{d}x + \boldsymbol{u}_y \mathrm{d}y + \boldsymbol{u}_z \mathrm{d}z \tag{11}$$

When the reference particle follows a curved trajectory with curvature $h = 1/\rho_0$ the line element is described by the following equation.

$$\mathrm{d}\boldsymbol{r} = \boldsymbol{u}_x \mathrm{d}x + \boldsymbol{u}_y \mathrm{d}y + \boldsymbol{u}_s \left(1 + hx\right) \mathrm{d}s \tag{12}$$

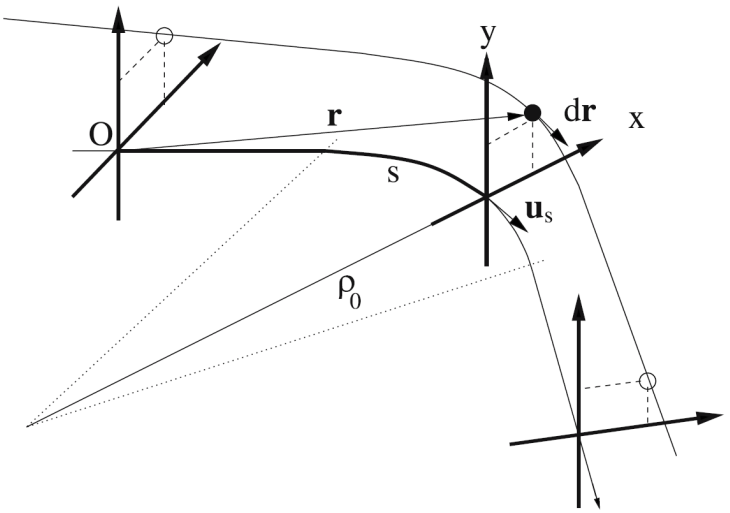

Figure 6: Coordinate system which is used to derive the linear ion optics [1].

For a formal full description of a particle, a total of six coordinates are needed, which are the position and momentum components of the particle along each axis (x,p_x,y,p_y,z,p_z). However, this form is not well suited to be expressed in terms of the solutions to the equations of motion. To achieve this we divide the transverse momenta by the momentum of the reference particle p_0.

$$\begin{aligned} \frac{p_x}{p_0} &= \frac{m\gamma \frac{dx}{dt}}{m\gamma \frac{ds}{dt}} = \frac{dx}{ds} = x' \\ \frac{p_y}{p_0} &= \frac{m\gamma \frac{dy}{dt}}{m\gamma \frac{ds}{dt}} = \frac{dy}{ds} = y' \end{aligned} \tag{13}$$

in the linear approximation the following equations can be used instead, which are derived from Eqs. (11) and (12)

$$\begin{aligned} x' &= \frac{dx}{ds} = \frac{dx}{(1+\frac{x}{\rho_0})dz} \approx \frac{dx}{dz} \\ y' &= \frac{dy}{ds} = \frac{dy}{(1+\frac{x}{\rho_0})dz} \approx \frac{dy}{dz} \end{aligned} \tag{14}$$

the expressions of z and p_z are written down in terms of solutions to the equations of motion. First z is replaced with l, which is the distance between the described particle and reference particle projected along the reference trajectory. For p_z the approximation is made that the longitudinal momentum p_z is much larger than the transverse momenta p_x and p_y. This allows the total momentum p to be written as $p_z \approx p$, which gives

$$\frac{p_z - p_0}{p_0} \approx \frac{p - p_0}{p_0} = \delta \tag{15}$$

where p is the momentum of the described particle and p_0 is the momentum of the reference particle. Using the quantities defined above the 6-dimensional vector $\boldsymbol{x}(s)$ is defined, which contains all of the necessary particle information.

$$\boldsymbol{x(s)} = \begin{pmatrix} x_1 \\ x_2 \\ x_3 \\ x_4 \\ x_5 \\ x_6 \end{pmatrix} = \begin{pmatrix} x \\ x' \\ y \\ y' \\ l \\ \delta \end{pmatrix} = \begin{pmatrix} \text{Radial position deviation} \\ \text{Radial angle deviation} \\ \text{Axial position deviation} \\ \text{Axial angle deviation} \\ \text{Longitudinal position deviation} \\ \text{Relative impulse deviation} \end{pmatrix} \tag{16}$$

It should be noted that often x' and y' will be described in terms of angles, θ and, ϕ instead of the definition given by Eq. (13).

$$\begin{aligned} x' &= \frac{dx}{dz} = \tan\theta \approx \theta \\ y' &= \frac{dy}{dz} = \tan\phi \approx \phi \end{aligned} \tag{17}$$

the last approximation is valid for x' and $y' \ll 1$.

2.4 Equations of Motion and First Order Approximation

The motion of the particles under the effect of an external force $\boldsymbol{F}$ is described by the relativistic form of Newton's second law of motion

$$\frac{\mathrm{d}\boldsymbol{p}}{\mathrm{d}t} = \boldsymbol{F} \tag{18}$$

the relativistic momentum of the particle is

$$\boldsymbol{p} = m\gamma\boldsymbol{v} \tag{19}$$

where m is the rest mass of the particle, γ is the Lorentz factor and $\boldsymbol{v}$ is the particle velocity. The external force is equal to the Lorentz force with zero electric field

$$\boldsymbol{F} = q\boldsymbol{v} \times \boldsymbol{B} \tag{20}$$

note that since the force is always perpendicular to the velocity the magnitude of the velocity does not change, which means that $m\gamma$ is constant. Substituting Eqs. (19) and (20) into Eq. (18) gives

$$m\gamma\dot{\boldsymbol{v}} = q\boldsymbol{v} \times \boldsymbol{B} \tag{21}$$

For a general case $\dot{\boldsymbol{v}}$ can be replaced by $\ddot{\boldsymbol{r}}$ where $\boldsymbol{r}(t)$ is a vector, which depends on the time t, containing the particle coordinates defined with respect to an arbitrary stationary point in the space

$$m\gamma\ddot{\boldsymbol{r}} = q\boldsymbol{v} \times \boldsymbol{B} \tag{22}$$

the coordinate system, which we have defined in Section 2.3, is attached to the central particle which travels with velocity v_s and has a radius of curvature ρ_0, these quantities are related via the angular velocity ω

$$v_s = \omega\rho_0 \tag{23}$$

the trajectory of a particle which does not follow the reference trajectory is described in Figure 7, its z velocity component v_z, expressed in the reference coordinate system, is equal to

$$v_z = \omega\left(\rho_0 + x\right) \tag{24}$$

its centripetal acceleration a_r is given by

$$a_r = -\omega^2\left(\rho_0 + x\right) \tag{25}$$

next, Eq. (22) is split into an x and y component. The total acceleration in the x-direction is the sum $\ddot{x} + a_r$.

$$\begin{aligned} \ddot{x} - \omega^2\left(\rho_0 + x\right) &= \frac{q}{\gamma m}\left(v_y B_z - v_z B_y\right) \\ \ddot{y} &= \frac{q}{\gamma m}\left(v_z B_x - v_x B_z\right) \end{aligned} \tag{26}$$

to simplify these equations some approximations will be made. The velocity components v_x and v_y are much smaller than v_z, likewise B_z is much smaller than B_x and B_y, the products of these quantities is therefore negligible. Furthermore in the linear approximation

$$\begin{aligned} v &= \sqrt{v_x^2 + v_y^2 + v_z^2} = v_z\sqrt{1 + x'^2 + y'^2} \approx v_z \\ p &= \gamma m v \approx \gamma m v_z = \gamma m \rho_0 \omega \left(1 + \frac{x}{\rho_0}\right) \end{aligned} \tag{27}$$

using these approximations Eq. (26) transforms into

$$\begin{aligned} \ddot{x} - \omega^2 (\rho_0 + x) &= -\frac{q}{p} v_z^2 B_y \\ \ddot{y} &= \frac{q}{p} v_z^2 B_x \end{aligned} \tag{28}$$

to eliminate time from this equation the relation $\mathrm{d}s \,/\, \mathrm{d}t = v_s = \rho_0\omega$ is used

$$\begin{aligned} \frac{\mathrm{d}}{\mathrm{d}t} &= \frac{\mathrm{d}}{\mathrm{d}t} = \frac{\mathrm{d}}{\mathrm{d}s}\frac{\mathrm{d}s}{\mathrm{d}t} = \rho_0\omega\frac{\mathrm{d}}{\mathrm{d}s} \\ \frac{\mathrm{d}^2}{\mathrm{d}t^2} &= \frac{\mathrm{d}}{\mathrm{d}t}\frac{\mathrm{d}}{\mathrm{d}t} = (\rho_0\omega)^2 \frac{\mathrm{d}^2}{\mathrm{d}s^2} \end{aligned} \tag{29}$$

substituting this result together with the relation $v_z = \omega(\rho_0 + x)$ into in Eq. (28) gives (where the position derivative is indicated with apostrophes instead of dots for time derivative)

$$\begin{aligned} x'' - \frac{1}{\rho_0}\left(1 + \frac{x}{\rho_0}\right) &= -\frac{q}{p} B_y \left(1 + \frac{x}{\rho_0}\right)^2 \\ y'' &= \frac{q}{p} B_x \left(1 + \frac{x}{\rho_0}\right)^2 \end{aligned} \tag{30}$$

To simplify even further the magnetic fields are expanded using a Taylor expansion. Since the $x - z$ plane is chosen as the magnetic symmetry plane $B_x(-y) = -B_x(y)$, which eliminates any even terms from the Taylor expansion

$$\begin{aligned} B_y(x) &= B_y(0) + \frac{\mathrm{d}B_y}{\mathrm{d}x}x + \frac{1}{2!}\frac{\mathrm{d}^2 B_y}{\mathrm{d}x^2}x^2 + \mathcal{O}(x^3) \\ B_x(y) &= \frac{\mathrm{d}B_x}{\mathrm{d}y}y + \frac{1}{3!}\frac{\mathrm{d}^3}{\mathrm{d}y^3}y^3 + \mathcal{O}(y^5) \end{aligned} \tag{31}$$

for the first-order approximation, these expressions are truncated to the first order. Furthermore, the momentum of the particles is also approximated linearly

$$\begin{aligned} p &= p_0 + p - p_0 = p_0 + \Delta p = p_0 \left(1 + \frac{\Delta p}{p_0}\right) = p_0 \left(1 + \delta\right) \\ \frac{1}{p} &= \frac{1}{p_0}\frac{1}{1+\delta} = \frac{1}{p_0}\frac{1-\delta}{(1+\delta)(1-\delta)} = \frac{1}{p_0}\frac{1-\delta}{1-\delta^2} \approx \frac{1-\delta}{p_0} \end{aligned} \tag{32}$$

under the assumption that $\delta = (p - p_0)/p_0 \ll 1$. This result is substituted into equation (30) together with $p_0 = qB_0\rho_0$. Furthermore we assume that x/ρ_0, y/ρ_0 and δ are all small such that their nonlinear or cross terms can be put to zero. Combining all these steps gives the following linear approximation to the equations of motion.

$$\begin{aligned} x'' + \frac{1 + \frac{\mathrm{d}B_y}{\mathrm{d}x}\frac{\rho_0}{B_0}}{\rho_0^2} x &= \frac{\delta}{\rho_0} \\ y'' - \frac{1}{\rho_0^2}\left(\frac{\mathrm{d}B_x}{\mathrm{d}y}\frac{\rho_0}{B_0}\right) y &= 0 \end{aligned} \tag{33}$$

in a quadrupole magnet the field gradients are equal in magnitude and are described by the dimensionless field index n

$$n = -\frac{\mathrm{d}B_y}{\mathrm{d}x}\frac{\rho_0}{B_0} = -\frac{\mathrm{d}B_x}{\mathrm{d}y}\frac{\rho_0}{B_0} \tag{34}$$

this simplifies the equations of motion to

$$\begin{aligned} x'' + \frac{1-n}{\rho_0^2} x &= \frac{1}{\rho_0}\delta \\ y'' + \frac{n}{\rho_0^2} y &= 0 \end{aligned} \tag{35}$$

In a hard edge model of the magnets where the field is constant with respect to s within the magnet and zero outside n is constant, this reduces the equations of motion to the equation of a harmonic oscillator with spring constants $k_x = (1-n)/\rho_0^2$ and $k_y = n/\rho_0^2$.

$$\begin{aligned} x'' + k_x x &= \frac{1}{\rho_0}\delta \\ y'' + k_y y &= 0 \end{aligned} \tag{36}$$

The equation of motion in y is homogeneous, with the initial conditions $y'(0) = y'_0, y(0) = y_0$, its solutions are

$$y(s) = \begin{cases} y_0 \cos\sqrt{k_y}s + y'_0 \frac{\sin\sqrt{k_y}s}{\sqrt{k_y}} & \text{for } k_y > 0 \\ y_0 \cosh\sqrt{k_y}s + y'_0 \frac{\sinh\sqrt{k_y}s}{\sqrt{k_y}} & \text{for } k_y < 0 \\ y_0 + y'_0 s & \text{for } k_y = 0 \end{cases} \tag{37}$$

The equation of motion for x inhomogeneous, which means that the solution is the sum of the homogeneous solution and particular solution.

$$x(s) = x(s)_{hom} + x(s)_{part} \tag{38}$$

The homogeneous solutions are the harmonic oscillator solutions

$$x(s)_{hom} = \begin{cases} c_1 \cos\sqrt{k_x}s + c_2 \sin\sqrt{k_x}s & \text{for } k_x > 0 \\ c_3 \mathrm{e}^{\sqrt{k_x}s} + c_4 \mathrm{e}^{-\sqrt{k_x}s} & \text{for } k_x < 0 \\ c_5 + c_6 s & \text{for } k_x = 0 \end{cases} \tag{39}$$

where c_1 through c_6 are constants determined by the initial conditions of the system. A particular solution can be found via inspection and is equal to

$$x(s)_{part} = \frac{\delta}{k_x \rho_0} \tag{40}$$

using these results together with the initial conditions $x'(0) = x'_0, x(0) = x_0$, the following solutions are obtained

$$x(s) = \begin{cases} x_0 \cos\sqrt{k_x}s + x'_0 \frac{\sin\sqrt{k_x}s}{\sqrt{k_x}} + \delta \frac{1-\cos\sqrt{k_x}s}{k_x \rho_0} & \text{for } k_x > 0 \\ x_0 \cosh\sqrt{k_x}s + x'_0 \frac{\sinh\sqrt{k_x}}{\sqrt{k_x}} - \delta \frac{1-\cosh\sqrt{k_x}s}{k_x \rho_0} & \text{for } k_x < 0 \\ x_0 + x'_0 s + \delta \frac{s^2}{2\rho_0} & \text{for } k_x = 0 \end{cases} \tag{41}$$

for elements in which the reference trajectory follows a straight line, these equations can be simplified using $\rho_0 \to \infty$ and $B_0 \rho_0 = p_0$

$$x(s) = \begin{cases} x_0 \cos\sqrt{k_x}s + x'_0 \frac{\sin\sqrt{k_x}s}{\sqrt{k_x}} & \text{for } k_x > 0 \\ x_0 \cosh\sqrt{k_x}s + x'_0 \frac{\sinh\sqrt{k_x}}{\sqrt{k_x}} & \text{for } k_x < 0 \\ x_0 + x'_0 s & \text{for } k_x = 0 \end{cases} \tag{42}$$

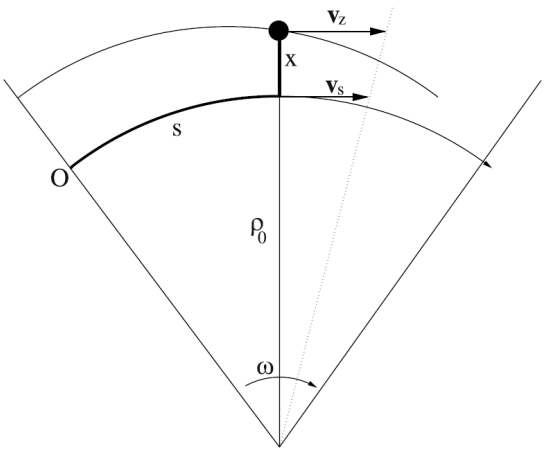

Figure 7: Illustration of a particle which does not follow the central trajectory of the beamline [1].

2.5 Transfer matrices

The equations derived in Section 2.4 are linear in x_0, x_0' and δ, this allows each ion optical element to be described in terms of a 6x6 transfer matrix R. The particle vector after the element can be deduced from the vector before the element using this matrix

$$\boldsymbol{x}_1 = R\boldsymbol{x}_0 \tag{43}$$

if a system consists out of multiple elements the total transfer matrix can be determined by multiplying the individual matrices. The total transfer matrix of a particle that first travels through element R_1, then R_2, until R_n is given by

$$R = R_n \cdots R_2 R_1 \tag{44}$$

next, the matrices for all the beam elements are given. Each transfer matrix can be found from the solutions of the equations of motion with a certain spring constant. It should be noted that the determinant of every transfer matrix R is equal to one, which is a consequence of the conservation of phase space volume of a beam.

2.5.1 Drift Space

For a drift space $k_x = k_y = 0$ and which gives

$$R = \begin{pmatrix} 1 & L & 0 & 0 & 0 & 0 \\ 0 & 1 & 0 & 0 & 0 & 0 \\ 0 & 0 & 1 & L & 0 & 0 \\ 0 & 0 & 0 & 1 & 0 & 0 \\ 0 & 0 & 0 & 0 & 1 & L/\gamma^2 \\ 0 & 0 & 0 & 0 & 0 & 1 \end{pmatrix} \tag{45}$$

where L is the drift space length and γ is the Lorentz factor.

2.5.2 Quadrupole

For the quadrupole matrices we define a parameter k

$$k = \frac{|B_0|}{a} \frac{1}{(B\rho)_0} \tag{46}$$

where a is the radius of the aperture, B_0 is the magnetic field at the pole tips, and $(B\rho)_0$ is the momentum of the reference particle divided by its charge

$$(B\rho)_0 = \frac{p_0}{q}. \tag{47}$$

For a radial focusing and axial defocusing quadrupole $k_x = k$ and $k_y = -k$ and vice versa for radial defocusing quadrupole and axial focusing dipole. The effective length of the quadrupole is denoted by L.

radial focusing and axial defocusing

$$R = \begin{pmatrix} \cos\sqrt{k}L & \frac{\sin\sqrt{k}L}{\sqrt{k}} & 0 & 0 & 0 & 0 \\ -\sqrt{k}\sin\sqrt{k}L & \cos\sqrt{k}L & 0 & 0 & 0 & 0 \\ 0 & 0 & \cosh\sqrt{k}L & \frac{\sinh\sqrt{k}L}{\sqrt{k}} & 0 & 0 \\ 0 & 0 & \sqrt{k}\sinh\sqrt{k}L & \cosh\sqrt{k}L & 0 & 0 \\ 0 & 0 & 0 & 0 & 1 & L/\gamma^2 \\ 0 & 0 & 0 & 0 & 0 & 1 \end{pmatrix} \tag{48}$$

radial defocusing and axial focusing

$$R = \begin{pmatrix} \cosh\sqrt{k}L & \frac{\sinh\sqrt{k}L}{\sqrt{k}} & 0 & 0 & 0 & 0 \\ \sqrt{k}\sinh\sqrt{k}L & \cosh\sqrt{k}L & 0 & 0 & 0 & 0 \\ 0 & 0 & \cos\sqrt{k}L & \frac{\sin\sqrt{k}L}{\sqrt{k}} & 0 & 0 \\ 0 & 0 & -\sqrt{k}\sin\sqrt{k}L & \cos\sqrt{k}L & 0 & 0 \\ 0 & 0 & 0 & 0 & 1 & L/\gamma^2 \\ 0 & 0 & 0 & 0 & 0 & 1 \end{pmatrix} \tag{49}$$

2.5.3 Parallel Pole Wedge Bending Magnet

For a parallel pole wedge bending magnet we only have the spring constant part resulting from the curved trajectory in the x-direction

$$k_x = \frac{1}{\rho_0^2}, \qquad k_y = 0 \tag{50}$$

the bending angle α can be calculated via

$$\alpha = \frac{L}{\rho_0} \tag{51}$$

where ρ_0 is the radius of curvature of the central trajectory and L is the effective length of the magnet.

$$R = \begin{pmatrix} \cos\alpha & \rho_0 \sin\alpha & 0 & 0 & 0 & \rho_0 (1 - \cos\alpha) \\ \frac{\sin\alpha}{\rho_0} & \cos\alpha & 0 & 0 & 0 & \sin\alpha \\ 0 & 0 & 1 & \rho_0\alpha & 0 & 0 \\ 0 & 0 & 0 & 1 & 0 & 0 \\ -\sin\alpha & -\rho_0 (1 - \cos\alpha) & 0 & 0 & 1 & \rho_0 \frac{\alpha}{\gamma^2} - \rho_0 (\alpha - \sin\alpha) \\ 0 & 0 & 0 & 0 & 0 & 1 \end{pmatrix} \tag{52}$$

2.5.4 Combined Function Magnet

The combined function magnet is a dipole magnet whose poles are not parallel, an example can be seen in Figure 8. This type of magnet is described by a combination of a parallel pole dipole magnet and a quadrupole magnet. The magnet is characterized by a field index n

$$n = -\frac{\rho}{B_0} \left(\frac{\partial B_z}{\partial r} \right)_{r=\rho} \tag{53}$$

where ρ is the radius of curvature of the central trajectory, B_0 is the magnetic field at the central trajectory and, r is the radius of curvature of the described particle. This field index can be written in terms of the quadrupole and dipole parameters

$$n = k\rho_0^2 \tag{54}$$

where ρ_0 and k are the parameters described in Eqs. (51) and (46) respectively. For $0 < n < 1$ the magnet is weak focusing and the transfer matrix (excluding the entries for l) is given by

$$R = \begin{pmatrix} \cos\sqrt{1-n}\alpha & \frac{\rho_0 \sin\sqrt{1-n}\alpha}{\sqrt{1-n}} & 0 & 0 & \frac{\rho_0\left(1-\cos\sqrt{1-n}\alpha\right)}{1-n} \\ -\frac{\sqrt{1-n}\sin\sqrt{1-n}\alpha}{\rho_0} & \cos\sqrt{1-n}\alpha & 0 & 0 & \frac{\sin\sqrt{1-n}\alpha}{\sqrt{1-n}} \\ 0 & 0 & \cos\sqrt{n}\alpha & \frac{\rho_0 \sin\sqrt{n}\alpha}{\sqrt{n}} & 0 \\ 0 & 0 & \frac{\sqrt{n}\sin\sqrt{n}\alpha}{\rho_0} & \cos\sqrt{n}\alpha & 0 \\ 0 & 0 & 0 & 0 & 1 \end{pmatrix} \tag{55}$$

Strong focusing magnets are characterised by $|n| > 1$. A strong focusing magnets which focus in the radial direction and defocus in the axial direction have $n < 0$,

$$R = \begin{pmatrix} \cos\sqrt{1-n}\alpha & \frac{\rho_0 \sin\sqrt{1-n}\alpha}{\sqrt{1-n}} & 0 & 0 & \frac{\rho_0\left(1-\cos\sqrt{1-n}\alpha\right)}{1-n} \\ -\frac{\sqrt{1-n}\sin\sqrt{1-n}\alpha}{\rho_0} & \cos\sqrt{1-n}\alpha & 0 & 0 & \frac{\sin\sqrt{1-n}\alpha}{\sqrt{1-n}} \\ 0 & 0 & \cosh\sqrt{|n|}\alpha & \frac{\rho_0 \sinh\sqrt{|n|}\alpha}{\sqrt{|n|}} & 0 \\ 0 & 0 & \frac{\sqrt{|n|}\sinh\sqrt{|n|}\alpha}{\rho_0} & \cosh\sqrt{|n|}\alpha & 0 \\ 0 & 0 & 0 & 0 & 1 \end{pmatrix} \tag{56}$$

a strong focusing magnet with $n > 1$ focuses strongly in the axial direction and defocuses in the radial direction

$$R = \begin{pmatrix} \cosh\sqrt{|1-n|}\alpha & \frac{\rho_0 \sinh\sqrt{|1-n|}\alpha}{\sqrt{|1-n|}} & 0 & 0 & \frac{\rho_0\left(1-\cosh\sqrt{|1-n|}\alpha\right)}{1-n} \\ \frac{\sqrt{|1-n|}\sinh\sqrt{|1-n|}\alpha}{\rho_0} & \cosh\sqrt{|1-n|}\alpha & 0 & 0 & \frac{\sinh\sqrt{|1-n|}\alpha}{\sqrt{|1-n|}} \\ 0 & 0 & \cos\sqrt{n}\alpha & \frac{\rho_0 \sin\sqrt{n}\alpha}{\sqrt{n}} & 0 \\ 0 & 0 & -\frac{\sqrt{n}\sin\sqrt{n}\alpha}{\rho_0} & \cos\sqrt{n}\alpha & 0 \\ 0 & 0 & 0 & 0 & 1 \end{pmatrix} \tag{57}$$

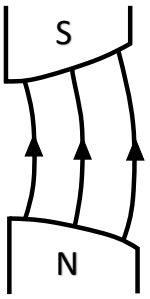

Figure 8: Shape of the magnetic field inside a focusing bending magnet. Image adapted from [4].

2.5.5 Rotation of Transverse Coordinates

To describe a magnet element that is rotated around the z-axis, a rotation of the transverse coordinates is required. This rotation is described by the following matrix, in which the rotation angle α is positive for a clock-wise rotation around the z-axis, as indicated in Figure 9

$$R = \begin{pmatrix} \cos\alpha & 0 & \sin\alpha & 0 & 0 & 0 \\ 0 & \cos\alpha & 0 & \sin\alpha & 0 & 0 \\ -\sin\alpha & 0 & \cos\alpha & 0 & 0 & 0 \\ 0 & -\sin\alpha & 0 & \cos\alpha & 0 & 0 \\ 0 & 0 & 0 & 0 & 1 & 0 \\ 0 & 0 & 0 & 0 & 0 & 1 \end{pmatrix} \tag{58}$$

the total transfer matrix R_t of a magnet element R_e that has been rotated under an angle α, can be obtained by sandwiching R_e between two rotation matrices

$$R_t = R(-\alpha)R_eR(\alpha) \tag{59}$$

the matrix $R(\alpha)$ rotates the axes such that they coincide with the local coordinate system of R_e. After the transformation R_e is applied the axes are transformed back to the original coordinate system using $R(-\alpha)$.

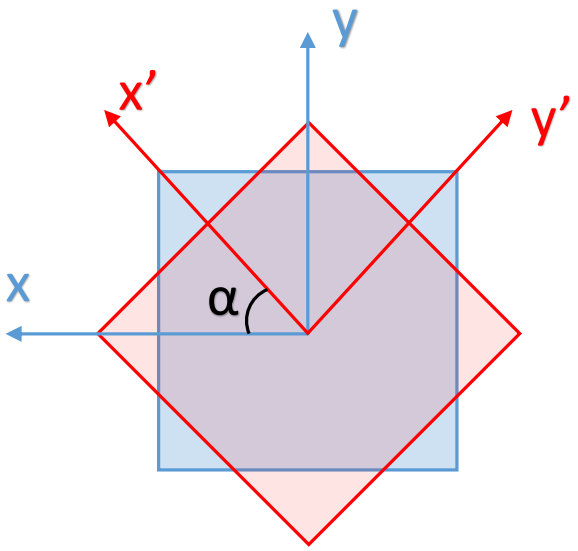

Figure 9: Original (blue) and rotated (red) coordinate systems, the axes which are rotated under a positive angle α are indicated with a prime, the rotated element is indicated with a square.

2.6 Phase Ellipse

The theory that is developed so far allows the description of the trajectory of a single particle through the system. To describe the beam, which consists of many particles, a phase space ellipse is used. First, the simple case of a 2-dimensional ellipse is described, afterwards, the description of the full 6-dimensional ellipse is given. The fact that the beam can be described by an ellipse is a direct consequence of the first-order description of the ion-optics and can be derived from Eq. (35), with a non-constant k, which is also known as Hill's equation.

$$x''(s) - k(s)x(s) = 0 \tag{60}$$

the full derivation can be found in [2].

For a two dimensional particle beam which travels in the x-z plane, the phase ellipse is represented by the symmetric 2x2 matrix

$$\sigma_x = \begin{pmatrix} \sigma_{11} & \sigma_{12} \\ \sigma_{12} & \sigma_{22} \end{pmatrix} \tag{61}$$

the equation for the phase ellipse is

$$\boldsymbol{x}^\top \sigma_x^{-1} \boldsymbol{x} = 1 \tag{62}$$

with $\boldsymbol{x} = [x, x']^\top$ is the vector from the origin to a point on the ellipse. Expanding the equation yields the equation of an ellipse.

$$x'^2\sigma_{11} - 2xx'\sigma_{12} + x^2\sigma_{22} = \sigma_{11}\sigma_{22} - \sigma_{12}^2 = \epsilon_x^2 \tag{63}$$

the quantity ϵ_x is related to the area of the ellipse, which is also called the emittance E_x of the beam

$$E_x = \pi\epsilon_x = \pi\sqrt{\det \sigma_x} = \pi\sqrt{\sigma_{11}\sigma_{22} - \sigma_{12}^2} \tag{64}$$

the ellipse is plotted in Figure 10, together with the physical interpretation of the ellipse parameters. These physical parameters of the beam, which are the maximum half-width (x_{max}) and divergence (x'_{max}) are given by

$$\begin{aligned} x_{max} &= \sqrt{\sigma_{11}} \\ x'_{max} &= \sqrt{\sigma_{22}} \end{aligned} \tag{65}$$

the correlation between these parameters is given by the dimensionless parameter

$$r_{12} = \frac{\sigma_{12}}{\sqrt{\sigma_{11}\sigma_{22}}}. \tag{66}$$

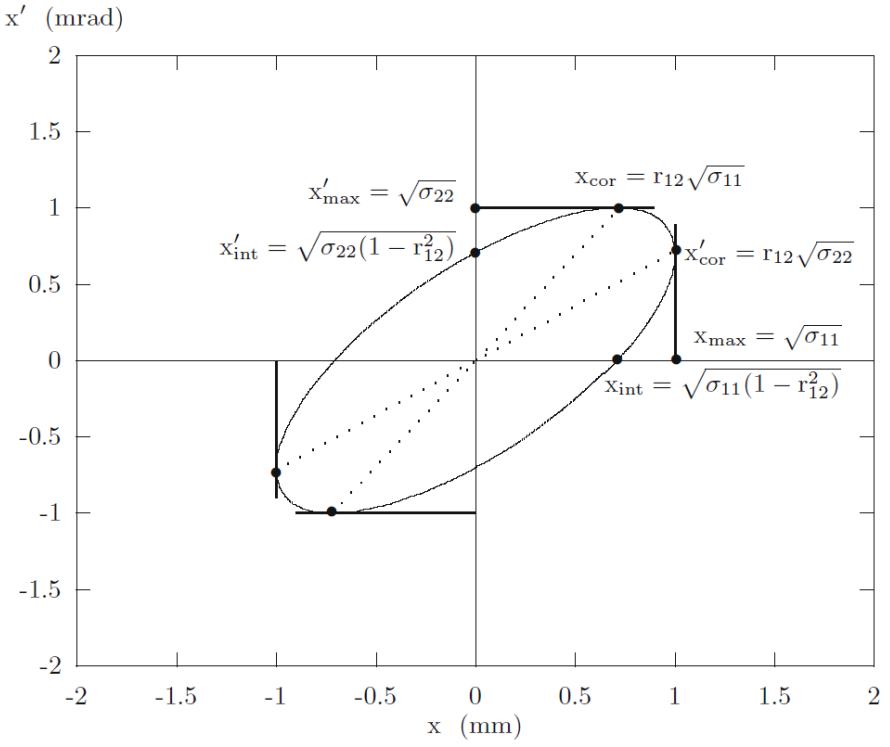

Figure 10: Phase ellipse plotted with the physical interpretation of the parameters [1].

To describe the beam in the full six dimensional phase space, the following symmetric 6x6 matrix is used

$$\sigma = \begin{pmatrix} \sigma_{11} & \sigma_{12} & \sigma_{13} & \sigma_{14} & \sigma_{15} & \sigma_{16} \\ \sigma_{12} & \sigma_{22} & \sigma_{23} & \sigma_{24} & \sigma_{25} & \sigma_{26} \\ \sigma_{13} & \sigma_{23} & \sigma_{33} & \sigma_{34} & \sigma_{35} & \sigma_{36} \\ \sigma_{14} & \sigma_{24} & \sigma_{34} & \sigma_{44} & \sigma_{45} & \sigma_{46} \\ \sigma_{15} & \sigma_{25} & \sigma_{35} & \sigma_{45} & \sigma_{45} & \sigma_{56} \\ \sigma_{16} & \sigma_{26} & \sigma_{36} & \sigma_{46} & \sigma_{46} & \sigma_{66} \end{pmatrix} \tag{67}$$

the diagonal elements give the physical parameters of the beam

$$\begin{aligned} x_{max} &= \sqrt{\sigma_{11}}, & x'_{max} &= \sqrt{\sigma_{22}} \\ y_{max} &= \sqrt{\sigma_{33}}, & y'_{max} &= \sqrt{\sigma_{44}} \\ l_{max} &= \sqrt{\sigma_{55}}, & \delta_{max} &= \sqrt{\sigma_{66}} \end{aligned} \tag{68}$$

the off-diagonal elements specify the correlation between the parameters via

$$r_{ij} = \frac{\sigma_{ij}}{\sqrt{\sigma_{ii}\sigma_{jj}}}. \tag{69}$$

To transform the phase space ellipsoid through a system, represented by a transfer matrix R, it can be proven from Eq. (62) that the following relation holds

$$\sigma(s) = R(0 \to s)\sigma(0)R(0 \to s)^\top \tag{70}$$

using this transformation it can be proven that the volume of the phase space ellipsoid is conserved. The volume of a six-dimensional ellipsoid is given by

$$V = \frac{16}{3}\pi\sqrt{\det\sigma} \tag{71}$$

from the transformation we obtain that

$$\det\sigma(s) = \det(R\sigma(0)R) = \det(R)\det(\sigma(0))\det(R) = \det\sigma(0) \tag{72}$$

since $\det(R) = \det\left(R^\top\right) = 1$, this means that the volume of the phase space ellipsoid is conserved.

2.7 Statistical Definition of the Beam

In this section a statistical description of the beam will be given. To introduce the topic an example is first given for the radial phase ellipse, afterwards the theory is extended to the full six-dimensional phase space.

In the previous section it was noted that the particles are encircled by the phase ellipse, however it was not yet mentioned what the density distribution of the particles inside the phase ellipse is. A realistic description of the beam uses the Gaussian distribution, whose two-dimensional form is given by

$$\rho(\boldsymbol{x}) = \frac{1}{2\pi\det(\Sigma)}\exp\left(-\frac{1}{2}\boldsymbol{x}^\top\Sigma^{-1}\boldsymbol{x}\right) \tag{73}$$

where $\boldsymbol{x} = (x, x')^\top$ is vector containing the particle coordinates, and Σ is the covariance matrix of the distribution. The entries of Σ can be calculated as

$$\begin{aligned}
\Sigma_{11} &= \frac{1}{n-1}\sum_{i=1}^{n}(x_i - \overline{x})^2 \\
\Sigma_{12} &= \frac{1}{n-1}\sum_{i=1}^{n}(x_i - \overline{x})(x_i' - \overline{x'}) \\
\Sigma_{22} &= \frac{1}{n-1}\sum_{i=1}^{n}(x_i - \overline{x'})^2
\end{aligned} \tag{74}$$

where the sums are taken over all particles in the cross-section of the beam. An example plot of Eq. (73) can be seen in Figure 11.

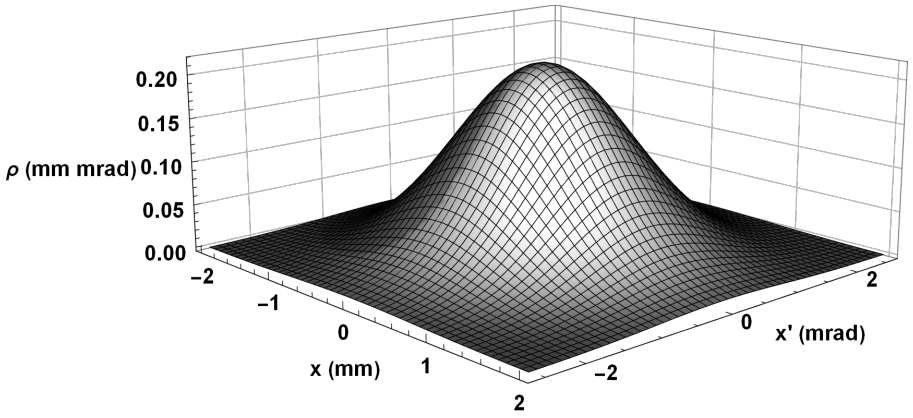

Figure 11: Two dimensional Gaussian, with $\Sigma_{11} = 0.6\,\mathrm{mm}^2$, $\Sigma_{22} = 0.9\,\mathrm{mrad}^2$, and $\Sigma_{12} = 0\,\mathrm{mm\,mrad}$, describing the density distribution of the particles within the phase ellipse.

The relation between Σ and σ_x as defined in Eq. (61) is not fixed. One definition, referred to as the 1σ-emittance is to use $\sigma_x = \Sigma$ such that the phase ellipse described in Eq. (62) becomes

$$\boldsymbol{x}^\top \Sigma^{-1} \boldsymbol{x} = 1 \tag{75}$$

the contour line described by this equation encloses 39.3% of the total intensity. The emittance of this distribution can be calculated using Eq.(64)

$$\epsilon_x^{1\sigma} = \sqrt{\det \sigma_x} = \sqrt{\Sigma_{11}\Sigma_{22} - \Sigma_{12}^2}. \tag{76}$$

Another possibility is to use the 2σ-emittance, such that $\sigma_x = 4\Sigma$, this time the contour line described by

$$\boldsymbol{x}^\top \Sigma^{-1} \boldsymbol{x} = 4 \tag{77}$$

encloses 86.5% of the intensity, the emittance becomes

$$\epsilon_x^{2\sigma} = \sqrt{\det \sigma_x} = 4\sqrt{\Sigma_{11}\Sigma_{22} - \Sigma_{12}^2} = 4\epsilon_x^{1\sigma} \tag{78}$$

.

The last common definition is to use the 3σ-emittance, such that $\sigma_x = 9\Sigma$, the contour line described by

$$\boldsymbol{x}^\top \Sigma^{-1} \boldsymbol{x} = 9 \tag{79}$$

encloses 98.9% of the total intensity, the emittance is equal to

$$\epsilon_x^{3\sigma} = \sqrt{\det \sigma_x} = 9\sqrt{\Sigma_{11}\Sigma_{22} - \Sigma_{12}^2} = 9\epsilon_x^{1\sigma} \tag{80}$$

.

It is clear that depending on the definition of σ_x the values of the emittances vary greatly, therefore it should always be mentioned which definition is used, these σ-emittance definitions hold for any dimensions of Σ. In the rest of this thesis the 2σ-emittance will be used unless otherwise stated.

To obtain the beam profile as measured on the beam monitors the projection of the two dimensional Gaussian distribution is made onto the x-axis, which yields another one-dimensional Gaussian. This Gaussian, when normalized to one, is described by the equation

$$\rho(x) = \frac{1}{\sqrt{2\pi\Sigma_{11}}} \exp\left(-\frac{1}{2}\frac{x^2}{\Sigma_{11}}\right) \tag{81}$$

A plot of this can be seen in 12. It should be noted that this approximation only works well in the range of $\sqrt{\Sigma_{11}} \leq x \leq 3\sqrt{\Sigma_{11}}$. Inside the beam pipe there is always a background of scattered particles, this background deviates strongly from a Gaussian distribution and therefore causes the intensity at positions outside of $\sqrt{\Sigma_{11}} \leq x \leq 3\sqrt{\Sigma_{11}}$, to be higher than expected from Eq. (81). Furthermore the Gaussian distribution extends to infinity, while the actual beam size is limited by the beam pipe diameter.

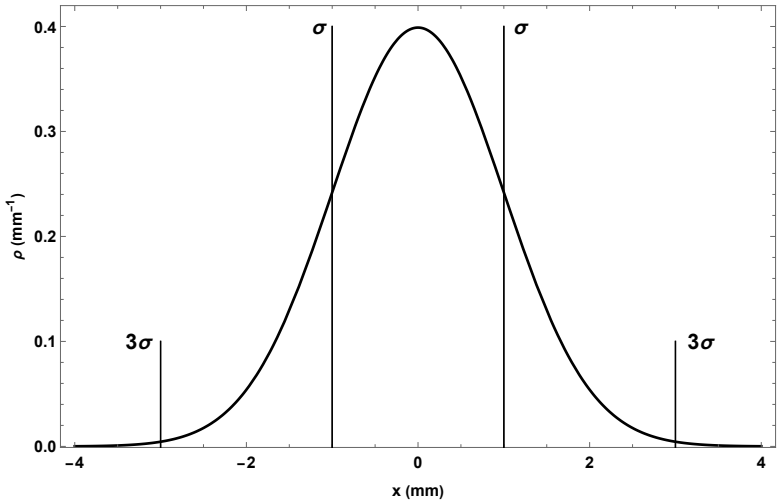

Figure 12: Normal distribution, using $\Sigma_{11} = 1.0\,\mathrm{mm}^2$ of a x-profile as measured on the beam monitors, the σ in the graph corresponds to $\sqrt{\Sigma_{11}}$. Image adapted from [1].

To extend this theory to the six-dimensional phase space we define the six dimensional Gauss distribution

$$\rho(\boldsymbol{x}) = \frac{1}{(2\pi)^3\sqrt{\det(\Sigma)}} \exp\left(-\frac{1}{2}\boldsymbol{x}^\top \Sigma^{-1}\boldsymbol{x}\right) \tag{82}$$

where σ is the 6x6 beam matrix and $\boldsymbol{x} = (x, x', y, y', l, \delta)$ is now the six-dimensional vector containing the coordinates. The lower dimensional phase spaces, such as the phase ellipse or the beam profile, can be obtained by projecting this distribution onto the appropriate axes. The entries of the Σ matrix can in general be calculated as

$$\begin{aligned} \Sigma_{ii} &= \frac{1}{n-1}\sum_{j=1}^{n}((x_i)_j - \overline{x_i})^2 \\ \Sigma_{ik} &= \frac{1}{n-1}\sum_{j=1}^{n}((x_i)_j - \overline{x})((x_k)_j - \overline{x_k}) \end{aligned} \tag{83}$$

where x_i is the ith component of the particle vector.

2.8 Quadrupole Variation Method

To perform corrections to the beam centroid, both the position and angle of the beam need to be known at specific locations. The beam monitors which are stationed at different positions along the beamline are only able to measure the beam profile, from which the position can be derived. To obtain the angle of the beam centroid the quadrupole variation method is used.

In the quadrupole variation method, multiple measurements need to be made under different settings of the quadrupole magnets in the beamline. The quadrupoles which are varied need to be in between the location at which the angle should be known and a beam monitor downstream of this position. At least two measurements need to be made, however, more measurements will lead to a more accurate value of the angle and position.

For the quadrupole variation method it is known that there is no coupling between the x and y coordinates in the beamline, as can be seen from the transfer matrices of the elements that are used in the system. This allows the transfer matrix to be simplified to a two-dimensional form. The resulting equations will be derived for the x-direction, however, the same equations can be applied to the y-direction.

The total transfer matrix of the system between the initial position and beam profile monitor is given by

$$R = \begin{pmatrix} R_{11} & R_{12} \\ R_{21} & R_{22} \end{pmatrix} \tag{84}$$

from Eq. (43) the x-coordinate is given by

$$x_1 = R_{11}x_0 + R_{12}x_0' = f(g) \tag{85}$$

where $f(g)$ is a function depending on the gradients of the quadrupoles which are varied. If a total of N measurements are taken then the initial beam conditions can be determined by minimising the following function [5]

$$\sum_{i=1}^{N} (x_{m_i} - f(g_i)) \tag{86}$$

where x_m is the measured position of the centroid of the beam. The beam is measured using wire harps, which project the intensity of the beam onto the x and y axes, therefore x_m is calculated as [6]

$$x_m = \frac{\sum_{i=1}^{N} xI}{\sum_{i=1}^{N} I} \tag{87}$$

where I is the measured intensity at location x.

For an accurate measurement, the beam size must be kept small, therefore in the case where multiple quadrupoles can be used their combined settings should give a small beam size at the beam profile monitor. Furthermore, the sensitivity of x_m to the quadrupole strengths needs be sufficiently high such that random errors do not dominate the measurements.

To demonstrate the effect of quadrupole settings on the beam size an example section of the beamline is taken in which a quadrupole triplet is present, which can be seen in Figure 13. In a quadrupole triplet, the same current is fed through the outer two quadrupoles, which also have the same dimensions. The current through the inner quadrupole has opposite polarity, such that it has an opposite focus with respect to the outer ones.

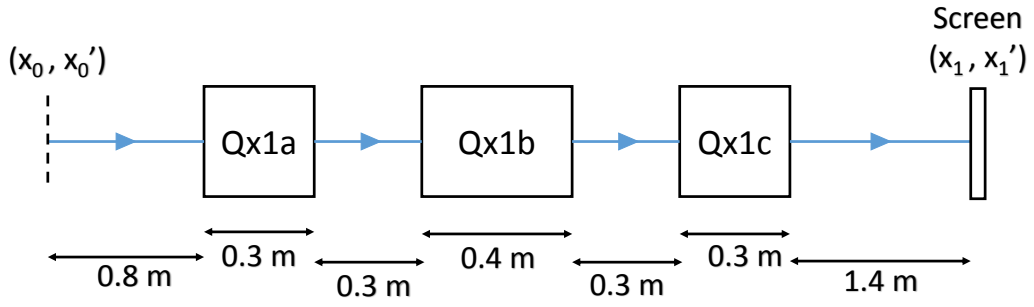

Figure 13: Image of a quadrupole triplet in the beamline.

For this example a beam matrix will is taken with $\sigma_{11} = 1\,\text{cm}^2$, $\sigma_{22} = 10\,\text{mrad}^2$ and all other entries zero. The field gradient of the first and third quadrupole is g_1 and the field gradient of the inner quadrupole is g_2. The plot of the beam size as a function of the field gradients can be seen in Figure 14, it is observed that there are multiple combinations possible which give a small beam size.

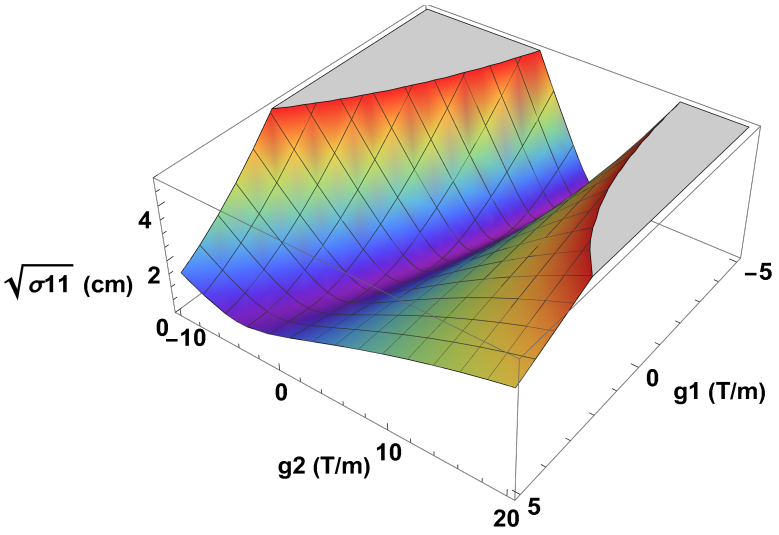

Figure 14: Graph of beam size in the x-direction as a function of varying the magnetic field settings in a triplet quadrupole variation.

3 Control System

To set up the control system several pieces of information are needed. Below an overview of the beam guidance system is given with the positions of all the steering, bending, and quadrupole magnets as well as the beam profile monitors. Also, the equations of magnets with incorrect settings will be derived, and the relation between the magnetic field flux density and current supplied to the magnets is given.

3.1 Beam Guidance system

The full beamline guidance system can be seen in Figure 15. At the start of the system, pairs of steering magnets are present to correct the angle and position of the beam coming from the cyclotron. After this point, the beam centroid should be aligned with the designed trajectory. If the bending magnets are set correctly the beam should stay aligned along the entire system which means that no further steering magnets are needed. To monitor the beam several profile monitors are installed in the system. Most monitors can measure the beam in both the axial and radial direction, these have a label starting with HX, some monitors are present which can only measure in the axial radial or axial direction, indicated with labels starting with HH or HV respectively. There is also a section in the beamline in which the beam is bent upwards by 2.6°, indicated by Bup. This section will be ignored initially since it requires a different control system from the rest of the system.

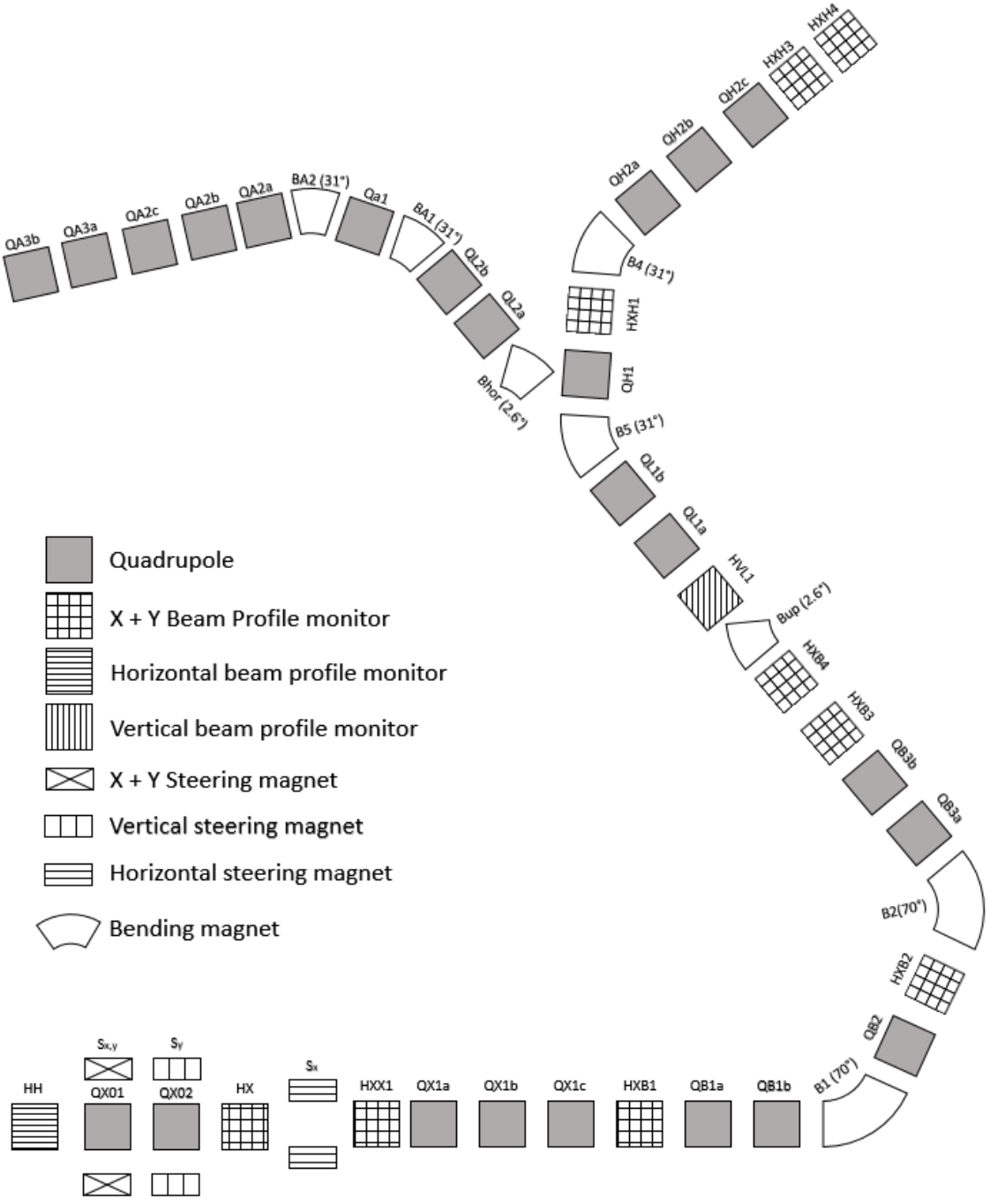

Figure 15: Schematic overview of the beamline.

3.2 Equations of Magnets with Incorrect Settings

The transfer matrices above are derived for the case where the beam centroid is aligned with the reference particle trajectory. However, initially, the beam will be misaligned which means that these matrices are not valid. In this section equations describing the particle motion in the misaligned system will be given for steering and bending magnets. Two general equations that hold for every dipole magnet are

$$\rho = \frac{p}{B} \tag{88}$$

$$\alpha = \frac{BL}{p} \tag{89}$$

where ρ is the radius of curvature of the particles in the field of the magnet, p is the momentum of the particle divided by its charge, B is the magnetic flux density, α is the bend angle of the magnet, and L is the effective length of the magnet.

3.2.1 Steering Magnet

The equations for a steering magnet will be derived for a two-dimensional case, which is allowed since there is no coupling between the x and y coordinates in the beam. Therefore these equations hold in both the radial and axial direction.

The typical length of a steering magnet is around 20-30 cm, and the bending angle is small, in the order of mrad. This means that its effect can be approximated by an instantaneous kick that occurs at the center of the magnet, which is proven in Appendix A. To correct for both angle and position, a pair of steering magnets is needed, which can be seen in Figure 16. This system can be written into the following matrix equation

$$\begin{bmatrix} x_1 \\ x_1' \end{bmatrix} = \begin{bmatrix} L_1 & L_2 \\ 1 & 1 \end{bmatrix} \begin{bmatrix} \alpha_1 \\ \alpha_2 \end{bmatrix} + \begin{bmatrix} x_0 + x_0' L_1 \\ x_0' \end{bmatrix} \tag{90}$$

where x_0 and x_0' are the position and angle deviation of the beam centroid at the center of the first steering magnet, x_1 and x_1' are the position and angle deviation of the beam centroid at a distance L_2 from the center of the second steering magnet, and L_1 and L_2 are the distances from the centers of the first and second steering magnet respectively to the end of the section, as can be seen in Figure 16, and α_1 and α_2 are the bending angles of the first and second steering magnet respectively.

In the desired case of $x_1 = x_1' = 0$ the system reduces to

$$\begin{bmatrix} L_1 & L_2 \\ 1 & 1 \end{bmatrix} \begin{bmatrix} \alpha_1 \\ \alpha_2 \end{bmatrix} = - \begin{bmatrix} x_0 + x_0' L_1 \\ x_0' \end{bmatrix} \tag{91}$$

By solving this system of equations it is possible to obtain the required values of α_1 and α_2. The change in angle α for a steering magnet is equal to the bending angle of a dipole, which means they can be calculated using Eq. (89).

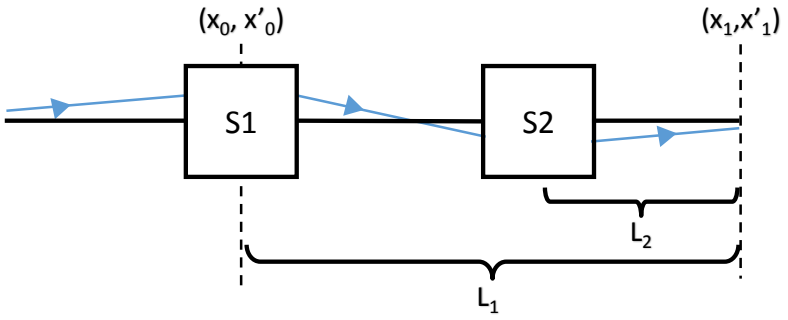

Figure 16: Pair of steering magnets which can be used to correct for position and angle. Reference trajectory is indicated in black, while the described particle trajectory is given in blue.

3.2.2 Bending Magnet

An image of a bending magnet with incorrect settings can be seen in Figure 17, the resulting equations are as follows, the derivation can be found in Appendix B

$$\begin{aligned} x_1 &= \cos(\alpha_0)x_0 + \rho\sin(\alpha_0)x_0' + \rho(1-\cos\alpha_0)\frac{\rho-\rho_0}{\rho} \\ x_1' &= -\frac{\sin\alpha_0}{\rho}x_0 + \cos(\alpha_0)x_0' + \sin(\alpha_0)\frac{\rho-\rho_0}{\rho} \end{aligned} \tag{92}$$

where α_0 and ρ_0 are the designed bending angle and radius of curvature, and ρ is the actual radius of curvature. These equations can be written into a matrix form as follows

$$\begin{bmatrix} x_1 \\ x_1' \\ \delta_\rho \end{bmatrix} = \begin{pmatrix} \cos\alpha_0 & \rho\sin\alpha_0 & \rho(1-\cos\alpha_0) \\ -\frac{\sin\alpha_0}{\rho} & \cos\alpha_0 & \sin\alpha_0 \\ 0 & 0 & 1 \end{pmatrix} \begin{bmatrix} x_0 \\ x_0' \\ \delta_\rho \end{bmatrix} \tag{93}$$

where $\delta_\rho = (\rho-\rho_0)/\rho$. These equations are analogous to Eq. (52), which is because p and ρ are related through Eq. (88). This means that a wrong value of the magnetic field is essentially the same as a wrong momentum of the described particle.

The equation describing a bending magnet which bend to the left can be found using Eq. (59), a magnet bending to the left is rotated by an angle of 180° with respect to a magnet bending to the right

$$\begin{bmatrix} x_1 \\ x_1' \\ \delta_\rho \end{bmatrix} = \begin{pmatrix} \cos(-180°) & 0 & 0 \\ 0 & \cos(-180°) & 0 \\ 0 & 0 & 1 \end{pmatrix} \begin{pmatrix} \cos\alpha_0 & \rho\sin\alpha_0 & \rho(1-\cos\alpha_0) \\ -\frac{\sin\alpha_0}{\rho} & \cos\alpha_0 & \sin\alpha_0 \\ 0 & 0 & 1 \end{pmatrix} \begin{pmatrix} \cos(180°) & 0 & 0 \\ 0 & \cos(180°) & 0 \\ 0 & 0 & 1 \end{pmatrix} \begin{bmatrix} x_0 \\ x_0' \\ \delta_\rho \end{bmatrix}$$

$$\begin{bmatrix} x_1 \\ x_1' \\ \delta_\rho \end{bmatrix} = \begin{pmatrix} \cos\alpha_0 & \rho\sin\alpha_0 & -\rho(1-\cos\alpha_0) \\ -\frac{\sin\alpha_0}{\rho} & \cos\alpha_0 & -\sin\alpha_0 \\ 0 & 0 & 1 \end{pmatrix} \begin{bmatrix} x_0 \\ x_0' \\ \delta_\rho \end{bmatrix} \tag{94}$$

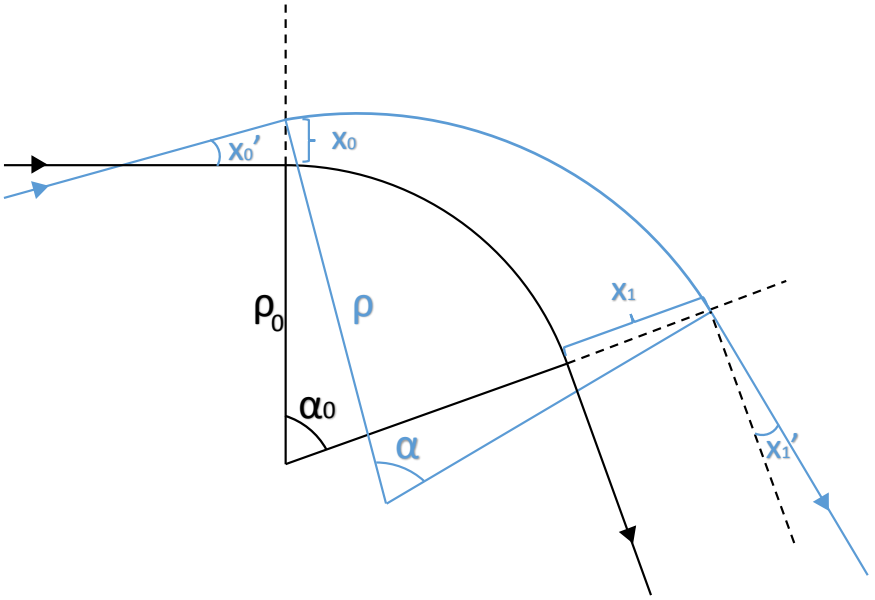

Figure 17: Image of a bending magnet with a wrong magnetic field value (blue), compared to a bending magnet with the correct magnetic field value (black).

3.2.3 Combined Function Magnet

Some magnets in the beamline are a combination of a dipole and quadrupole magnet. These are also needed to align the beam centroid, however, the equations are different to that of a steering magnet due to the added quadrupole field. Because the bending angle is small we approximate the effect of this magnet to a quadrupole in which an instantaneous kick is applied at the center, the proof of this can be found in Appendix C. The transfer matrices can be found using Eqs. (48) and (49). If the quadrupole component of the field is focusing it is equal to

$$\begin{bmatrix} x_1 \\ x_1' \end{bmatrix} = \begin{pmatrix} \cos\sqrt{k}L & \frac{\sin\sqrt{k}L}{\sqrt{k}} \\ -\sqrt{k}\sin\sqrt{k}L & \cos\sqrt{k}L \end{pmatrix} \begin{bmatrix} x_0 \\ x_0' \end{bmatrix} + \begin{bmatrix} \frac{\alpha\sin\frac{\sqrt{k}L}{2}}{\sqrt{k}} \\ \alpha\cos\frac{\sqrt{k}L}{2} \end{bmatrix} \tag{95}$$

if the quadrupole component is defocussing the following transfer function holds

$$\begin{bmatrix} x_1 \\ x_1' \end{bmatrix} = \begin{pmatrix} \cosh\sqrt{k}L & \frac{\sinh\sqrt{k}L}{\sqrt{k}} \\ \sqrt{k}\sinh\sqrt{k}L & \cosh\sqrt{k}L \end{pmatrix} \begin{bmatrix} x_0 \\ x_0' \end{bmatrix} + \begin{bmatrix} \frac{\alpha\sinh\frac{\sqrt{k}L}{2}}{\sqrt{k}} \\ \alpha\cosh\frac{\sqrt{k}L}{2} \end{bmatrix} \tag{96}$$

4 Control Algorithms

4.1 General Strategy

The goal of the control system is to achieve a beam whose centroid is aligned with the reference trajectory of the system and whose size is minimized at specified locations in the system. For the initial alignment of the system a lookup table is used, this will result in approximately correct values which allows the ion beam to reach the beam monitors at which the cross-sectional profile of the beam is measured. To perform subsequent fine-tuning of the magnet settings information on the beam position and angle needs to be known. The position can be calculated using the measured cross-sectional beam profile, the angle can be measured from the quadrupole variation method.

For the alignment of the beam centroid it is important to note that a beam can only be adjusted using elements upstream of its position. This allows the control to be done sequentially, where the beam centroid is first aligned in one section before moving on to the next. This greatly reduces the number of parameters that need to be tweaked simultaneously.

The overview in Figure 15 shows that the steering magnets are located at the start of the beamline. Since a pair of steering magnets is present for the x and y coordinate, it is possible to align the beam centroid with the reference trajectory after steering magnet S_x. If the beam centroid is not aligned with a quadrupole axis when the quadrupole strength is changed, the beam centroid trajectory will change. Therefore it is import to first adjust the quadrupole component of the combined function magnets $S_{x,y}$ and S_y such that the desired spot size is achieved at Hx, before doing the beam centroid alignment. Once the steering magnets have been used to align the beam, it will stay aligned until it encounters a bending magnet with incorrect settings. Using the control algorithm this bending magnet will be adjusted such that the beam will be aligned again. This step is repeated for each bending magnet in the beamline until the end is reached.

4.2 Control Loop Steering Magnet

4.2.1 General Form

The goal of the control loop for the steering magnets is to achieve zero beam centroid angle and position at the end of the steering magnet pair. Since measurements of the beam centroid can only be made in discrete steps, see Section 2.8, a control loop is proposed which operates in the discrete-time domain. The controller which is proposed performs corrections to the beam centroid based on a measured error, the loop can be seen in Figure 18, the state-space form of this system is

$$\begin{aligned} \mathbf{x}(k+1) &= A\mathbf{x}(k) + B\mathbf{u}(k) \\ \mathbf{y}(k) &= C\mathbf{x}(k) + D\mathbf{u}(k) + \mathbf{y_0} \end{aligned} \tag{97}$$

where $\mathbf{x}$ is the state vector, $\mathbf{y}$ the output vector, $\mathbf{u}$ the input vector and $\mathbf{y_0}$ is a constant disturbance term. For the case of the steering magnets the output vector is equal to the beam centroid position and angle at the end of the steering magnet pair, and the state vector is equal to the current supplied to the steering magnets,

$$\mathbf{y} = \begin{pmatrix} x_1 \\ x_1' \end{pmatrix}, \qquad \mathbf{x} = \begin{pmatrix} I_1 \\ I_2 \end{pmatrix}, \tag{98}$$

the matrices C and D, and the vector $\mathbf{y_0}$ can be determined from Eqs. (5), (89) and (90)

$$C = \frac{\mu_0 n}{p} \begin{bmatrix} \frac{L_1 L_{s1}}{g_1} & \frac{L_2 L_{s2}}{g_2} \\ \frac{L_{s1}}{g_1} & \frac{L_{s2}}{g_2} \end{bmatrix}, \qquad D = \begin{bmatrix} 0 & 0 \\ 0 & 0 \end{bmatrix}, \qquad \boldsymbol{y_0} = \begin{pmatrix} x_0 + x_0' L_1 \\ x_0' \end{pmatrix} \tag{99}$$

where L_{s1} and L_{s2} are the lengths of the first and second steering magnet respectively, L_1 and L_2 are the lengths as described in Figure 16, g_1 and g_2 are the gap sizes of the first and second steering magnet respectively and p is the particle momentum divided by its charge. The goal of the controller is to put $\mathbf{y}$ to zero, it can be shown from simple block diagram algebra, using the loop in Figure 18, that

$$\mathbf{y}(k+1) = (CAC^{-1} - CB)\mathbf{y}(k) + (I - CAC^{-1})\mathbf{y_0} \tag{100}$$

By inspection the following matrices are proposed, where I_n denotes the n x n identity matrix

$$A = I_2, \qquad B = C^{-1} = \frac{p}{\mu_0 n (L_1 - L_2)} \begin{bmatrix} \frac{g_1}{L_{s1}} & -\frac{g_1 L_2}{L_{s1}} \\ -\frac{g_2}{L_{s2}} & \frac{g_2 L_1}{L_{s2}} \end{bmatrix} \tag{101}$$

substituting these equations into Eq. (100) gives the trivial solution

$$\mathbf{y}(k+1) = 0 \tag{102}$$

from this, it is observed that under ideal circumstances the control loop should always converge to the desired solution in one step. The effect of deviations from our ideal model is discussed in the next section.

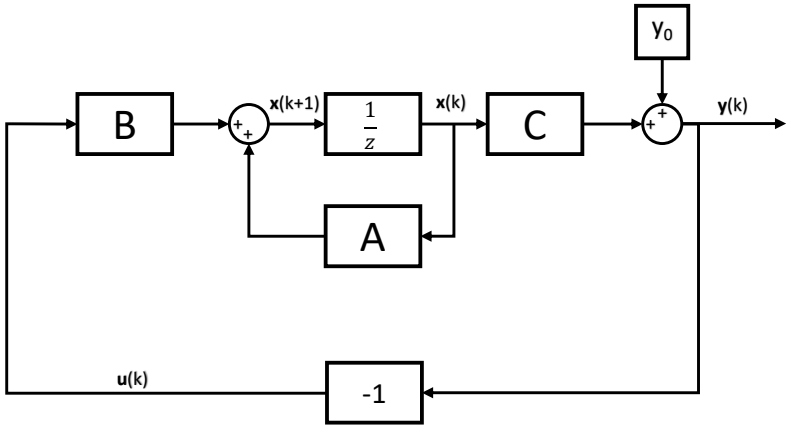

Figure 18: Control loop for the steering magnets.

4.2.2 Stability and Convergence Rate

In the previous section it was determined that for an ideal system, the system would converge in a single step, however since the plant parameters are not exactly known it will not be possible to choose our controller exactly as the inverse of the plant. Furthermore, a paraxial approximation was used in deriving the plant model. To analyze this problem a new matrix $\widetilde{B}$ is defined, which is not exactly equal to C^{-1}, writing down the closed-loop equation again gives

$$\mathbf{y}(k+1) = (I_2 - C\widetilde{B})\mathbf{y}(k) \tag{103}$$

After n iterations the value of $\mathbf{y}$ will be given by [7]

$$\mathbf{y}(n) = (I_2 - C\widetilde{B})^n\mathbf{y}(0) \tag{104}$$

this system will be stable if the eigenvalues λ_i of $(I_2 - C\widetilde{B})$ satisfy $|\lambda_i| \leq 1$ [8]. To estimate the magnitude of error that is allowed $\widetilde{B}$ is written as B multiplied by a constant value γ, which simplifies the matrices to

$$I_2 - \gamma CB = I_2 - \gamma CC^{-1} = (1-\gamma)I_2 \tag{105}$$

which has eigenvalues $\lambda_1 = \lambda_2 = 1 - \gamma$, therefore the system is stable if $0 \leq \gamma \leq 2$. This would mean that for instability of the system to occur, the estimate of the plant behaviour would have to be off by a factor 2, or be negative of the real plant. This margin far exceeds the deviations caused by measurement uncertainties or approximations, therefore the system is deemed stable. The stable behaviour of the system depends on the value of γ, for $0 < \gamma < 1$ the system will asymptotically go to

zero without oscillating, for $1 < \gamma < 2$ the system will go asymptotically to zero, but it will cross the zero position multiple times. These behaviours are demonstrated in Figure 19.

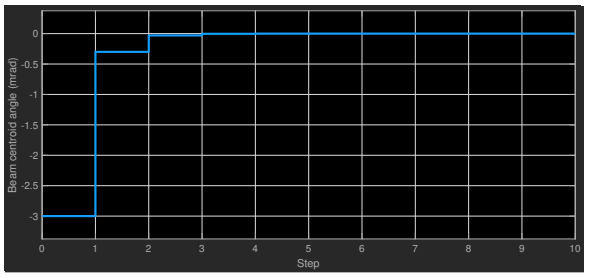

(a) Angle of the beam centroid versus the step number of the algorithm for γ=0.9

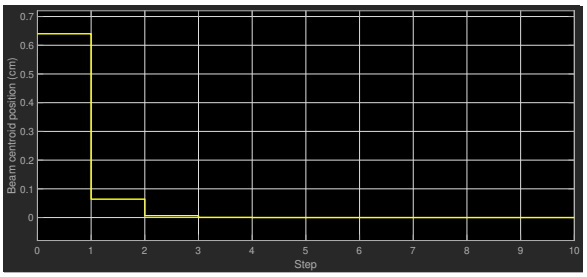

(b) Position of the beam centroid versus the step number of the algorithm for γ=0.9

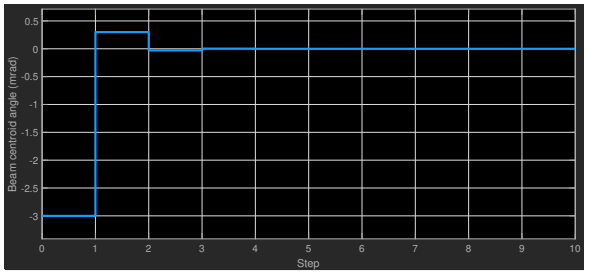

(c) Angle of the beam centroid versus the step number of the algorithm for γ=1.1

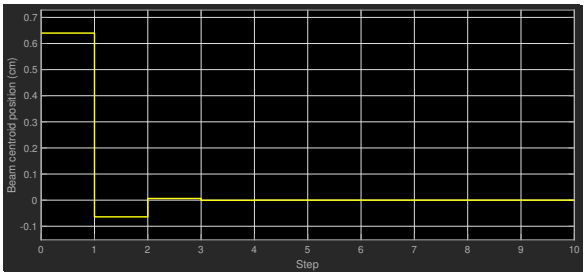

(d) Position of the beam centroid versus the step number of the algorithm for γ=1.1

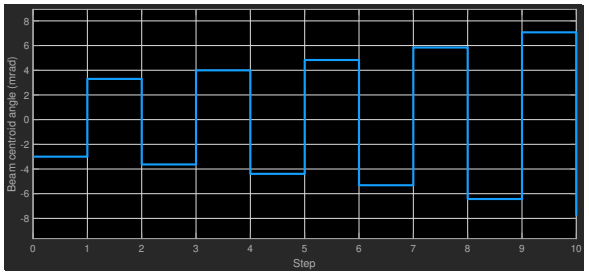

(e) Angle of the beam centroid versus the step number of the algorithm for γ=2.1

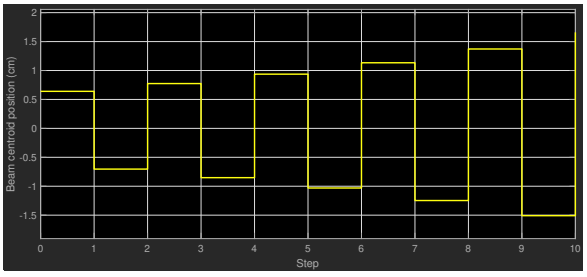

(f) Position of the beam centroid versus the step number of the algorithm for γ=2.1

Figure 19

4.2.3 Effect of Measurement Errors

One aspect that has not been considered yet is the possibility of positional misalignments of the magnets in the beamline. The equation describing a particle traveling through a misaligned quadrupole or dipole magnet is [9]

$$\boldsymbol{x}(\mathbf{1}) = R\boldsymbol{x}(\mathbf{0}) + F\boldsymbol{m} + G\boldsymbol{x}(\mathbf{0}) \tag{106}$$

where R is the transfer matrix of the magnet, F and G are matrices depending on the magnet properties and magnitude of misalignment, and $\boldsymbol{m}$ is the misalignment vector

$$\boldsymbol{m} = \begin{pmatrix} \delta x \\ \theta x \\ \delta y \\ \theta y \\ \delta z \\ \theta z \end{pmatrix} \tag{107}$$

where δx, δy, δz are the displacements of the magnet in the x, y, and z direction and θx, θy, and θz are the rotations about the x, y, and z axes respectively. All rotations are defined to be positive when rotating in the clockwise direction looking in the positive direction of the axis. Since the quadrupoles are used for measuring, a misalignment of them will add a fixed error in the measurement step, this can be seen in Figure 20, where the added error can, in general, be described by a matrix E and an added vector b, these both depend on the magnet settings and the magnitude of the misalignment. Using this the closed-loop solution of the system is

$$\mathbf{y}(k+1) = (CAC^{-1} - CBE)\mathbf{y}(k) - CB\mathbf{b} + (I - CAC^{-1})\mathbf{y_0} \tag{108}$$

Using the matrices given in Eq. (101), this simplifies to

$$\mathbf{y}(k+1) = (I - E)\mathbf{y}(k) - \mathbf{b} \tag{109}$$

which, assuming the system is stable, has the steady state solution,

$$\mathbf{y}_{steady} = -E^{-1}\mathbf{b} \tag{110}$$

which means that when misalignment is present in the system there will always be a steady-state error whose magnitude depends on the settings of the magnets and magnitude of the misalignment. Note that this steady-state error cannot be removed using an integrator because it is caused by an error in the measurements and not by the properties of the plant. The misalignment is also unknown so it is not possible to correct for it by correcting the error signal before it is fed into the controller. For a numerical example using values from the beamline see Section 5.2.

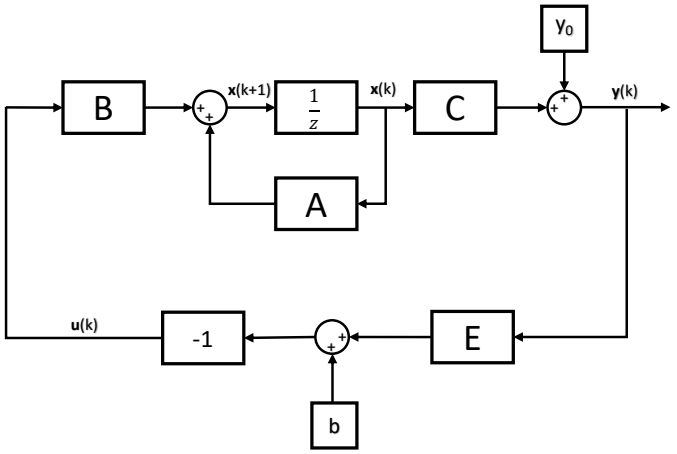

Figure 20: Discrete control loop with measurement error represented by the matrice E and vector b.

4.3 Control Loop bending Magnet

4.3.1 General Form

The goal of the bending magnet control system is to achieve zero beam centroid angle and position at the exit face of the bending magnet, which means that there are two controlled variables. There is only one tunable parameter, which is the current supplied to the magnet, which means that the system is overdetermined. For now, it will be assumed that the beam centroid angle and position are zero at the entrance face ($x_0 = x_0' = 0$), which makes the system solvable. Later on, solutions will be discussed for when this is not the case.

According to Eq. (93), under the assumptions that $x_0 = x_0' = 0$, x_1 and x_1' will be zero when $\rho = \rho_0$, which is the goal of the control loop. To reduce the sensitivity to misalignment errors of the beam profile monitors a least squares solution for calculating ρ is proposed, for a right bending magnet this yields

$$\rho = -\frac{(x_1 + 2\rho_0)(-1 + \cos\alpha_0) + x_1'\rho_0 \sin\alpha_0}{2 + x_1'^2 - 2\cos\alpha_0 - 2x_1' \sin\alpha_0} \tag{111}$$

where x_1 and x_1' are the beam centroid position and angle at the exit of the bending magnet, and can be obtained from the quadrupole variation method. The bending radius for a left bending magnet is calculated using

$$\rho_{\text{left}} = \frac{(x_1 - 2\rho_0)(-1 + \cos\alpha_0) + x_1'\rho_0 \sin\alpha_0}{2 + x_1'^2 - 2\cos\alpha_0 + 2x_1' \sin\alpha_0} \tag{112}$$

The control loop can be seen in Figure 21. The following state-space description is used,

$$\begin{aligned} \mathrm{x}(k+1) &= A\mathrm{x}(k) + B\mathrm{u}(k) \\ \mathrm{y}(k) &= C\mathrm{x}(k) + D\mathrm{u}(k) \end{aligned} \tag{113}$$

where the output vector $y(k)$ is $\frac{1}{\rho}$ and the state vector is the current of the magnet I, from Eqs. (5), (88) and (93) it can be seen that the matrices C and D are equal to

$$C = \frac{\mu_0 n}{pg}, \qquad D = 0 \tag{114}$$

From block diagram algebra the following closed loop solution can be found for y, where $r = \frac{1}{\rho_0}$ is the reference value

$$y(k+1) = C(AC^{-1} - B)y(k) + CBr \tag{115}$$

for the desired solution, where y tracks the reference value r the following gains A and B are proposed

$$A = 1, \qquad B = C^{-1} = \frac{pg}{\mu_0 n} \tag{116}$$

which simplifies the closed-loop solution to

$$y(k+1) = r \tag{117}$$

it is observed that under ideal conditions the output converges to the reference value within one step.

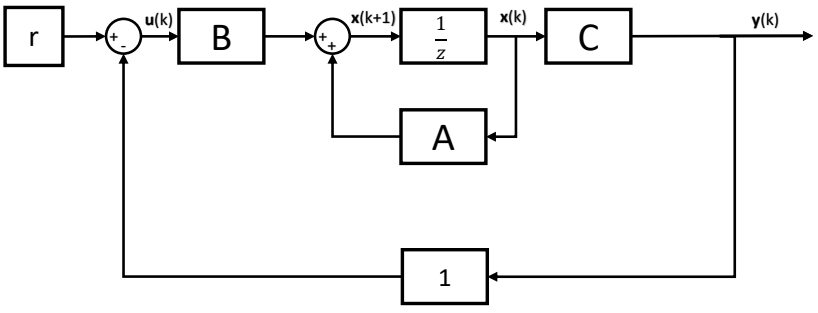

Figure 21: Control loop for a bending magnet, r is the reference value, C is a gain determined by the plant, the gains A and B can be adjusted for optimal control.

4.3.2 Stability and Convergence rate

Similarly to the steering magnet control, the plant model will not be exactly equal to the real system. To check the stability in this case a matrix $\widetilde{B}$ is defined, which is approximately equal to $B = C^{-1}$, writing out the closed-loop solution again gives

$$y(k+1) = (1 - C\widetilde{B})y(k) + C\widetilde{B}r \tag{118}$$

which, assuming the system is stable has the following steady-state solution [7]

$$y_{steady} = \frac{C\widetilde{B}}{1 - (1 - C\widetilde{B})}r = r \tag{119}$$

so as long as the choice of B does not cause instability, the output vector will converge asymptotically to the reference value r. The speed of convergence depends on how well $\widetilde{B}$ approximates C^{-1}. Similarly for the steering magnets, $\widetilde{B}$ can be written as B multiplied by a constant gain γ, such that $\widetilde{B} = \gamma B$, substituting this into the closed-loop solution gives

$$y(k+1) = (1 - \gamma CB)y(k) + \gamma CBr = (1 - \gamma)y(k) + \gamma r \tag{120}$$

after n iterations the value of y is equal to

$$y(n) = (1 - \gamma)^n(y_0 - r) + r \tag{121}$$

Calculating the rate of convergence gives

$$\lim_{n\to\infty} \frac{y(n+1) - r}{y(n) - r} = \lim_{n\to\infty} \frac{(1-\gamma)^{n+1}(y_0 - r)}{(1-\gamma)^n(y_0 - r)} = 1 - \gamma \tag{122}$$

Similarly to the steering magnet control loop, the convergence rate is determined by γ.

4.3.3 Effect of Measurement Errors

Similar to Section 4.2.3 measurement errors can occur by the misalignment of the quadrupole magnets used in the quadrupole variation method. Again these effects can be simulated by a gain E and an added scalar b as indicated in Figure 22. The closed-loop solution, assuming A=1 and B=C^{-1} is given by

$$y(k+1) = (1 - E)y(k) + (r - b) \tag{123}$$

The steady-state solution, assuming the system is stable is given by

$$y_{steady} = \frac{r - b}{E} \tag{124}$$

again it is observed that the effect of misaligned quadrupoles causes a steady-state error, this error can also not be corrected by using an integrator. For a numerical example using values from the beamline see Section 5.2.

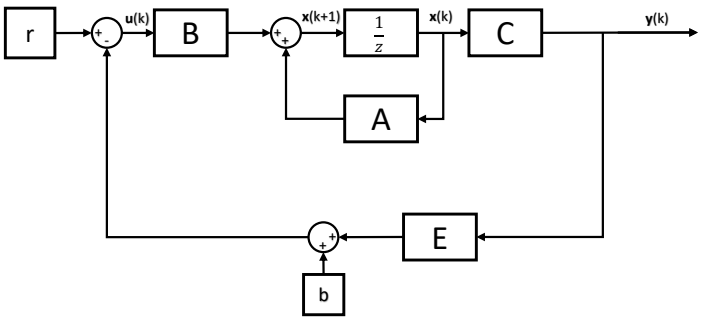

Figure 22: Control loop for a bending magnet, r is the reference value, C is a gain determined by the plant, the gains A and B can be adjusted for optimal control. The effect of positional misalignment of the quadrupoles used for measuring is simulated using the gain E and the scalar b.

5 Simulation Results and Discussion

5.1 Sensitivity Analysis of Quadrupole Variation Method

In the methods that are developed so far it is assumed that there is no error or uncertainty present in the system. However in a real system there will always be some noise present due to natural fluctuations of the involved parameters, further uncertainty is added due to the finite precision of measurements of the required parameters. In this section the effects of these uncertainties on the behaviour of the quadrupole variation method is investigated.

In general for a function $y = f(x_1, x_2, \ldots, x_3)$ the standard deviation of y can be estimated using [10]

$$s_y = \sqrt{\left(\frac{\partial y}{\partial x_1}\right)^2 s_{x_1}^2 + \left(\frac{\partial y}{\partial x_2}\right)^2 s_{x_2}^2 + \ldots + \left(\frac{\partial y}{\partial x_1}\right)\left(\frac{\partial y}{\partial x_2}\right) s_{x_1 x_2}^2 + \ldots} \tag{125}$$

where s_y is the standard deviation of y, s_{x_i} is the standard deviation of x_i and $s_{x_i x_j}$ is the covariance between x_i and x_j. This equation is an approximation that holds when the standard deviations are sufficiently small such that the first order is dominant in the expansion of f around $x_1, x_2, \ldots, x_n$. The partial derivative terms inside the square root are sometimes also called the sensitivity coefficients since they indicate how sensitive s_y is to the standard deviations of the variables x_i

The equations describing x_0 and x_0' as obtained from the quadrupole variation method are

$$
\begin{aligned}
x_0 &= \frac{C_{21}x_2 - C_{22}x_1}{C_{12}C_{21} - C_{11}C_{22}} \\
x_0' &= \frac{C_{12}x_1 - C_{11}x_2}{C_{12}C_{21} - C_{11}C_{22}}
\end{aligned}
\tag{126}
$$

where the following notation was used

$$
C_{1j} = [R_{11}]_j, \qquad C_{2j} = [R_{12}]_j \tag{127}
$$

where C_{j1}, C_{j2} are the elements of total transfer matrix R for the jth measurement. Using this notation the sensitivity coefficients for the non-covariance terms become,

$$
\begin{aligned}
\left(\frac{\partial x_0}{\partial x_1}\right)^2 &= \frac{C_{22}^2}{(C_{12}C_{21} - C_{11}C_{22})^2}, \quad \left(\frac{\partial x_0}{\partial x_2}\right)^2 = \frac{C_{21}^2}{(C_{12}C_{21} - C_{11}C_{22})^2} \\
\left(\frac{\partial x_0}{\partial C_{11}}\right)^2 &= \frac{C_{22}^2(C_{22}x_1 - C_{21}x_2)^2}{(C_{12}C_{21} - C_{11}C_{22})^4}, \quad \left(\frac{\partial x_0}{\partial C_{12}}\right)^2 = \frac{C_{12}^2(C_{22}x_1 - C_{21}x_2)^2}{(C_{12}C_{21} - C_{11}C_{22})^4} \\
\left(\frac{\partial x_0}{\partial C_{22}}\right)^2 &= \left(\frac{x_1}{C_{12}C_{21} - C_{11}C_{22}} + \frac{C_{11}(C_{22}x_1 - C_{21}x_2)^2}{(C_{12}C_{21} - C_{11}C_{22})^2}\right)^2 \\
\left(\frac{\partial x_0}{\partial C_{21}}\right)^2 &= \left(\frac{x_2}{C_{12}C_{21} - C_{11}C_{22}} + \frac{C_{12}(C_{22}x_1 - C_{21}x_2)^2}{(C_{12}C_{21} - C_{11}C_{22})^2}\right)^2
\end{aligned}
\tag{128}
$$

it is observed that every denominator term in these expressions contains some power of $C_{12}C_{21} - C_{11}C_{22}$, if this term gets small the sensitivity coefficients will blow up. To give a numerical example a simple section of beamline is considered where only one quadrupole is used to adjust the bending magnet B1, which is shown in Figure 23.

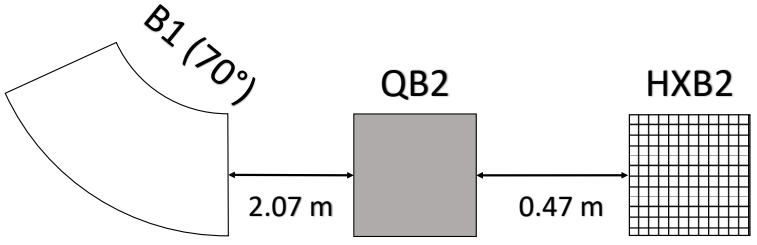

Figure 23: Section of the beamline that is used to tune B1

The only parameter that can be changed in this system is the magnetic field gradient of the quadrupole QB2.In this example this is done by giving a base value G_0 and a fractional change x such that the

two magnetic field values used in the measurement are given by $G_0(1-x)$ and $G_0(1+x)$. The constant variables in this problem are given in Table 2

Table 2: Numerical values used in testing sensitivity of quadrupole variation method.

Element	Item	Value	Unit
Beam properties at exit face B1	x_0	0.1	cm
	x_0'	1	mrad
	p	0.6144	GeV c^{-1}
Drift spaces	B1→QB2	2.07	m
	QB2 →HXB2	0.47	m
Quadrupole QB2	Effective Length	0.3	m
Bending magnet B1	Effective Length	2.88307	m
	Bending angle	70	°

Using these values the sensitivity values are plotted against the fractional change in magnetic field strength for different base magnetic field values, this can be seen in Figure 24.

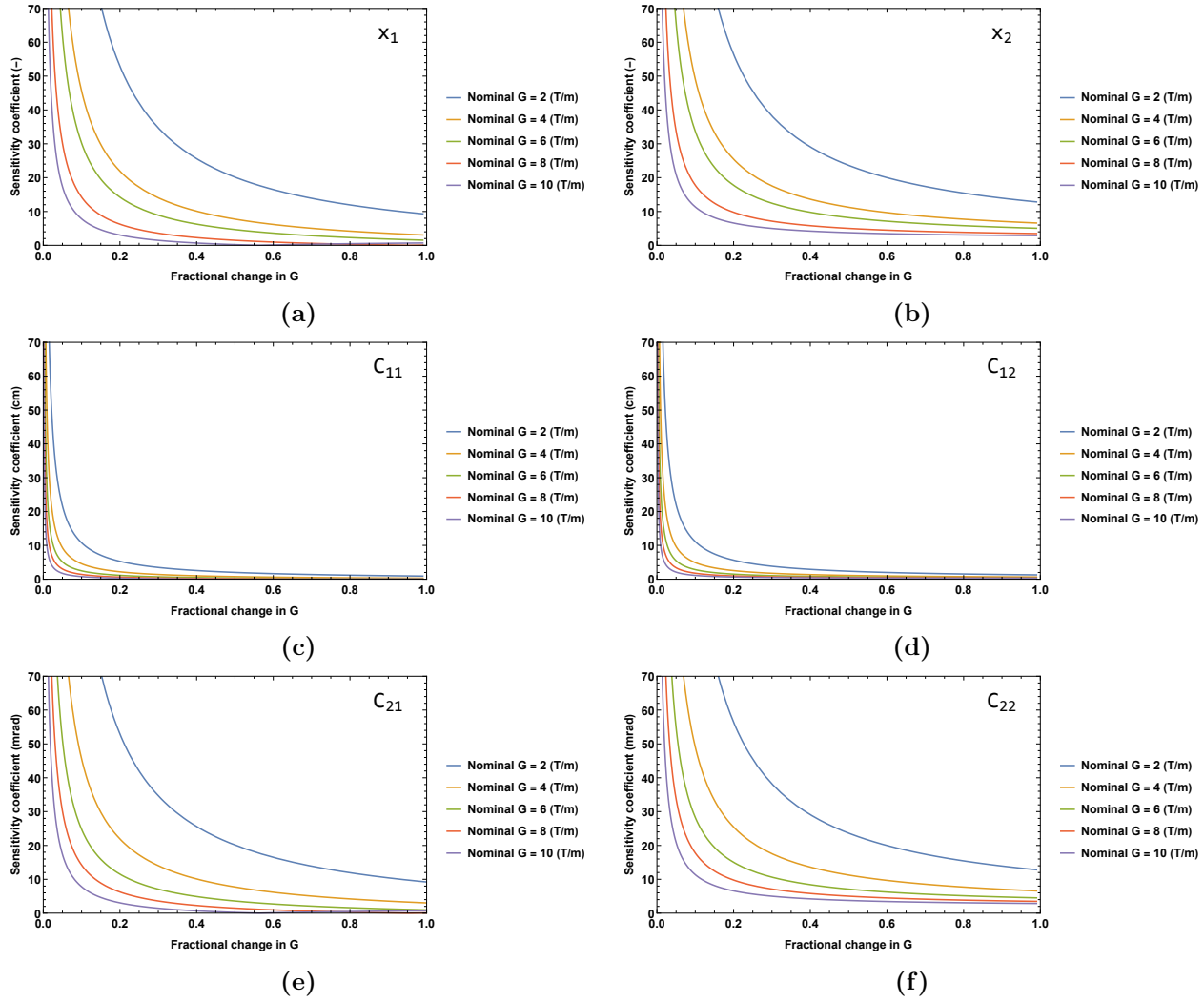

Figure 24: Sensitivity coefficients of the respective parameters describing x_0, the denominator of the sensitivity coefficient is indicated in the top right of each graph.

The same steps are repeated for the sensitivity analysis of x_0'

$$
\begin{aligned}
\left(\frac{\partial x_0'}{\partial x_1}\right)^2 &= \frac{C_{12}^2}{(C_{12}C_{21}-C_{11}C_{22})^2}, \quad \left(\frac{\partial x_0'}{\partial x_2}\right)^2 = \frac{C_{11}^2}{(C_{12}C_{21}-C_{11}C_{22})^2} \\
\left(\frac{\partial x_0'}{\partial C_{21}}\right)^2 &= \frac{C_{12}^2(C_{12}x_1-C_{11}x_2)^2}{(C_{12}C_{21}-C_{11}C_{22})^4}, \quad \left(\frac{\partial x_0'}{\partial C_{22}}\right)^2 = \frac{C_{11}^2(C_{12}x_1-C_{11}x_2)^2}{(C_{12}C_{21}-C_{11}C_{22})^4} \\
\left(\frac{\partial x_0'}{\partial C_{12}}\right)^2 &= \left(\frac{x_1}{C_{12}C_{21}-C_{11}C_{22}} + \frac{C_{21}(C_{12}x_1-C_{11}x_2)^2}{(C_{12}C_{21}-C_{11}C_{22})^2}\right)^2 \\
\left(\frac{\partial x_0'}{\partial C_{11}}\right)^2 &= \left(\frac{x_2}{C_{12}C_{21}-C_{11}C_{22}} - \frac{C_{22}(C_{12}x_1-C_{11}x_2)^2}{(C_{12}C_{21}-C_{11}C_{22})^2}\right)^2
\end{aligned}
\tag{129}
$$

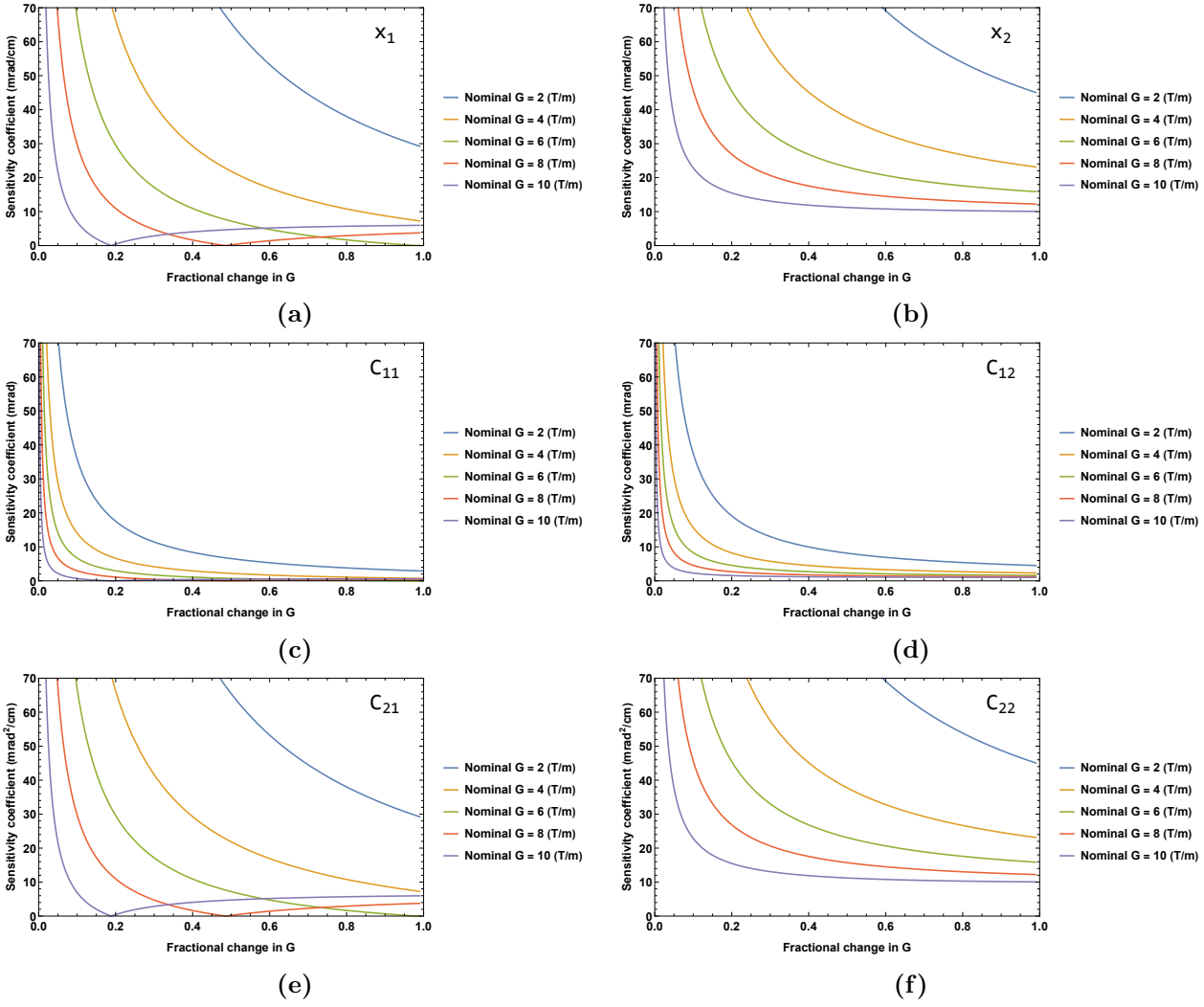

Figure 25: Sensitivity coefficients of the respective parameters describing x_0', the denominator of the sensitivity coefficient is indicated in the top right of each graph.

In the real system the sensitivity of x_0 and x_0' to measurement errors the variables involved in the quadrupole variation method should be minimized, according to the results presented here this means that the magnetic field gradient in the quadrupoles should have to varied as much as possible. However, when changing the magnetic field gradient away from the optimal value the beam size is increased. The beamsize should not exceed the dimensions of the transport pipes, since then beam intensity will be lost to the walls. Furthermore, a larger beam size will lead to a larger statistical error in the determination of the beam centroid paramters. Therefore an optimum value will have to be found, this value will be different for different sections of the beamline.

5.2 Effect of Misalignment of Magnet Elements on Algorithms

When a magnet element is misaligned it will introduce a systematic error into the system. This will affect the convergence properties of the algorithm. These effects will first be tested on a small scale, starting with the algorithm which controls the steering magnets. The section of the beamline which is used for this includes steering magnets $S_{x,y}$ and S_x as well as the quadrupole triplet QX1a, QX1b and QX1c, the measurements for the quadrupole variation method are made using beam monitor HXB1. The misalignments are initially only applied to the quadrupole triplet magnets. The maximum misalignment for a single magnet is estimated to be approximately 0.3 mm. Depending on how these misalignments are distributed throughout the system the size of the beam centroid displacement varies. First a worst case scenario is assumed where the effect of the misalignment is largest. The relevant parameters are given in Table 3, for the quadrupole variation method quadrupoles QX1a and QX1c where simultaneously varied by $\pm 10\%$ of their original values for a total of two measurements.

Table 3: Numerical values used in testing the effect of misalignment of magnet elements on the developed algorithms, the drift space distances are measured from the exit of one element to the face of the next, negative magnetic field gradients indicate a defocusing quadrupole.

Element	Item	Value	Unit
Beam properties at entrance face QX01	x_0	0.2	cm
	x_0'	2	mrad
	p	0.6144	GeV c^{-1}
Drift spaces	$S_{x,y}\rightarrow$ QX02	0.8	m
	QX02 $\rightarrow S_x$	0.174	m
	$S_x \rightarrow$HXX1	0.6440	m
	HXX1 $\rightarrow$QX1a	0.174	m
	QX1a $\rightarrow$QX1b	0.3	m
	QX1b $\rightarrow$QX1c	0.3	m
	QX1c $\rightarrow$HXB1	1.227	m
Quadrupole QX01	Effective Length	0.2	m
	Magnetic field gradient	17.46	T m^{-1}
Quadrupole QX02	Effective Length	0.2	m
	Magnetic field gradient	-9.37	T m^{-1}
Steering magnet S_x	Effective Length	0.2	m
Quadrupole QX1a	Effective Length	0.3	m
	Magnetic field gradient	10.7	T m^{-1}
	misalignment (x-direction)	0.3	mm
Quadrupole QX1b	Effective Length	0.4	m
	Magnetic field gradient	-9.96	T m^{-1}
	misalignment (x-direction)	-0.3	mm
Quadrupole QX1c	Effective Length	0.4	m
	Magnetic field gradient	10.7	T m^{-1}
	misalignment (x-direction)	0.3	mm

The results from using the steering algorithm on this system can be seen in Figure 26. We see that after one iteration the algorithm converges to a steady state error, of 0.14 cm for the position and -0.41 mrad for the angle. This is because the measured values from the quadrupole variation algorithm are different than the actual values of the system, due to misalignment of the magnets. This systematic error in the measurement also causes a systematic error in the correction using the steering magnets.

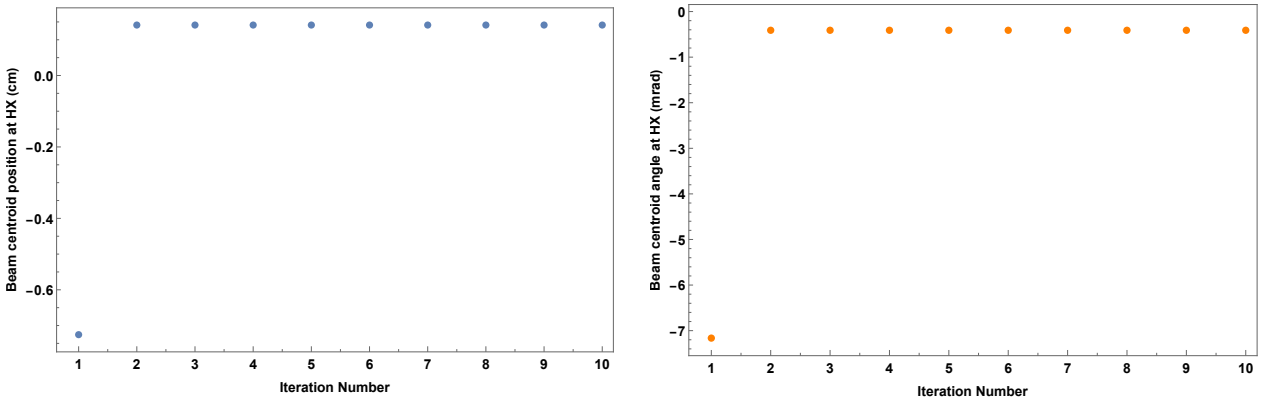

(a) **(b)**

Figure 26: Convergence of a) position and b) angle of the beam centroid when using the steering magnet algorithm if misalignment is present

The algorithm for the bending magnet is also tested using the same geometry as described in Figure 23 and Table 2. Measurement using the quadrupole variation method were made using QB2 with a base magnetic field gradient of $5.31\,\mathrm{T\,m^{-1}}$ and a variation of $\pm 10\%$. The beam centroid at the entrance was assumed to be aligned and QB2 was misaligned by 0.3 mm in the x-direction. Initially a the bending radius of the bending magnet was set to 1.01 times the designed value. The convergence plots can be seen in Figure 27. Again the algorithm converges in one iteration, the steady state errors for position and angle are 0.08 mm 0.05 mrad respectively. These error are much smaller than for the steering magnets since there is only one misaligned magnet which is used for measuring.

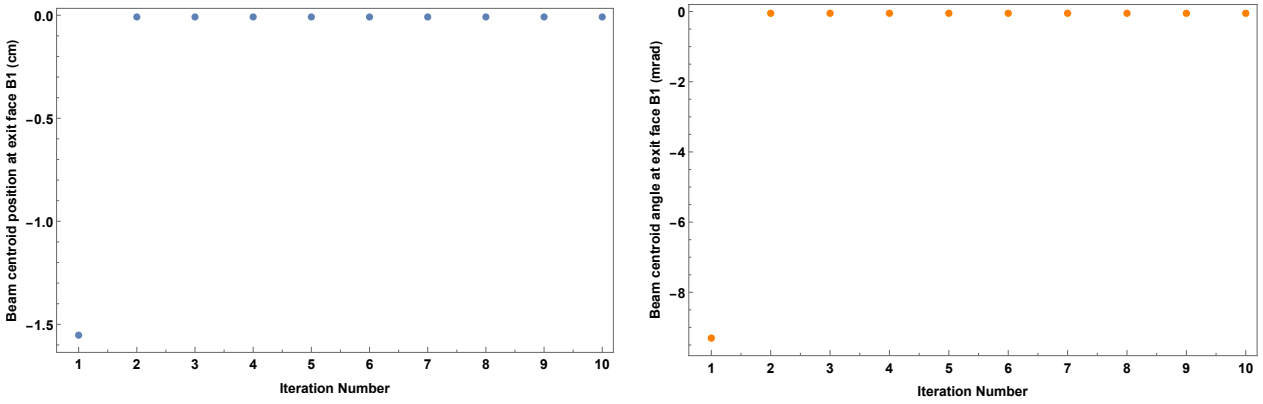

(a) **(b)**

Figure 27: Convergence of a) position and b) angle of the beam centroid when using the bending magnet algorithm on B1 if misalignment is present

5.3 Measuring the Magnet Misalignment

In this section, it will be investigated whether it is possible to measure the misalignment of a magnet using the beam profile monitors. Two methods are proposed, in the first method, the misalignment is measured for a single quadrupole at a time, while in the second method the misalignments of multiple magnets can be measured simultaneously. An analysis on the accuracy of both methods is also done.

5.3.1 Measuring the Misalignment of a Single Magnet

In this method, two beam profile monitors are used, which need to be located on either side of the quadrupole magnet whose misalignment is being measured. In the first step, all of the quadrupoles in between the two beam profile monitors are turned off, this allows the beam centroid position and angle at the first beam monitors to be calculated.

$$x_0' = \frac{x_1 - x_0}{L_{tot}} \tag{130}$$

where x_0 and x_0' are the beam centroid position and angle measured at the first beam monitor, x_1 is the beam centroid position measured at the second beam monitor, and L_{tot} is the distance between the monitors. Afterwards, the quadrupole is turned on. The effect of a misaligned quadrupole on the beam is described by [9]

$$\boldsymbol{x}(1) = R\boldsymbol{x}(0) + F\boldsymbol{m} + G\boldsymbol{x}(0) \tag{131}$$

where $\boldsymbol{x}(0)$ and $\boldsymbol{x}(1)$ are the particle vectors at the entrance and exit of the quadrupole magnet, R is the transfer matrix of the quadrupole, $\boldsymbol{m}$ is the misalignment vector

$$\boldsymbol{m} = \begin{pmatrix} \delta x \\ \theta x \\ \delta y \\ \theta y \\ \delta z \\ \theta z \end{pmatrix} \tag{132}$$

where δx, δy, δz are the displacements of the magnet in the x, y, and z direction and θx, θy, and θz are the rotations about the x, y, and z axes respectively. All rotations are defined to be positive when rotating in the clockwise direction, looking in the positive direction of the axis. The origin of the rotation axes is the reference trajectory position at the entrance of the magnet. The matrices F and G are given by

$$\begin{aligned} F &= A_1 - RA_0 \\ G &= RB_0 - B_1R \end{aligned} \tag{133}$$

where R is again the transfer matrix of the quadrupole and the matrices A_0, A_1, B_0, and B_1 are given by

$$A_0 = \begin{pmatrix} 1 & 0 & 0 & 0 & 0 & 0 \\ 0 & 0 & 0 & 1 & 0 & 0 \\ 0 & 0 & 1 & 0 & 0 & 0 \\ 0 & -1 & 0 & 0 & 0 & 0 \\ 0 & 0 & 0 & 0 & 1 & 0 \\ 0 & 0 & 0 & 0 & 0 & 0 \end{pmatrix}, \qquad A_1 = \begin{pmatrix} 1 & 0 & 0 & L & 0 & 0 \\ 0 & 0 & 0 & 1 & 0 & 0 \\ 0 & -L & 1 & 0 & 0 & 0 \\ 0 & -1 & 0 & 0 & 0 & 0 \\ 0 & 0 & 0 & 0 & 1 & 0 \\ 0 & 0 & 0 & 0 & 0 & 0 \end{pmatrix}$$
$$B_0 = B_1 = \begin{pmatrix} 0 & \delta z & \theta z & 0 & 0 & 0 \\ 0 & 0 & 0 & \theta z & 0 & 0 \\ -\theta z & 0 & 0 & \delta z & 0 & 0 \\ 0 & -\theta z & 0 & 0 & 0 & 0 \\ 0 & 0 & 0 & 0 & 0 & 0 \\ 0 & 0 & 0 & 0 & 0 & 0 \end{pmatrix}, \tag{134}$$

using Eq. (131) a particle traveling through a drift space, a quadrupole, and another drift space can be described as

$$\boldsymbol{x}(1) = R_{d2} R_q R_{d1} \boldsymbol{x}(0) + R_{d2} F \boldsymbol{m} + R_{d2} G R_{d1} \boldsymbol{x}(0) \tag{135}$$

where R_{d1} and R_{d2} are the transfer matrices of the first and second drift space and R_q is the transfer matrix of the quadrupole.

The misalignment vector has 6 components, to limit the number of measurements that have to be made only the components which affect the beam significantly should be considered. From Eq. (131) it can be seen that δz and θz only appear as cross terms with components from the $\boldsymbol{x}$ vector, since both quantities are small, their product can be neglected. The rotational misalignments θx and θy are defined with respect to the face of the magnet. This rotation around the face can be split into a rotation around the center and a displacement. Rotation around the center of the magnet does not affect the beam significantly since the average distance from the axis remains approximately the same. Therefore only the displacement components δx and δy remain. The x and y coordinates are still decoupled, therefore they can be determined separately, the equations for x are written down here.

Using the above assumptions the displacement vector components simplify to $\theta x = \theta y = \delta z = \theta z = 0$. Using this, the first component from Eq. (135) for a quadrupole which focuses in x can be written in terms of the individual matrix elements as

$$x_m = \left(R_q^{11} + R_{d2}^{12} R_q^{21}\right) x_0 + \left(R_q^{12} + R_{d1}^{12}\left(R_q^{11} + R_{d2}^{12} R_q^{21}\right) + R_{d2}^{12} R_q^{22}\right) x_0' + \left(F^{11} + F^{21} R_{d2}^{12}\right) \delta x \tag{136}$$

where the matrix indices are given in superscript, x_m is the beam centroid position measured at the second beam profile monitor when the quadrupole is turned on, and x_0 and x_0' are the beam centroid position and angle at the first beam profile monitor respectively.

This equation can be solved for the unknown variable δx,

$$\delta x = \frac{-(R_q^{11} + R_{d2}^{12}R_q^{21})x_0 - (R_q^{12} + R_{d1}^{12}(R_q^{11} + R_{d2}^{12}R_q^{21}) + R_{d2}^{12}R_q^{22})x_0' + x_m}{F^{11} + F^{21}R_{d2}^{12}} \tag{137}$$

the value for x_0' can be found using Eq. (130), x_0 and x_m can be measured, and the other variables are known, which means that δx can be calculated.

To estimate the precision of this measurement a sensitivity analysis is performed via propagation of error using partial derivatives. The analytical derivatives of Eq. (137) are too complex to analyze directly, therefore numerical values are substituted in, which can be found in Table 5. The numerical values correspond to the first quadrupole triplet in the beamline consisting of quadrupoles QX1a, QX1b, and QX1c. The imaging properties under in standard operating conditions of this triplet can be seen in Figure 28.

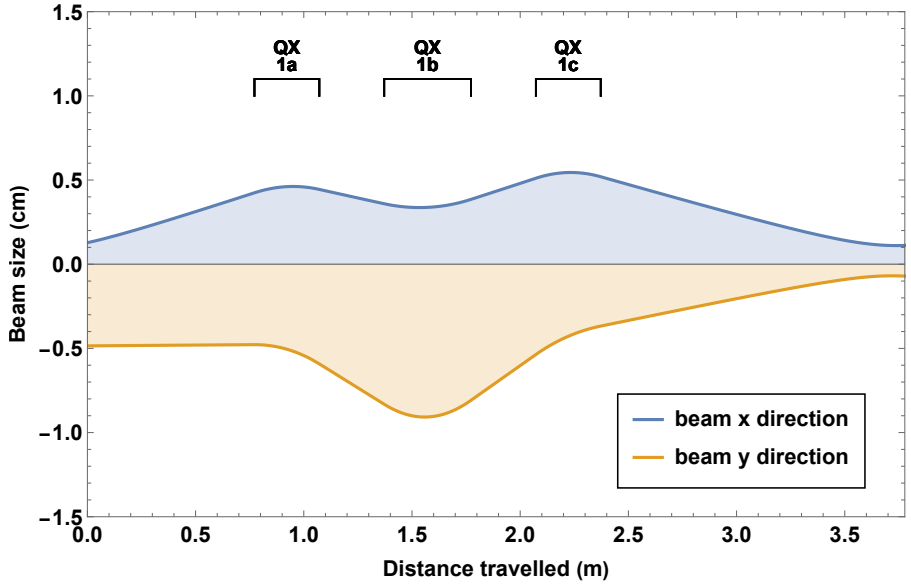

Figure 28: Imaging properties of the quadrupole triplet QX1a, QX1b, and QX1c under standard operating conditions, the first and last quadrupoles focus in the x-direction, while the center quadrupole focuses in the y-direction. The location and size of the quadrupoles is indicated with an open bracket.

The sensitivity coefficients are defined as

$$\frac{\partial Y}{\partial X} \tag{138}$$

where Y is the output variable and X is an input value. The sensitivity coefficients corresponding to the magnet displacement measurements can be found in Table 4. It can be seen that all the sensitivity coefficients are relatively small. It is estimated that the displacements of the magnets are in the order of 0.3 mm, using the calculated sensitivity coefficients, estimated errors, and Eq. (125) it can be seen that using this method the precision of the beam profile monitors needs to be of the same order to measure the displacements accurately.

Table 4: Sensitivity coefficients of the displacements of quadrupoles QX1a, QX1b and QX1c, denoted by δx_1. δx_2 and δx_3 respectively. The predicted error indicates the estimate of the measurement uncertainty of the respective input variables.

		Magnet displacement (m)				
		δx_1	δx_2	δx_3		
Input variable	Unit	Sensitivity Coefficient (m/Unit)			Predicted error	Unit
x_0	m	0.798	0.605	0.411	0.5	mm
x_1	m	-0.296	-0.130	0.056	0.5	mm
x_m	m	0.498	0.526	0.533	0.5	mm
L_{d1}	m	5.95×10^{-4}	4.51×10^{-4}	3.06×10^{-4}	2.0	mm
L_{d2}	m	3.00×10^{-4}	5.66×10^{-4}	1.14×10^{-3}	2.0	mm
L_q	m	4.16×10^{-3}	4.33×10^{-3}	6.98×10^{-3}	4.0	mm
k	m^{-2}	4.46×10^{-4}	6.54×10^{-4}	4.15×10^{-4}	0.075	m^{-2}

Table 5: Numerical values used in determining the sensitivity of the method used to determine the alignment error of a single quadrupole. The beam properties at HXB1 are different for measuring the misalignment of the different quadrupoles, these different measurements are indicated by writing δx_1, δx_2, and δx_3 in parenthesis for the measurements corresponding to quadrupole QX1a, QX1b, and QX1c respectively.

Element	Item	Value	Unit
Beam properties at HXX1	p	0.6144	GeV c^{-1}
	x_0	1.0	mm
Beam properties at HXB1	x_1	3.5	mm
	x_m (δx_1)	1.1	mm
	x_m (δx_2)	1.8	mm
	x_m (δx_3)	-0.58	mm
	$\sqrt{\sigma_x}$ (δx_1)	5.7	mm
	$\sqrt{\sigma_y}$ (δx_1)	15	mm
	$\sqrt{\sigma_x}$ (δx_2)	3.7	mm
	$\sqrt{\sigma_y}$ (δx_2)	15	mm
	$\sqrt{\sigma_x}$ (δx_3)	2.7	mm
	$\sqrt{\sigma_y}$ (δx_3)	15	mm
Drift spaces	HXX1→QX1a	0.526	m
	HXX1→QX1b	1.126	m
	HXX1→QX1c	1.826	m
	QX1a →HXB1	2.527	m
	QX1b →HXB1	1.827	m
	QX1c →HXB1	1.227	m
Quadrupole QX1a	Effective Length	0.3	m
	Field gradient	5.3	T m^{-1}
	misalignment (x-direction)	0.3	mm
Quadrupole QX1b	Effective Length	0.4	m
	Field gradient	5.1	T m^{-1}
	misalignment (x-direction)	0.3	mm
Quadrupole QX1c	Effective Length	0.3	m
	Field gradient	10	T m^{-1}
	misalignment (x-direction)	0.3	mm

5.3.2 Measuring the Misalignment of Multiple Magnets

In this section, it is explained how the misalignment of multiple quadrupole magnets can be measured simultaneously. Similar to the previous section only the displacements of the magnets will be considered since they have the largest effect on the beam centroid. Using these assumptions it will be

possible to write down a system of multiple quadrupoles and drift spaces into equations that are linear in the misalignment parameters and the initial beam conditions. This system can be easily solved using an inverse matrix operation to solve for these unknown parameters.

The assumption that $\delta z = \theta z = 0$ is important to keep the linearity of the system. This can be demonstrated by setting up a simple system consisting out of two drift spaces with a misaligned quadrupole in between. The full expression becomes

$$\boldsymbol{x}(1) = \underbrace{R_{d2}R_qR_{d1}}_{M}\boldsymbol{x}(0) + \underbrace{R_{d2}F}_{N}\boldsymbol{m} + \underbrace{R_{d2}GR_{d1}}_{O}\boldsymbol{x}(0) \tag{139}$$

The matrices A and B do not depend on any of the misalignments or on the $x(0)$ vector, however the matrix O, since it includes G, is a function of δz and θz, which means that it adds cross terms of the misalignment vector and the $\boldsymbol{x}(0)$ vector to the equation. By setting $\delta z = \theta z = 0$, the matrix G becomes zero and the cross-terms disappear, preserving the linearity of the system. For the case when $\delta z = \theta z = 0$, it is possible to expand the system of $n+1$ drift spaces and n quadrupoles to

$$\begin{aligned}\boldsymbol{x}(1) = Rd_{n+1}(Rq_nRd_nRq_{n-1}Rd_{n-1}\dots Rq_1Rd_1)\boldsymbol{x}(0)& \\ + Rd_{n+1}\sum_{i=1}^{n} Rq_nRd_nRq_{n-1}Rd_{n-1}\dots Rq_{i+1}Rd_{i+1}F_i\boldsymbol{m}_i&\end{aligned} \tag{140}$$

where Rd_i and Rq_i are the transfer matrices corresponding to the ith drift space and ith quadrupole in the system respectively, and m_i is the misalignment vector corresponding the ith quadrupole. From this equation it can easily be seen that the system is linear in terms of the misalignment parameters and the initial beam conditions. To calculate the quadrupole displacements it is possible to take the first component of Eq. (140) and set up a linear system of equations, this is demonstrated for a system of four drift spaces and three quadrupoles, as also found in the beamline

$$\boldsymbol{x}(1) = \underbrace{R_{d4}R_{q3}R_{d3}R_{q2}R_{d2}R_{q1}R_{d1}}_{A}\boldsymbol{x}(0) + \underbrace{R_{d4}R_{q3}R_{d3}R_{q2}R_{d2}F_1}_{B}\boldsymbol{m}_1 + \underbrace{R_{d4}R_{q3}R_{d3}F_2}_{C}\boldsymbol{m}_2 + \underbrace{R_{d4}F_3}_{D}\boldsymbol{m}_3 \tag{141}$$

where the matrices A B C and D are defined to simplify the system. For this system there are 5 unknowns, which are the three magnet displacements and the initial beam centroid position and angle, this also means that at minimum 5 measurements need to be made. Writing down the first component of Eq. (141) in matrix form for 5 measurements gives

$$\begin{pmatrix} A^1_{11} & A^1_{12} & B^1_{11} & C^1_{11} & D^1_{11} \\ A^2_{11} & A^2_{12} & B^2_{11} & C^2_{11} & D^2_{11} \\ A^3_{11} & A^3_{12} & B^3_{11} & C^3_{11} & D^3_{11} \\ A^4_{11} & A^4_{12} & B^4_{11} & C^4_{11} & D^4_{11} \\ A^5_{11} & A^5_{12} & B^5_{11} & C^5_{11} & D^5_{11} \end{pmatrix} \begin{pmatrix} x_0 \\ x'_0 \\ \delta x_1 \\ \delta x_2 \\ \delta x_3 \end{pmatrix} = \begin{pmatrix} x_{m1} \\ x_{m2} \\ x_{m3} \\ x_{m4} \\ x_{m5} \end{pmatrix} \tag{142}$$

where x_{mi} is the ith measurement taken from the beam profile monitor at the end of the last drift space, the superscripts of the matrix elements indicate different values corresponding to the different quadrupoles gradients used during the measurements. Next, it will be determined how sensitive this method is to errors, for now only errors from the measurements are considered. The sensitivity coefficients can be seen in Table 6, these values were minimized with respect to the magnetic field gradients of the quadrupoles using the constraint that the magnetic field values are between $-15\,\mathrm{T\,m^{-1}}$ and $15\,\mathrm{T\,m^{-1}}$ and that the maximum beam size at the second beam profile monitor is 1.5 cm in both the x and y direction, the beam size is defined as 2σ, where σ is the standard deviation of the Gaussian beam profile. The simulated annealing algorithm was used for minimization [1], the magnetic field gradients resulting from this optimization can be found in Table 7. The geometry of the system is the same as given in Table 5.

The obtained sensitivity values in Table 6 are significantly larger than the values found in Table 4. The sensitivity values indicate how much the uncertainty of the δx_i variables increases with the uncertainty of the measurements beam centroid position x_{mi}. The norm in Table 6, when multiplied with the measurement uncertainty of a beam profile monitor, gives the minimum uncertainty of the measured δx_i values. The calculated uncertainty of δx_i will increase even further if the sensitivity coefficients of the magnetic field gradients and drift and quadruple lengths are added. When looking at the norm of the sensitivity coefficients in Table 6, the accuracy of the beam monitors needs to be a at least a factor 20-40 times better than the alignment errors in order to be able to measure the alignment errors. Since the alignment errors are expected to be around 0.3 mm the required beam monitor accuracy must be at minimum 7.5 µm-15 µm which is not realistic.

Table 6: Sensitivity values, the norm is calculated as $\sqrt{\sum_{i=1}^{5} s_i^2}$, where s_i are the sensitivity coefficients corresponding to one outcome variable.

	Outcome variables (m)				
	x_0	x_0'	δx_1	δx_2	δx_3
Input variable (m)	Sensitivity Coefficient (unitless)				
x_{m1}	−27.1	7.08	−22.0	−17.4	−14.0
x_{m2}	−29.4	9.96	−22.9	−16.4	−8.82
x_{m3}	17.6	−5.32	14.2	10.83	7.48
x_{m4}	26.5	−7.85	21.1	16.0	10.9
x_{m5}	13.4	6.862	10.6	8.08	5.44
norm	52.8	15.9	42.0	31.8	21.9

[1] Minimization was done in Mathematica Version 12.2, Wolfram Research, Champaign, IL

Table 7: Magnetic field gradients used in measuring the quadrupole displacements which minimize the sensitivity coefficients found in Table 6.

Measurement number	Gradient QX1a (T/m)	Gradient QX1b (T/m)	Gradient QX1c (T/m)
1	8.54	1.11	-11.1
2	8.20	0.664	-8.09
3	5.29	11.0	-9.00
4	11.9	-10.5	-6.66
5	-15.0	10.9	-15.0

5.4 Misalignment of Steering Magnets

The effects of misalignment of the quadrupoles which are used in the quadrupole variation method are discussed in Section 5.2, however, effects of misalignment of the steering magnets which are used to control the beam centroid have not been investigated.

The derivation of the equation describing the behaviour of the particle vector when travelling through a misaligned steering magnet is given in Appendix D. It can be derived by adjusting the equations for a misaligned bending magnet given in [9], to a steering magnet. The equation is given by

$$\boldsymbol{x}(1) = R\boldsymbol{x}(0) + (A_1 - RA_0)\,\boldsymbol{m} + (RB_0 - B_1R)\boldsymbol{x}(0) + (B_1 + I_3)\,\boldsymbol{b} \tag{143}$$

where $\boldsymbol{x}(1)$ and $\boldsymbol{x}(0)$ are the particle vectors at the exit and entrance face of the magnet respectively, the matrices A_0, A_1, B_0 and B_1 are identical to the matrices given in Eq. (134), $\boldsymbol{m}$ is the misalignment vector as given in Eq. (132), and I_3 is the 3x3 identity matrix. The matrix R and vector b describe the transport of the particle when no misalignment is present ($\boldsymbol{m} = B_0 = B_1 = 0$), such that

$$\boldsymbol{x}(1) = R\boldsymbol{x}(0) + \boldsymbol{b}. \tag{144}$$

Using the approximation that the effect of the steering magnets can be represented by an instantaneous kick at the center of the magnet, the matrix R and vector $\boldsymbol{b}$ describing the effect of a steering magnet are

$$R = \begin{pmatrix} 1 & L & 0 & 0 & 0 & 0 \\ 0 & 1 & 0 & 0 & 0 & 0 \\ 0 & 0 & 1 & L & 0 & 0 \\ 0 & 0 & 0 & 1 & 0 & 0 \\ 0 & 0 & 0 & 0 & 1 & 0 \\ 0 & 0 & 0 & 0 & 0 & 1 \end{pmatrix}, \qquad \boldsymbol{b} = \begin{pmatrix} \frac{\alpha L}{2} \\ \alpha \\ \frac{\phi L}{2} \\ \phi \\ 0 \\ 0 \end{pmatrix} \tag{145}$$

where L is the length of the steering magnet, α is the bending angle in the x-z plane and ϕ is the bending angle in the y-z plane.

substituting this into Eq. (143) and writing out all the terms gives

$$\boldsymbol{x}(1) = \boldsymbol{x}_u(1) + \boldsymbol{x}_p(1) = \begin{pmatrix} x_0 + Lx_0' + \frac{\alpha L}{2} \\ x_0' + \alpha \\ y_0 + Ly_0' + \frac{\phi L}{2} \\ y_0' + \phi \\ l \\ \delta \end{pmatrix} + \begin{pmatrix} \alpha\delta z + \frac{\phi L\theta z}{2} \\ \phi\theta z \\ \phi\delta z - \frac{\alpha L\theta z}{2} \\ -\alpha\theta z \\ 0 \\ 0 \end{pmatrix} \tag{146}$$

where $\boldsymbol{x}_u(1)$ is the unperturbed particle vector and $\boldsymbol{x}_p$ is a vector containing the perturbations due to misalignment. From this, it is observed that all misalignment parameters in $\boldsymbol{x}_p(1)$ appear as cross-terms with the bending angles α and ϕ, since these quantities are both small, their product can be neglected. Therefore any misalignment present in the steering magnet will not have a significant effect on the beam control.

Next misalignment in the combined function magnets is investigated, Eq. (143) is again used, the matrix R and vector b can be obtained from Eq. (95) and (96). The calculations will be done for combined function magnet whose quadrupole component focuses in the x direction and defocuses in the y direction, but the same conclusions can be found when switching the focusing direction

$$R = \begin{pmatrix} \cos\sqrt{k}L & \frac{\sin\sqrt{k}L}{\sqrt{k}} & 0 & 0 & 0 & 0 \\ -\sqrt{k}\sin\sqrt{k}L & \cos\sqrt{k}L & 0 & 0 & 0 & 0 \\ 0 & 0 & \cosh\sqrt{k}L & \frac{\sinh\sqrt{k}L}{\sqrt{k}} & 0 & 0 \\ 0 & 0 & \sqrt{k}\sin\sqrt{k}L & \cos\sqrt{k}L & 0 & 0 \\ 0 & 0 & 0 & 0 & 1 & 0 \\ 0 & 0 & 0 & 0 & 0 & 1 \end{pmatrix}, \qquad \boldsymbol{b} = \begin{pmatrix} \frac{\alpha\sin\frac{\sqrt{k}L}{2}}{\sqrt{k}} \\ \alpha\cos\frac{\sqrt{k}L}{2} \\ \frac{\alpha\sin\frac{\sqrt{k}L}{2}}{\sqrt{k}} \\ \alpha\cos\frac{\sqrt{k}L}{2} \\ 0 \\ 0 \end{pmatrix} \tag{147}$$

These values are also substituted into Eq. (143), the solution was simplified by eliminating all cross-terms involving the misalignment parameters, particle coordinates, or bending angles since these terms are very small, which means that their product can be neglected

$$\begin{aligned} \boldsymbol{x}(1) &= \boldsymbol{x}_u(1) + \boldsymbol{x}_p(1) \\ &= \begin{pmatrix} x_0\cos\sqrt{k}L + \frac{x_0'\sin\sqrt{k}L}{\sqrt{k}} + \frac{\alpha\sin\frac{\sqrt{k}L}{2}}{\sqrt{k}} \\ -x_0\sqrt{k}\sin\sqrt{k}L + x_0'\cos\sqrt{k}L + \alpha\cos\frac{\sqrt{k}L}{2} \\ y_0\cosh\sqrt{k}L + \frac{\sinh\sqrt{k}L}{\sqrt{k}} + \frac{\phi\sinh\frac{\sqrt{k}L}{2}}{\sqrt{k}} \\ y_0\sqrt{k}\sinh\sqrt{k}L + y_0'\cosh\sqrt{k}L + \phi\cosh\frac{\sqrt{k}L}{2} \\ l \\ \delta \end{pmatrix} + \begin{pmatrix} \delta x(1-\cos\sqrt{k}L) + \theta y(L - \frac{\sin\sqrt{k}L}{\sqrt{k}}) \\ \theta y(1-\cos\sqrt{k}L) + \sqrt{k}\delta x\sin\sqrt{k}L \\ \delta y(1-\cos\sqrt{k}L) + \theta x(-L + \frac{\sin\sqrt{k}L}{\sqrt{k}}) \\ \theta x(-1+\cos\sqrt{k}L) - \sqrt{k}\delta y\sin\sqrt{k}L \\ 0 \\ 0 \end{pmatrix} \end{aligned} \tag{148}$$

where $\boldsymbol{x}_u(1)$ is the unperturbed particle vector and $\boldsymbol{x}_p$ is a vector containing the perturbations due to misalignment. It is observed that $\boldsymbol{x}_p(1)$ does not depend on α or ϕ, i.e. $\boldsymbol{x}_p(1)$ does not change during the tuning process. When including the misalignment effect, Eq. (144) can be written as

$$\boldsymbol{x}(1) = R\boldsymbol{x}(0) + \boldsymbol{b} + \boldsymbol{c} \tag{149}$$

where $\boldsymbol{x}(1)$ and $\boldsymbol{x}(0)$ are the particle vectors at the entrance and exit of the combined function magnet, R and $\boldsymbol{b}$ are defined as before, and $\boldsymbol{c}$ is a vector containing the misalignment effect, which does not depend on the tuning parameters α and ϕ. To analyze the effect of the addition of $\boldsymbol{c}$ on the control algorithm, the forward equation for the pair of combined function magnets used to align the beam centroid in the y-coordinate is written down. This section consists out of two combined function magnets, S_{xy} and S_y, separated by a drift space of length L_1, followed by a second drift space from the combined function magnet S_y to beam monitor HX of length L_2. The equation relating the particle vector at the end of the section $\boldsymbol{x}(1)$ to the particle vector at the start of the section $\boldsymbol{x}(0)$, when no misalignment is present, is given by

$$\boldsymbol{x}(1) = R_{d2}R_{s2}R_{d1}R_{s1}\boldsymbol{x}(0) + R_{d2}R_{s2}R_{d1}\boldsymbol{b_{s1}} + R_{d2}\boldsymbol{b_{s2}} \tag{150}$$

where R_{d1} and R_{d2} are the transfer matrices of the first and second drift space respectively, R_{s1} and $\boldsymbol{b_{s1}}$ are the transfer matrix and constant vector of the first combined function magnet, and R_{s2} and $\boldsymbol{b_{s2}}$ are the transfer matrix and constant vector of the second combined function magnet.

By rewriting this to include the misalignment effect $\boldsymbol{c}$, the forward equation becomes

$$\boldsymbol{x}(1) = R_{d2}R_{s2}R_{d1}R_{s1}\boldsymbol{x}(0) + R_{d2}R_{s2}R_{d1}\boldsymbol{c_1} + R_{d2}\boldsymbol{c_2} + R_{d2}R_{s2}R_{d1}\boldsymbol{b_{s1}} + R_{d2}\boldsymbol{b_{s2}} \tag{151}$$

where $\boldsymbol{c_1}$ and $\boldsymbol{c_2}$ are the vectors containing the misalignment effects for the first and second combined function magnets respectively. Comparing Eqs. (150) and (151) it is observed that the terms in front of the $\boldsymbol{b}$ vectors, which contain the effect of the bending part of the combined function magnet, are the same. The only difference is that the terms $R_{d2}R_{s2}R_{d1}\boldsymbol{c_1}$ and $R_{d2}\boldsymbol{c_2}$ are added, which are independent of α and ϕ, in addition to the already present independent term $R_{d2}R_{s2}R_{d1}R_{s1}\boldsymbol{x}(0)$. In other words the added constants act like a different initial particle vector in Eq. (150), denoted by $\overline{\boldsymbol{x}}(0)$ given by

$$\overline{\boldsymbol{x}}(0) = \boldsymbol{x}(0) + R_{s1}^{-1}\boldsymbol{c_1} + \left(R_{s2}R_{d1}R_{s1}\right)^{-1}\boldsymbol{c_2} \tag{152}$$

where $\boldsymbol{x}(0)$ is the particle vector at the beginning of the system which has misalignment present. Since it is known that the system converges in one step for any initial vector $\boldsymbol{x}(0)$, it can be seen that the misalignment of the combined function magnets, or steering magnets, does not affect the performance of the algorithm, it only changes the applied current to the magnets once convergence is reached.

5.5 Finding the Optimal Beam Centroid Angle and Position

5.5.1 Optimal beam transport for steering magnets in x-direction

If misalignment is present in the system, it is not possible to align the beam centroid with the designed trajectory everywhere in the system. Therefore a criterion needs to be found which gives the optimal beam parameters in terms of the misalignment parameters. In the second step of the beam tuning process, the quadrupoles will be tuned to achieve minimum beam sizes at specified locations. If the beam centroid is far away from the quadrupole axes, the beam trajectory will change significantly during this tuning process, which should be avoided. Therefore, the objective will be to minimize the average distance from the beam centroid to the quadrupole axes in the beamline. As a secondary effect, this objective will also lower beam loses during transport, since the closer the beam follows the designed trajectory, the lower the number of particles lost in the beamline walls.

The distance from the beam centroid to the quadrupole axes is given by the x and y coordinates of the beam centroid. To calculate the average distance, these coordinates should be written as a function of the distance, s, along the reference trajectory. The function describing $x(s)$ and $y(s)$ in a beamline section will be a piecewise function, in which each sub-function corresponds to an element, e.g. a drift space, quadrupole, or bending magnet. From this piecewise function, the equations describing the beam trajectory in the quadrupoles are extracted and used to construct the objective function, which should be minimized to find the optimal beam parameters.

This piecewise function is constructed according to the diagram shown in Figure 29. The transfer matrices of each element can be written as a function of the distance along the reference trajectory s by replacing the element length L with s. To calculate the sub-function of a misaligned quadrupole Eq. (131) should be used instead of a single transfer matrix. By multiplying the transfer matrix with the beam vector at the start of the element, a sub-function describing the beam centroid trajectory is created, which is defined along the entire length of the element. To calculate the sub-function of the next element the starting distance L_0 and particle vector $\boldsymbol{x}$ are updated. Note that the updating of the starting point L_0 and the shift $R(s - L_0)$ in the piecewise functions are not strictly necessary, as can be seen in the objective function defined in Eq. (153), however, it makes the results easier to interpret. The result is a six-dimensional beam vector that contains the piecewise functions describing every beam coordinate in terms of the initial beam vector and distance s. For the objective function, only the piecewise functions describing x and y are required. An example of how such a piecewise function looks for x can be seen in Figure 30.

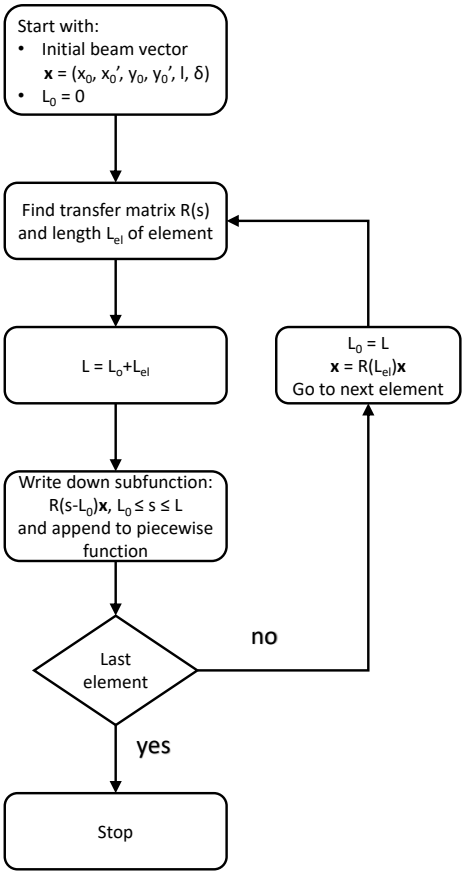

Figure 29: Diagram showing the construction of the piecewise functions describing the beam centroid trajectory through the beamline.

To create the objective function, the sub-functions corresponding to the quadrupoles, denoted by q_i for the ith quadrupole in the beamline section, are extracted from the piecewise function and the following objective function is constructed. Note that this objective function is defined for transport regarding the x-coordinate, an analogous expression can be found for the y-coordinate

$$f_{obj}(x_0, x_0') = \sum_{i=1}^{n} \left(\int_{Ls_i}^{Le_i} q_i(s) \mathrm{d}s \right)^2, \tag{153}$$

where f_{ojb} is the objective function, which is a function of the initial beam conditions x_0 and x_0', n is the number of quadrupoles, and Ls_i and Le_i are the starting and ending coordinates of the ith quadrupole. The optimal initial beam conditions can be found by minimizing Eq. (153) with respect to x_0 and x_0' since this will minimize the average distance from the beam centroid to the quadrupole axes. Since the functions q_i are linear in x_0 and x_0', the squared integrals will be convex functions,

the sum of convex functions is also convex [11], which means that the objective function f_{obj} will be convex. Therefore, minimization is straightforward and can be done using numerical or analytical methods.

It should be noted that since the square inside Eq. (153) is on the outside of the integral, solutions in which the beam centroid crosses the center of the quadrupole, i.e. the average value of x on the left and right side of the quadrupole is equal, will also yield a minimum value of the objective function, since for that quadrupole the integral term will be zero. For the purposes of beam tuning, this is also a valid solution since the symmetry will approximately cancel out the effects on the beam centroid due to changes in the quadrupole focusing strength.

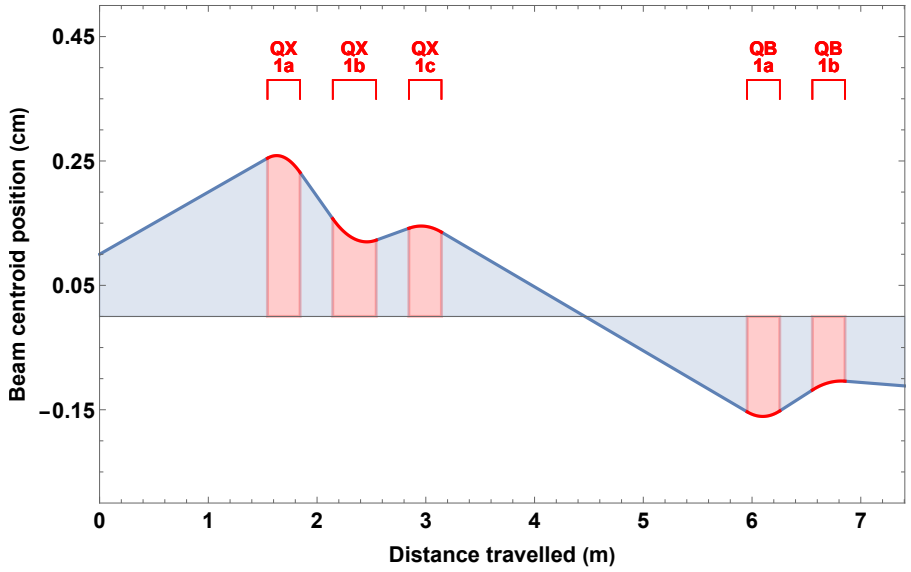

Figure 30: Plot of a piecewise function describing the transport of the beam centroid through the beamline. The subfunctions which give the transport through the quadrupoles are indicated in red. The area under the graph is shaded to indicated the size of the integral in that region.

To demonstrate this technique an example is given for the steering magnets $S_{x,y}$ and S_x, which steer the beam in the x-direction. At the exit of the steering magnets, it is possible to steer the beam to every possible combination of x_0 and x_0', therefore the goal is to pick these values such that Eq. (153) is minimized. The section of beamline which comes after the steering magnets is given in Figure 31. The settings for all the quadrupoles are given in Table 8.

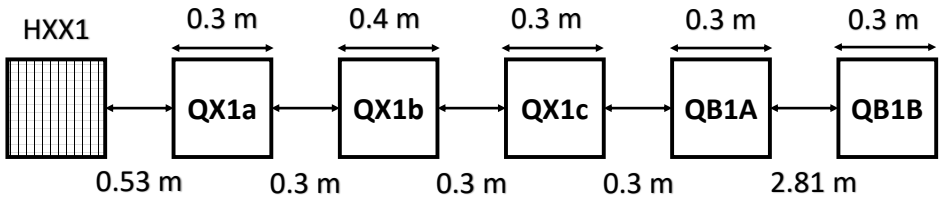

Figure 31: Section of the beamline which comes after steering magnets $S_{x,y}$ and S_x.

Figure 32 shows the beam centroid trajectory for the optimum solution, found by minimizing Eq. (153), and the trajectory when the beam conditions at HXX1 are set to $x = 0$ and $x' = 0$. The quadrupoles have misalignments as given in Table 8. It can be seen that the non-optimized solution performs much worse. The average absolute distances from the quadrupole axes for the optimized and non-optimized case are 0.338 mm and 0.783 mm respectively.

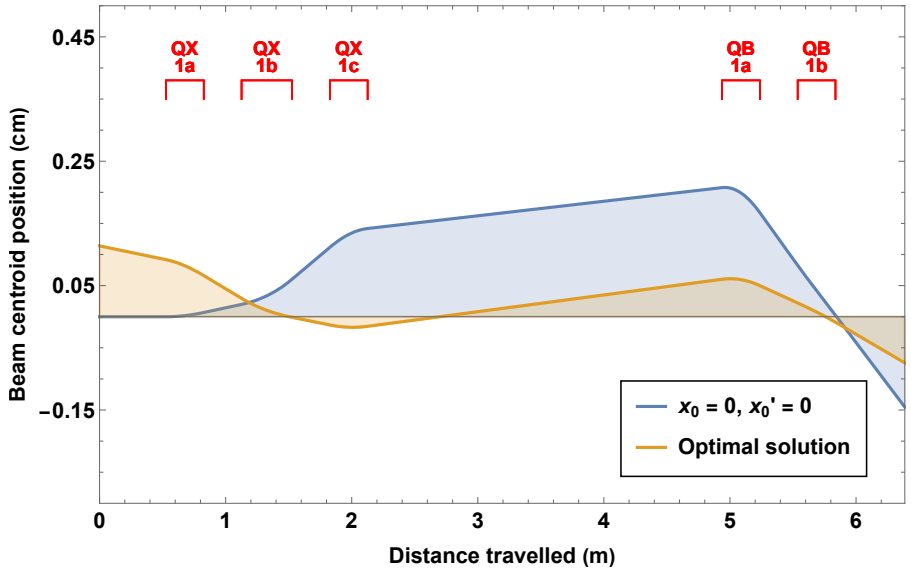

Figure 32: Plot of the beam centroid as it travels through the beamline section, the optimum solution where the distance to the center of the quadrupoles is minimized is shown in orange, the solution when setting the initial beam conditions x_0 and x_0' to zero is shown in blue.

To minimize Eq. (153) for a system with misalignments, the misalignments need to be known, which is usually not the case. To compare the performance of the algorithm, in which it is assumed that all misalignments are zero, to the optimum solution by given by minimizing Eq. (153), a Monte Carlo simulation is performed. If the optimum solution performs much better than the algorithm, it will be useful to measure the misalignment of quadrupoles in the real system, such that the optimum solution for the real system can be calculated and implemented into the algorithm.

For each run in this simulation, each quadrupole is given a random misalignment drawn from a uniform distribution with bounds of $-0.3\,\text{mm}$ and $0.3\,\text{mm}$. For each set of misalignments, the steady state response of the steering algorithm is computed, substituted into Eq. (153), and compared to the minimum of Eq. (153). The steady state solution is defined as values of x_0 and x_0' as the number of iterations of the algorithm goes to infinity.

The steady state solution depends on the measurements that the algorithm obtains from the quadrupole variation method. If the quadrupoles that are used in the measurement have a misalignment, but the algorithm assumes that all misalignments are zero, the measured beam conditions will deviate from the real beam conditions. Because the algorithm performs the corrections to the steering magnets based on wrong beam condition values, the steady state solution will be different from $x_0 = x_0' = 0$. The measured values from the quadrupole variation method, and therefore also the steady state solution, are dependent on the magnetic field gradients and misalignments of the quadrupoles used in the quadrupole variation method. To calculate the steady state solution, the quadrupole gradient values from Table 8 were used. During each quadrupole variation method, two measurements were taken, where QX1a and QX1c were set to 0.9 and 1.1 times the default values for the first and second measurement respectively, the other quadrupoles were kept constant. The misalignments were varied according to the Monte Carlo simulation, and the measurements for the quadrupole variation method were taken using beam profile monitor HXB1. The optimum solution, which could be achieved by the system if all misalignment parameters were known, was also calculated for each set of misalignments, by constructing the Eq. (153), which depends on the misalignments and minimizing it with respect to x_0 and x_0' using numerical methods. In total 10^4 runs were done.

Figure 33 shows the results of this simulation, it can be seen that the performance of the algorithm is close to that of the minimum solution. The average absolute distance to the quadrupole axes using the steady state solution was $0.178\,\text{mm}$, and for the minimum solution, it is $0.151\,\text{mm}$, the spread in the datapoints is given by the box-and-whisker plots in Figure 34. This means that, under the assumptions of this simulation, using the optimum solution does not yield significantly better performance than the standard algorithm.

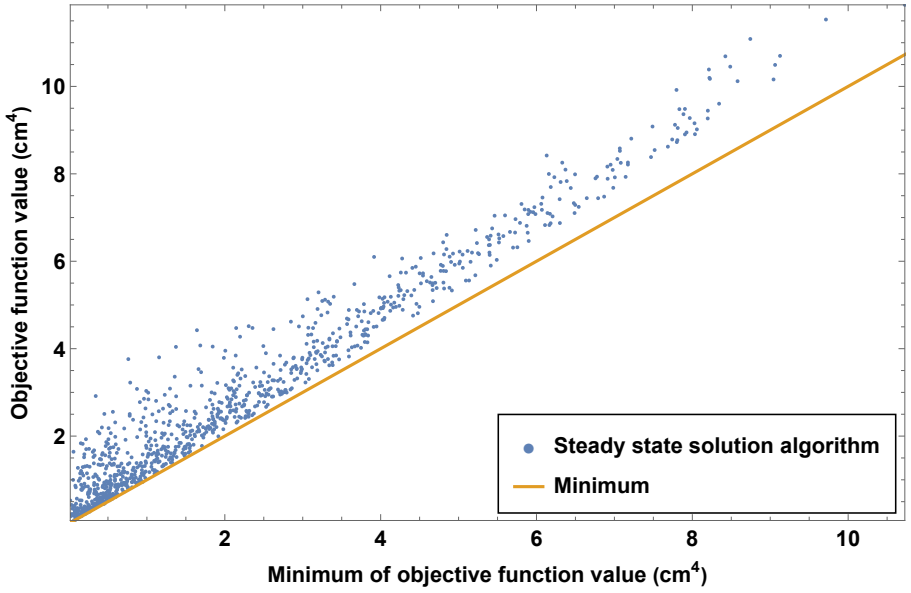

Figure 33: Monte Carlo simulation results showing the minimum values of the objective function and the values of the objective function that results from applying the algorithm. For clarity only 10^3 out of 10^4 runs are shown.

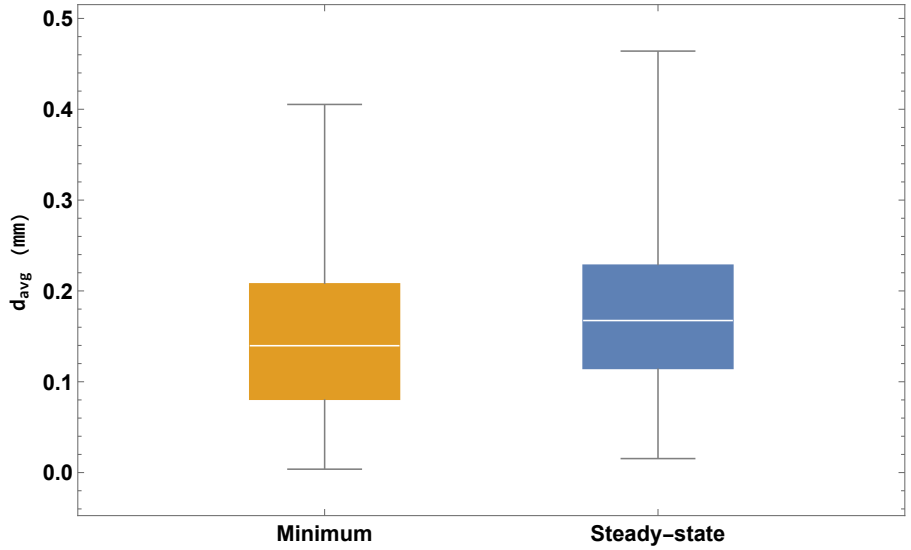

Figure 34: Box-and-whisker plot of the average absolute distance to the quadrupole axes d_{avg} for the minimum and steady state algorithm solution. The whiskers show the minimum and maximum value, the box shows the 25th percentile, median and 75th percentile.

Table 8: Numerical values used in optimizing beam transport for the x-coordinate, in the section after the pair of steering magnets.

Element	Item	Value	Unit
Beam properties	p	0.6144	GeV c^{-1}
Drift spaces	HXX1→QX1a	0.526	m
	QX1a→QX1b	0.300	m
	QX1b→QX1c	0.300	m
	QX1c →QB1A	2.811	m
	QB1A →QB1B	0.300	m
Quadrupole QX1a	Effective Length	0.3	m
	Field gradient	10.7	T m^{-1}
	misalignment (x-direction)	0.3	mm
Quadrupole QX1b	Effective Length	0.4	m
	Field gradient	-9.96	T m^{-1}
	misalignment (x-direction)	-0.3	mm
Quadrupole QX1c	Effective Length	0.3	m
	Field gradient	10.06	T m^{-1}
	misalignment (x-direction)	0.3	mm
Quadrupole QB1A	Effective Length	0.3	m
	Field gradient	9.28	T m^{-1}
	misalignment (x-direction)	-0.3	mm
Quadrupole QB1B	Effective Length	0.3	m
	Field gradient	-7.95	T m^{-1}
	misalignment (x-direction)	0.3	mm

5.5.2 Optimal beam transport for steering magnets in y-direction

Next, the optimal beam transport for the y-coordinate, using steering magnets $S_{x,y}$ and S_y, is investigated. The objective function in Eq, (153) is again used, where x_0 and x_0' are replaced with y_0 and y_0'. Using the same geometry as in Table 8, with the displacements in y instead of x, the optimum solution, found by minimizing Eq. (153), is compared with the solution where the initial beam parameters are $y_0 = 0$ and $y_0' = 0$. The result can be seen in Figure 35. It is observed that in the case of $y_0 = 0$ and $y_0' = 0$, the beam centroid deviates greatly from the reference trajectory, this is because quadrupoles QX1c and QB1a are both defocussing in y, which amplify the effects of the magnet misalignments. For the optimal solution the average absolute distance from the quadrupole axes is 0.166 mm and for the zero initial conditions, it is equal to 3.87 mm.

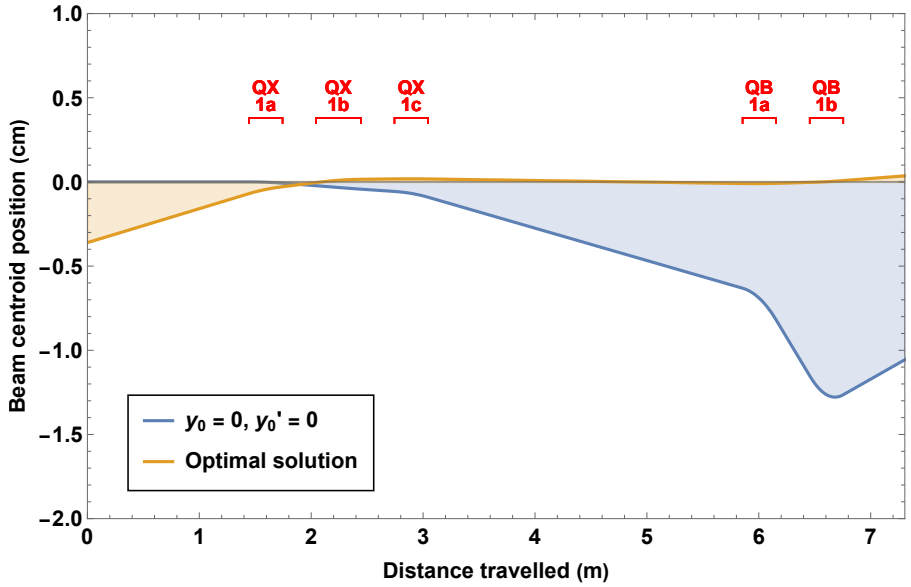

Figure 35: Plot of the beam centroid as it travels through the beamline section, the optimum solution where the distance from the beam centroid to the center of the quadrupoles is minimized is shown in orange, the solution when the initial beam conditions are set to zero is shown in blue.

To investigate the performance of the algorithm, which again assumes all misalignments are zero, a Monte Carlo simulation with the same settings as in Section 5.5.1, including the settings for the quadrupole variation method, was done. The results of this can be seen in Figure 36. It is observed that the steady state solution performs significantly worse for higher minimum values of the objective function, where the effect of the misalignment is the highest. For lower values of the minimum objective function, the performance of the algorithm becomes more in line with that of the optimum. Furthermore, most of the points are located near the lower left of the graph, this indicates that the situation where the misalignments have a small effect on the transport is more likely than the case where the misalignments have a large effect. The average absolute distance from the quadrupole axis for the optimum case is 0.067 mm, for the steady state value of the algorithm is it equal to 0.244 mm. This large discrepancy is most likely due to the fact the consecutive defocusing quadrupoles QX1c and QB1a, are not corrected for by the algorithm.

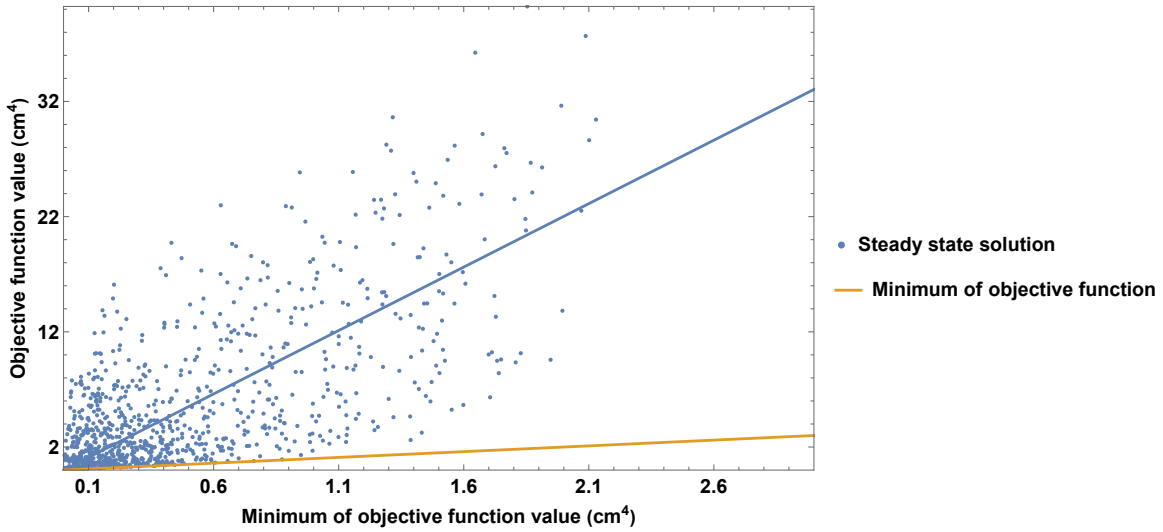

Figure 36: Monte Carlo simulation results showing the minimum the minimum value of the objective function and the value of the objective function that results from applying the algorithm. For clarity only 10^3 out of 10^4 runs are shown. A line showing the correlation of the datapoints has been added to better compare the two methods.

Since the algorithm performs much worse in this case, a different strategy is proposed. To implement the optimal solution in the algorithm it is necessary to know all the quadrupole misalignments with sufficient accuracy, which might be difficult. Therefore another method is proposed, which uses the fact that there is a certain correlation between the y-coordinate measured at beam profile HXB1 and the optimal solution, found by minimizing Eq. (153). By measuring this y, which is only a single measurement, it is possible to predict the optimal solution.

In this method y at HXB1 should be measured in a specific way, following these two steps:

1. First all the quadrupoles in between beam monitors HX and HXB1 are turned off, effectively turning them into drift spaces. The steering magnets $S_{x,y}$ and S_y are used to ensure that at beam monitor HX the beam conditions are $y = 0$ and $y' = 0$. This can be done by making sure that $y = 0$ at both monitors HX and HXB1.
2. In the second step the quadrupoles are turned back on and set to their default values, as given in Table 8. Depending on the misalignment of the quadrupoles, y at HXB1 should change. The new value, denoted by y_{HXB1} should be measured using the beam profile monitor.

There will be a certain correlation between y_{HXB1} and the optimum beam conditions at HX. By simulating many possible misalignments of the quadrupoles and calculating the optimal initial beam parameters at HX, denoted by y_0 and y_0', as well as y_{HXB1}, for each set of misalignments, it is possible to fit a function to the data, from which the optimal conditions can be predicted.

During this process measurement error due to displacements in the quadrupoles which are used for the quadrupole variation method should be taken into account. If the quadrupoles are not displaced

along or rotated around the z-axis, the measurement error can be represented by

$$\boldsymbol{y}_m = \boldsymbol{y}_r + \boldsymbol{b} \tag{154}$$

where $\boldsymbol{y}_m$ is the beam centroid vector, which is measured using the quadrupole variation method, $\boldsymbol{y}_r$ is the real beam centroid vector, and $\boldsymbol{b}$ is a vector containing the measurement error, which depends on the displacements of the quadrupoles and the magnet settings during the quadrupole variation method.

The objective of the algorithm is to steer the beam such that $y = y' = 0$ at the exit of the steering magnet pair. Since the algorithm only has access to the measured beam centroid vector $\boldsymbol{y}_m$, the steady state result of the algorithm will be $\boldsymbol{y}_m = 0$. The algorithm can easily be adapted, by making a substitution $\boldsymbol{y}_m = \widetilde{\boldsymbol{y}_m}$, such that after sufficient iterations, the end result $\widetilde{\boldsymbol{y}_m} = 0$ is achieved. Using this, the following value for $\widetilde{\boldsymbol{y}_m}$ is proposed.

$$\widetilde{\boldsymbol{y}_m} = \boldsymbol{y}_m - (\boldsymbol{b} + \boldsymbol{g}) \tag{155}$$

where $\boldsymbol{g}$ is a vector containing the desired values for $\boldsymbol{y}_r$, which are ideally equal to the optimal values obtained from minimizing Eq (153). This way, when the algorithm converges to $\widetilde{\boldsymbol{y}_m} = 0$, the following relation is obtained

$$0 = \boldsymbol{y}_m - (\boldsymbol{b} + \boldsymbol{g}) \Rightarrow \boldsymbol{y}_m = \boldsymbol{b} + \boldsymbol{g} \Rightarrow \boldsymbol{y}_r = \boldsymbol{g} \tag{156}$$

from which it is observed that the real $\boldsymbol{y}$ value indeed converges to the desired goal $\boldsymbol{g}$. We will refer to $\boldsymbol{b} + \boldsymbol{g}$ as the corrected optimal values. From this, it can be seen that if the corrected optimal values are known, they can be substituted into the algorithm via Eq. (155) and the optimal beam transport conditions $\boldsymbol{g}$ will be achieved at the exit of the steering magnets. Next, the simulations are performed to predict the corrected optimal values.

In each iteration of the simulation, a misalignment is drawn from a uniform distribution with bounds $-0.3\,\text{mm}$ and $0.3\,\text{mm}$, for each of the quadrupoles QX1a, QX1b, QX1c, QB1a en QB1b. A total of 10^4 iterations were done. For each iteration $\boldsymbol{b} + \boldsymbol{g}$ and y_{HXB1} are calculated. Figure 37 shows all of the data points obtained in this way. The figure also shows a linear relation that is fitted through the datapoints. Finding the correct optimal values is most important when the effect of misalignment is the greatest. This is the case when the corrected optimal values are the largest, therefore each point was assigned a weight equal to its y_0 or y_0' value before fitting. The relations were then fitted using a weighted least-squares approach and are equal to

$$\begin{aligned} y_{0,opt} &= 0.196 y_{\text{HXB1}} + 7.92 \times 10^{-5} \\ y'_{0,opt} &= -0.379 y_{\text{HXB1}} - 1.79 \times 10^{-4} \end{aligned} \tag{157}$$

where $y_{0,opt}$ and $y'_{0,opt}$ are the corrected optimal values at HX (equal to $\boldsymbol{b} + \boldsymbol{g}$), and y_{HXB1} is y measured at HXB1 using the previously described technique. By measuring y_{HXB1} in the beamline and plugging the obtained value into Eq. (157) the corrected optimal values can be predicted. Using Eq. (155) these values can be substituted into the algorithm.

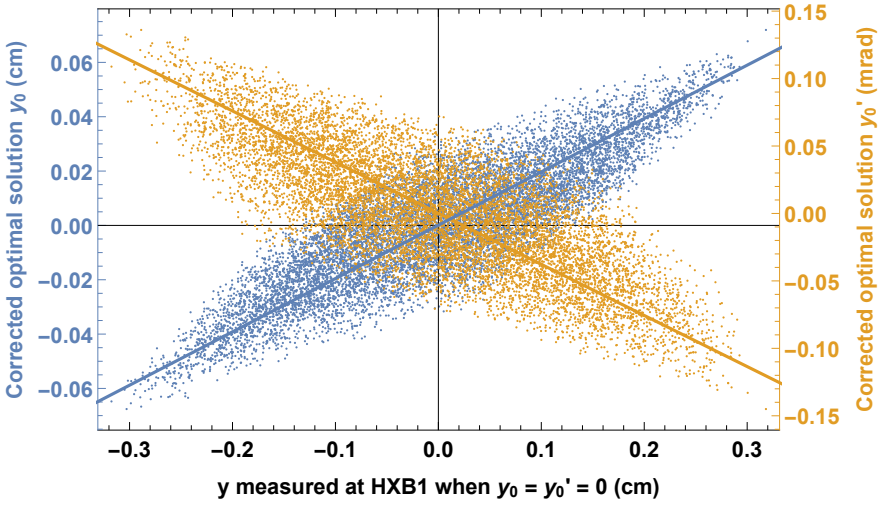

Figure 37: Graph of the Monte Carlo simulations, the values of $\boldsymbol{b} + \boldsymbol{g}$, whose components are denoted by the corrected optimal solution for y_0 and y'_0, are plotted against y measured at HXB1 when $y_0 = y'_0 = 0$. The linear relations were fitted to the datapoints using a least squares approach.

The performance of this method, compared to the steady state solution and optimum solution can be seen in Figure 38a. It can be seen that it performs better than the standard algorithm, which has no information on the misalignments, but worse than the optimum solution, which has access to all the misalignment values. Especially at higher values of the optimum values, this prediction method functions better than the steady state solution. The average absolute distance from the axis is equal to 0.146 mm, which is an improvement over the steady state solution of the algorithm, however still worse than the minimum solution.

To compare the prediction method to the steady state solution further, the ratio of their respective objective function values is plotted in Figure 38b. Points in which the ratio is smaller than one, indicate a point in which the objective function value of the prediction method is smaller than that of the steady state solution, therefore the performance of the prediction method is better for those points. In total 67% of the points have a value below one. Furthermore, most of the points which have values above one correspond to low values of the minimum of the objective function. For these points, the objective function, which is a measure of the deviation from the ideal trajectory, is already quite low for both methods, so the higher ratio results in a smaller performance difference, than it would be for points with a high minimum of the objective function.

The comparison of the average absolute distance from the beam centroid to quadrupole axes between the three different methods can be seen in Figure 39. It can be seen that for the best performance

of the algorithm, all misalignments of the quadrupoles would need to be measured, such that the optimum solution can be implemented into the algorithm. In the case that this is not possible, the prediction method can be used to yield better performance over the standard algorithm.

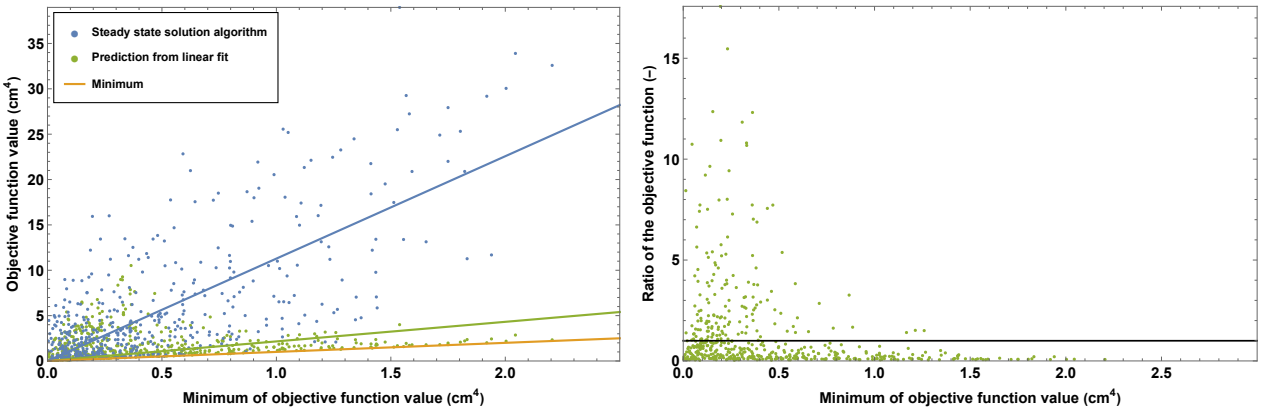

(a) Comparison of the two methods for determining the optimal beam conditions for transport. Lines showing the correlation of the datapoints have been added for easier comparison.

(b) Ratio of the objective function value of the prediction from the linear fit to the steady state solution. A horizontal line equal to one has been added to the plot.

Figure 38: Figures illustrating the performance of the method which predicts the optimal beam transport parameters from the linear models.

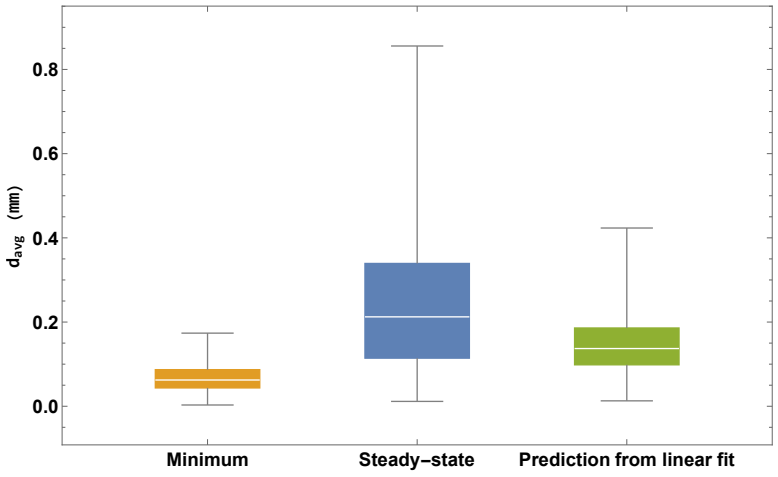

Figure 39: Box-and-whiskers plot of the average absolute distance to the quadrupole axes d_{avg} for the optimal solution obtained from minimizing the objective function, the steady state solution of the algorithm, and guess of optimal conditions based on a linear relation fitted from the simulations. The whiskers show the minimum and maximum value, the box shows the 25th percentile, median and 75th percentile.

5.5.3 Optimal beam conditions for a bending magnet

The same strategies as in Section 5.5.1 can be used to find the optimal settings for a bending magnet. The bending magnet has one free parameter, being the bending radius ρ, while the beam has two parameters that need to be controlled, which makes the system overdetermined. Since it is not possible to find an exact solution, this method provides a way to find the optimal setting.

As an example, the section in between the bending magnet B1 and B2 is taken, which can be seen in Figure 40. The magnet settings can be found in Table 9. To set up the objective function Eq. (153) is again used, where the initial vector, defined at the exit face of B1, is calculated using Eq. (93). It is assumed that the beam conditions at the entrance face of B1 are known, which leaves the bending radius ρ as the only free parameter. The objective function can be minimized with respect to ρ using any numerical convex minimization method.

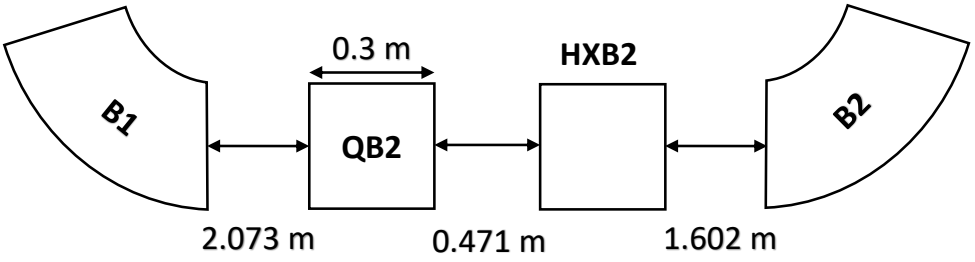

Figure 40: Section of the beamline which contains the bending magnet B1 and the quadrupole QB2

To compare this method to the current algorithm, a Monte Carlo study was performed in which the optimum solution is compared to the steady state solution of the algorithm. The displacement of quadrupole QB2 was taken from a uniform distribution between $-0.3\,\text{mm}$ and $0.3\,\text{mm}$. The initial beam conditions at the entrance face of magnet B1 were taken from uniform distributions with bounds $-1\,\text{mm} \leq x_0 \leq 1\,\text{mm}$ and $-1\,\text{mrad} \leq x_0' \leq 1\,\text{mrad}$, 10^4 runs were done. To calculate the steady state solution a quadrupole variation method was used where two measurements were taken in which QB2 was set to 0.9 and 1.1 the default value for the first and second measurement respectively. The measurement were taken using profile monitor HXB2.

The results can be seen in Figure 41. The minimum values of the objective function are not shown since they were equal to zero, within machine precision, for most runs. It can be seen that for the steady state solution of the algorithm most of the runs end up with a reasonably low value for the objective function. However, there is also a small possibility that the objective function value exceeds $5.0\,\text{cm}^4$, which corresponds to an average distance from the quadrupole axes of 0.75 mm. The average absolute distance from the beam centroid to the quadrupole axis, using the steady state solution, is equal to 0.22 mm, for the minimum solution the average distance is equal to 0.019 mm. The spread in datapoints is illustrated in Figure 42. This large discrepancy is because the algorithm for the bending magnets assumes that the beam centroid is aligned at the entrance face, and also suffers from measurement errors, due to magnet misalignments, in the quadrupole variation method. To improve

the performance of the algorithm ways to measure the beam centroid at the entrance of the bending magnet could be added to the algorithm. The closest beam monitors which could be used to measure this are HXB1 and HXB2. However due to magnet misalignments and uncertainty in the beam centroid momentum neither of these monitors will yield accurate enough measurements to be used for correction. Furthermore, by measuring the misalignment of quadrupole QB2, the measurement error can be corrected.

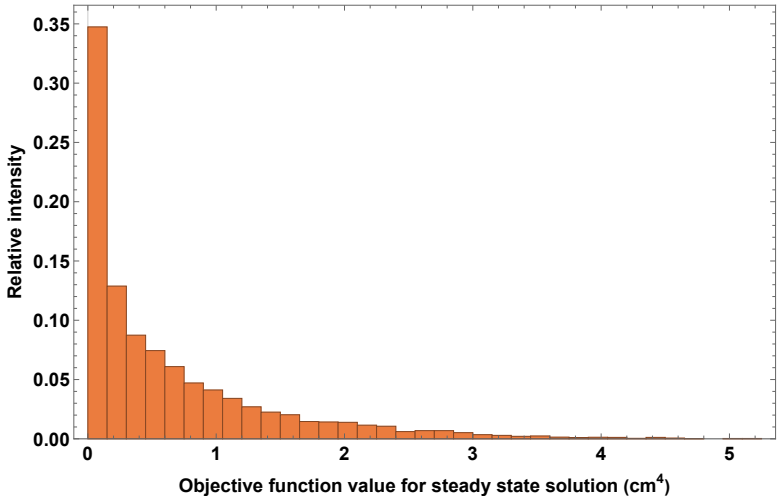

Figure 41: Histogram of the different objective function values obtained from the Monte Carlo simulation.

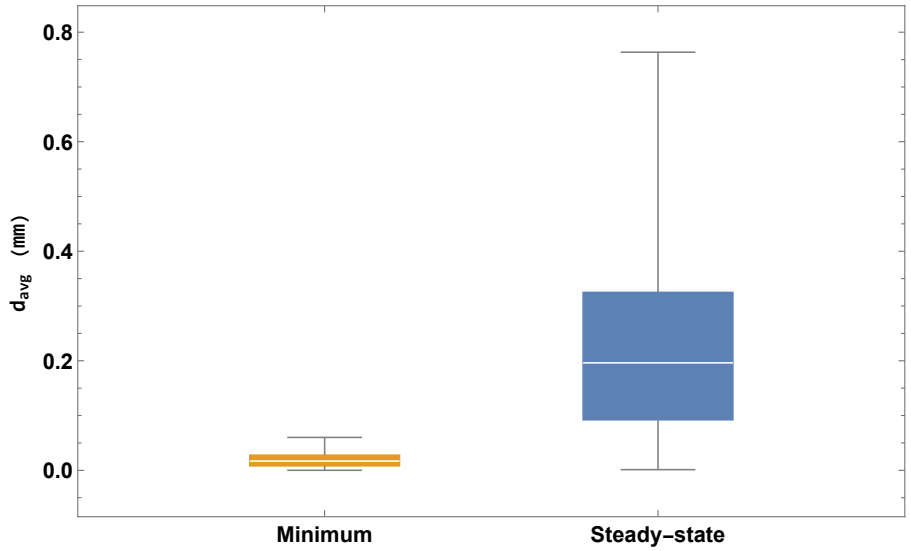

Figure 42: Box-and-whiskers plot of the average absolute distance to the quadrupole axis d_{avg}, for the minimum of the objective function, and the steady state solution achieved by the algorithm. The whiskers show the minimum and maximum value, the box shows the 25th percentile, median and 75th percentile.

Table 9: Numerical values used in optimizing beam transport in the section after bending magnet B1.

Element	Item	Value	Unit
Beam properties	p	0.6144	GeV c^{-1}
Drift spaces	B1→QB2	2.073	m
	QB2→HXB2	0.471	m
Quadrupole QB2	Effective Length	0.3	m
	Field gradient	10.7	T m^{-1}
	misalignment (x-direction)	0.3	mm
Bending Magnet B1	Effective Length	2.88307	m
	Bending angle	70	°

5.6 Finding Quadrupole Gradients which Create a Waist in the Beam

The goal of the second step of the tuning process is to find the quadrupole gradients which yield a beam waist at a desired location in the beamline. These beam waists are characterized by $\sigma_{12} = 0$ for a horizontal waist and $\sigma_{34} = 0$ for a vertical waist. It will be analyzed whether the criteria of finding a beam waist is sufficient to find the quadrupole settings which yield the best transport across the entire beamline. An example section of the beamline will be used involving quadrupoles QX1a,

QX1b, and QX1c, the goal is to achieve both a horizontal and vertical waist at the beam monitor HXB1. To find all of the possible quadrupole gradients which yield a beam waist, the sum of σ_{12} and σ_{34} is written as a function of the three quadrupole gradients. Then an equally spaced 3-dimensional grid of quadrupole gradients was created. From each point in this grid, a gradient descent minimizer was started. All of the minima found in this way, where $\sigma_{12} + \sigma_{34} = 0$, were stored and any duplicate positions were discarded. A plot of all these points can be seen in Figure 43. It is observed that many combinations are possible, a selection of the beam trajectories resulting from the found gradients can be seen in Figure 44. It is observed that quadrupole gradients found using this method result in a vastly different beam trajectory than the default settings which are used. Therefore it is concluded that the criterion of a simultaneous beam waist at one location is not sufficient to automatically find the optimal gradients for a quadrupole triplet. By adding criteria, such as a maximum beam size in both the x and y direction, the choice of quadrupole gradients can be limited further. However, this is still not sufficient to find the single best setting. To find the optimal setting it will be necessary to also place constraints at other locations in the beamline than the place where the waist should be found. This can be done by using the reference values for the other beamline elements and predicting the trajectory in the rest of the beamline using those values. The same analysis was done for a quadrupole doublet in which 4 possible gradient combinations were found which yield a simultaneous waist in the beam, these gradients lead to similar beam trajectories as seen in Figure 44. By also limiting the beam size at the waist location the best setting could be found from these 4 gradients.

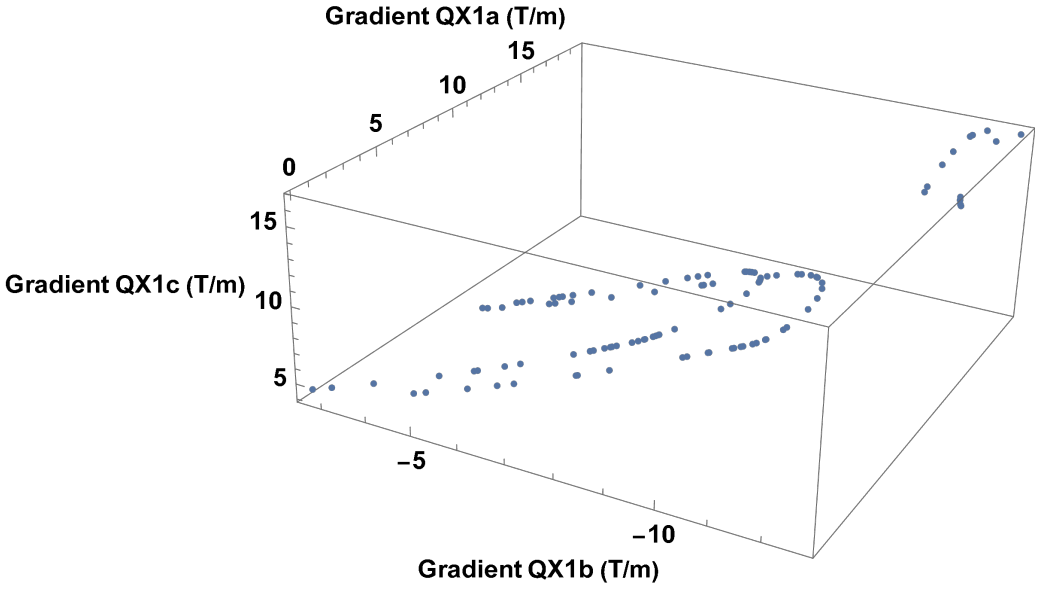

Figure 43: Combinations of quadrupole gradients which yield a simultaneous horizontal and vertical waist in the beam at HXB1

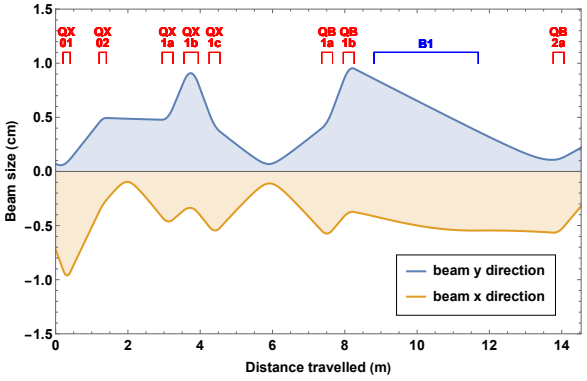

(a) Default settings: QX1a = 10.7 T m^{-1}, QX1b = −9.96 T m^{-1}, QX1c = 10.06 T m^{-1}.

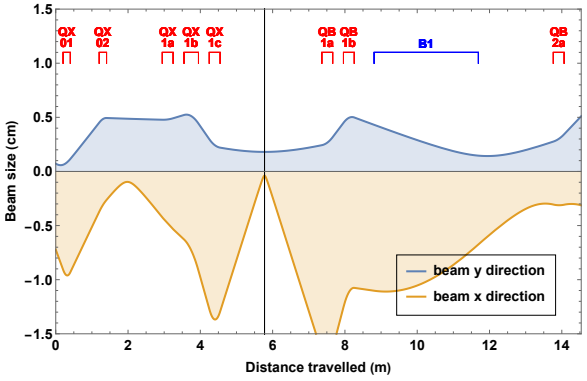

(b) QX1a = 1.52 T m^{-1}, QX1b = −5.97 T m^{-1}, QX1c = 11.4 T m^{-1}

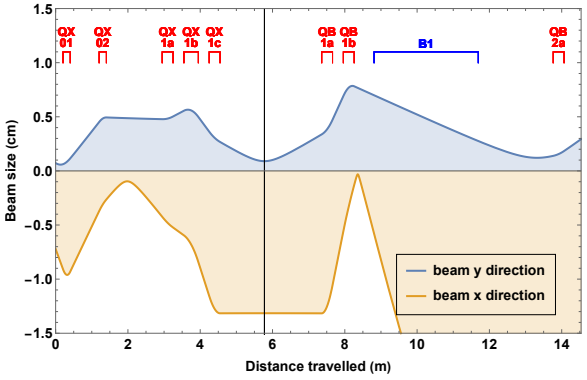

(c) QX1a = 2.58 T m^{-1}, QX1b = −5.90 T m^{-1}, QX1c = 5.65 T m^{-1}

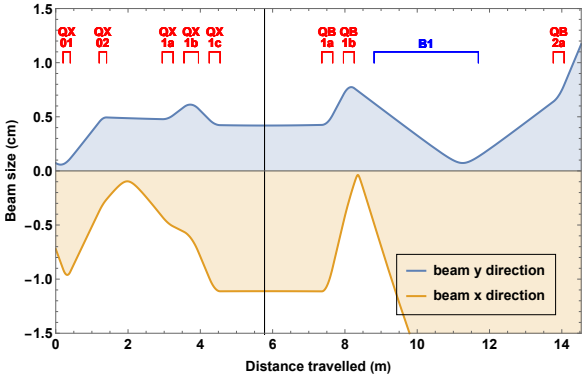

(d) QX1a = 3.64 T m^{-1}, QX1b = −5.03 T m^{-1}, QX1c = 5.10 T m^{-1}

Figure 44: Beam trajectory using the default quadrupole gradients compared to the beam trajectory using gradients obtained from finding a simultaneous horizontal and vertical beam waist at monitor HXB1.

Table 10: Bound of the quadrupole gradients which are used for finding all possible beam waists. Positive gradients indicate focusing in x, negative indicate defocusing in x.

Magnet	Lower bound (T/m)	Upper bound (T/m)
QX1a	0	20
QX1b	-20	0
QX1c	0	20

6 Experimental Results and Discussion

The verification of the steering magnet algorithm was done experimentally in the low energy beamline at KVI, which can be seen in Figure 45. This beamline uses electrostatic elements, instead of magnetic elements. This means that the state vector, defined in Eq. (98), contains the voltages supplied to the steering plates, instead of a current. However, once the voltage has been converted to a steering angle the control loop defined in Section 4.2, will also hold for the electrostatic steering plates. Similarly, the quadrupoles are also electrostatic, but by converting the voltage to a quadrupole strength k, all the equations defined earlier will still hold. To estimate the performance of the algorithm two experiments were performed. In the first experiment, the accuracy of Eq. (90) is determined, in the second experiment the accuracy of the quadrupole variation method was determined.

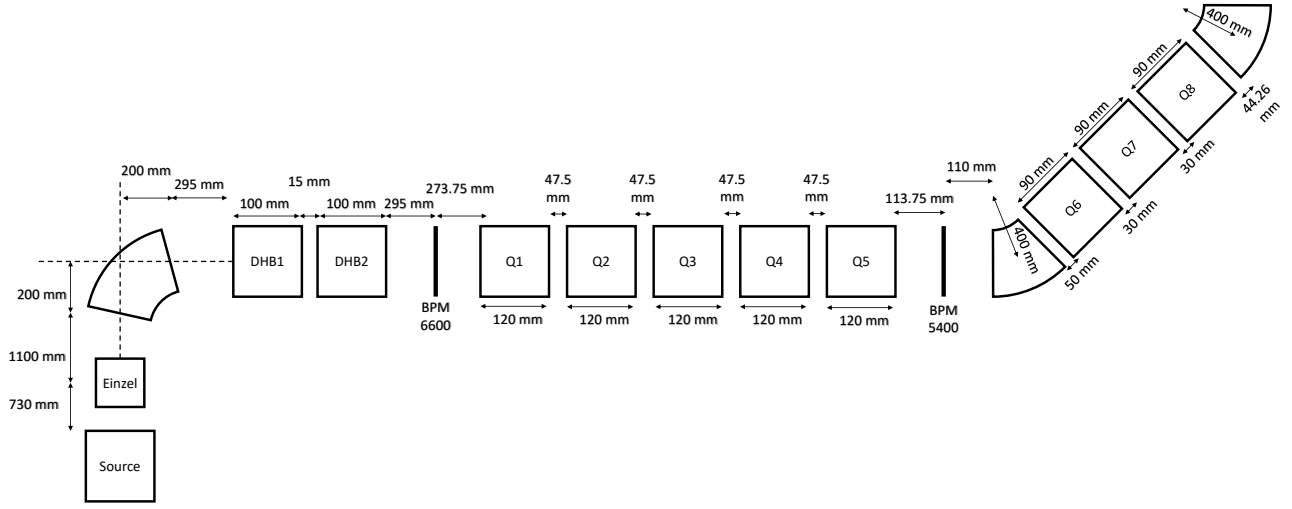

Figure 45: Layout of the low energy beamline, DHB1 and DHB2 are steering plates, Q1 through Q8 are quadrupoles.

6.1 Verifying the Plant Description

The following equation was used to convert the applied voltage to the steering magnet to the bending angle

$$\alpha = 29.96 \frac{L_s}{2V_a} \Delta V \tag{158}$$

where α is the bending angle in radians, L_s is the length of the steering plate in metres, V_a is the accelerating voltage of the ions in volts, and ΔV is the voltage across the steering plates in volts, the factor 29.96 was obtained by solving Poisson's equation of electrostatics for the steering plate geometry. The relevant values for the beamline are given in Table 12.

For the experiment the change in beam position at monitor 6600 was measured while varying the voltages on steering plates DHB1 and DHB2, for the reference value both steering plates were set at a voltage of 0 V, according to Eq. (90) the change in position Δx is then given by

$$\Delta x = L_1\alpha_1 + L_2\alpha_2. \tag{159}$$

Table 11 shows the results of this experiment compared to the predictions from the model. It is observed that the experimental Δx values are not equal in magnitude for voltages with opposite polarity, while this is predicted for the model. By adding 10 different noise-only profiles to a measurement and calculating Δx for each case the standard deviation of Δx was calculated and was estimated to be ± 0.03 mm. Therefore measurement uncertainty cannot explain this difference.

This asymmetry in the experimental Δx values could also occur if part of the beam was blocked by one of the elements in the beamline during some of the measurements. However, the mean and standard deviation of the intensity of the measured profiles is 5561 ± 233, since the standard deviation is small it is unlikely that this is the case. Therefore it is still unclear why the asymmetry occurs. For future experiments, it is recommended to sweep across a larger range of voltages to see if a linear trend can be observed which is equal to the trend predicted by the model.

It can also be seen that the model values deviate between 2.30%-23.0% from the experimental values. It is difficult to say if this error is due to errors in our model, or due to the same reason that the asymmetry in the measurements occurs. Errors in the model are most likely due to an incorrect value of L_1 and L_2, the technical drawings which were used to obtain these values were incomplete, which means that these values needed to be obtained by comparing multiple drawings, which might have introduced some error in the values. To check these values measurements should be done across a larger range of bending values. According to Eq. (159), a plane can be fitted to the datapoints, from which L_1 and L_2 can be extracted.

Finally, for future experiments, it is also recommended to take measurements where the voltages applied DHB1 and DHB2 are varied at the same time. From these measurements, it can be investigated whether there are any interaction effects between the steering magnets, which are not predicted by our model.

Table 11: Comparison of the change in position Δx measured at monitor 6600 for the experiment and the values predicted from the model. Voltage was only applied to one steering plate at a time.

Plate voltage ΔV (V)	Experimental Δx (mm)	Model Δx (mm)	Relative error (%)
DHB1 +50	1.78	1.37	23.0
DHB1 −50	−1.57	−1.37	12.6
DHB2 +50	1.14	1.03	10.0
DHB2 −50	−1.05	−1.03	2.30

Table 12: Values used in the experimental setup, L_{s1} and L_{s2} are the length of the steering plates DHB1 and DHB2 respectively.

Experiment Parameters	Value	Unit
V_a	25150	V
L_1	460	mm
L_2	345	mm
L_{s1}	100	mm
L_{s2}	100	mm

6.2 Accuracy of Quadrupole Variation Method

To check the accuracy of the quadrupole variation method the voltages applied to the quadrupoles Q1 through Q5 were changed and the beam position was measured at profile monitor 5400, this position was then used to calculate the initial beam position and angle, x_0 and x_0', at monitor 6600. The quadrupole focusing strength k for an electrostatic quadrupole is given by [1]

$$k = \frac{2|V_0|}{a^2}\frac{1}{(E\rho)_0} \tag{160}$$

where V_0 is the voltage applied to the quadrupole plates, a is the radial distance from the pole tips to the center of the quadrupole, and $(E\rho)_0$ is the electric rigidity of the particle, as defined in Eq. (2). Using this definition of k, the transfer matrices of the quadrupoles are given by Eqs. (48) and (49). The experiment data is given in Table 13.

First x_0 and x_0' were determined using all of the measurements, the resulting values and standard errors are $x_0 = (-0.26 \pm 0.02)\,\text{cm}$ and $x_0' = (3.2 \pm 0.2)\,\text{mrad}$. Next, to investigate a possible offset of the profile monitor, a constant offset was included in the fitting procedure. In this case the estimated beam parameters are equal to $x_0 = (-0.18 \pm 0.06)\,\text{cm}$ and $x_0' = (1.4 \pm 1.0)\,\text{mrad}$. The offset itself was determined to be $(0.12 \pm 0.07)\,\text{cm}$. From this it can be observed that the measured values of x_0 and x_0' are sensitive to small misalignments of the beam profile monitor.

To estimate the uncertainty in the measurements of x_0 and x_0' during the tuning process, the quadrupole variation calculations were also done using two sets of quadrupole settings at a time. For this, the first setting was always taken to have all quadrupole voltages set to zero, the second setting was scanned through the other measurement in Table 13. No constant offset of monitor 6600 was included in the fitting. The calculated values can be seen in Figure 46, the sensitivity coefficients are also included in the figure. Using the same definitions as in Eq. (128), these are defined as

$$\begin{aligned} \text{Sensitivity } x_0 &= \sqrt{\left(\frac{\partial x_0}{\partial x_1}\right)^2 + \left(\frac{\partial x_0}{\partial x_2}\right)^2} \\ \text{Sensitivity } x_0' &= \sqrt{\left(\frac{\partial x_0'}{\partial x_1}\right)^2 + \left(\frac{\partial x_0'}{\partial x_2}\right)^2} \end{aligned} \tag{161}$$

From the figure, it can be seen that the spread of the data is quite significant. However, the datapoints which seem to be outliers also have a high sensitivity to the measured positions at monitor 6600, which would explain why they deviate from the reference point.

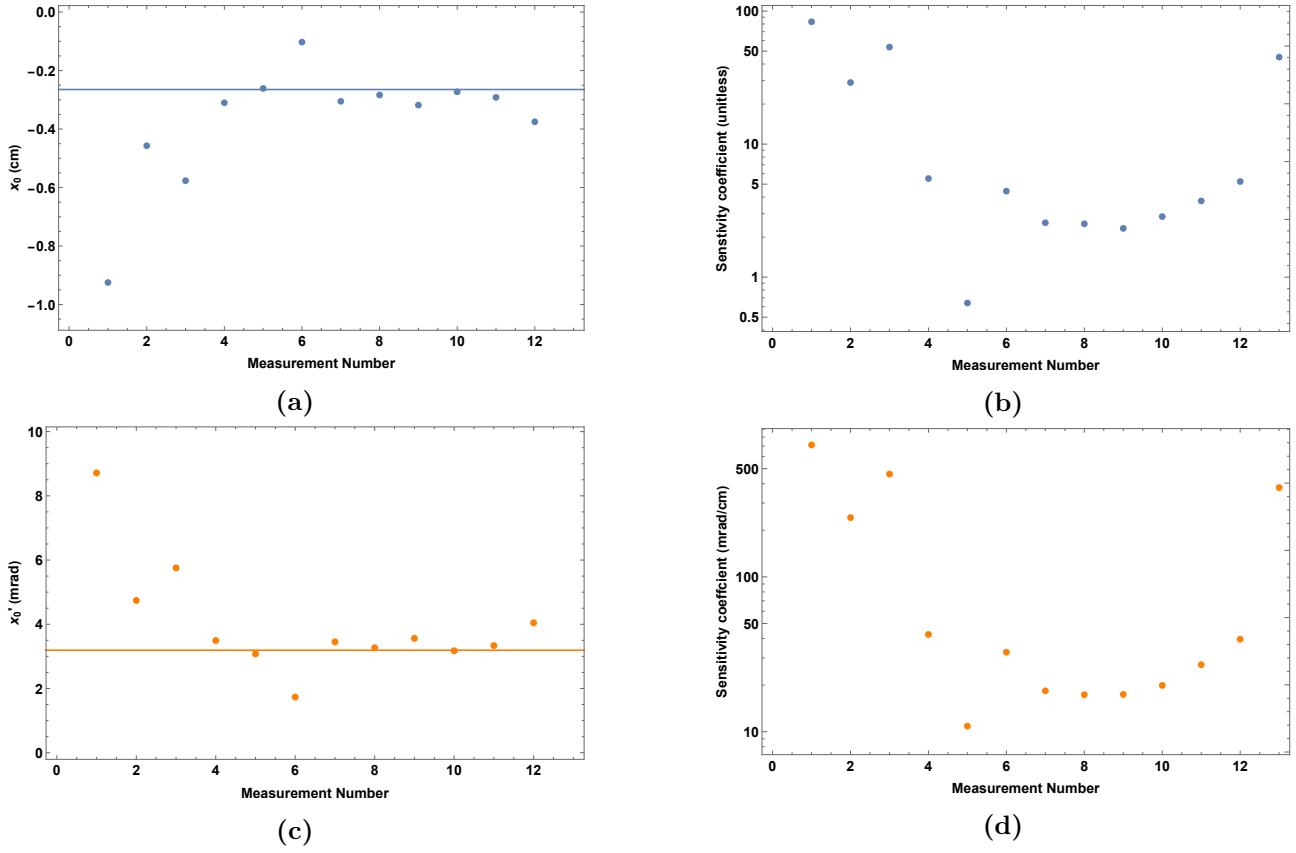

Figure 46: a) and b) show the beam centroid position measured using two sets of quadrupole settings and the associated sensitivity coefficients. c) and d) show the beam centroid angle measured using two sets of quadrupole settings and the associated sensitivity coefficients. The solid lines show the values calculated by including all measurements.

Another observation that can be made from the points is that the value for x_0 and x_0' seem to mirror each other, this is an indication that there is a high correlation between the determined x_0 and x_0'

values. This can be checked by looking at the confidence ellipses for x_0 and x_0', in Figure 47, these include all of the measured datapoints. It can be seen that the ellipse is tilted, which indicates a correlation in x_0 and x_0'. These correlations can arise from the fitting equation, the distribution of the independent data, or the experimental uncertainties [12]. To lower the correlation, and increase the accuracy of the measurements, more measurements could be taken. Furthermore, the quadrupole voltages should be chosen such that for some of the measurements $R_{11} = 0$ or $R_{12} = 0$. For those measurements, only x_0 or x_0' will contribute to the value of the beam centroid position. Therefore including these in the fit should reduce the correlation of the fitted parameters.

values corresponding to the individual measurements are spread out as much as possible since this increases the quality of the fit.

Another method to decrease this correlation is to include information of other beam profile monitors. Since x_0 and x_0' are measured at monitor 6600, it is possible to directly measure x_0 using monitor 6600, if the uncertainty of this measurement is taken into account it can serve as a constraint for the fitting of x_0 and x_0'. For the experiment x_0 at monitor 6600 was determined to be (0.01 ± 0.10) cm, where the error is an estimation based on the uncertainty in beam monitor position. Using this as a constraint in the fit gives $x_0 = (-0.11 \pm 0.05)$ cm and $x_0' = (2.13 \pm 0.50)$ mrad. If a constant monitor offset is used, $x_0 = (-0.11 \pm 0.06)$ cm and $x_0' = (0.06 \pm 1.10)$ mrad, the offset itself is fitted to be (0.22 ± 0.08) cm. The standard errors for the fit using the constraint were taken equal to the square root of the diagonal elements of the covariance matrix. It is observed that the associated standard errors of the determined values are larger than when not including a constraint on x_0.

For future experiments, the used voltages of the quadrupoles should be chosen more carefully to generate measured data which allows fitting with a lower correlation between x_0 and x_0'. Also, it should be investigated whether it would be possible to measure the positional misalignment of the beam monitors mechanically, to increase the accuracy of the fitted values.

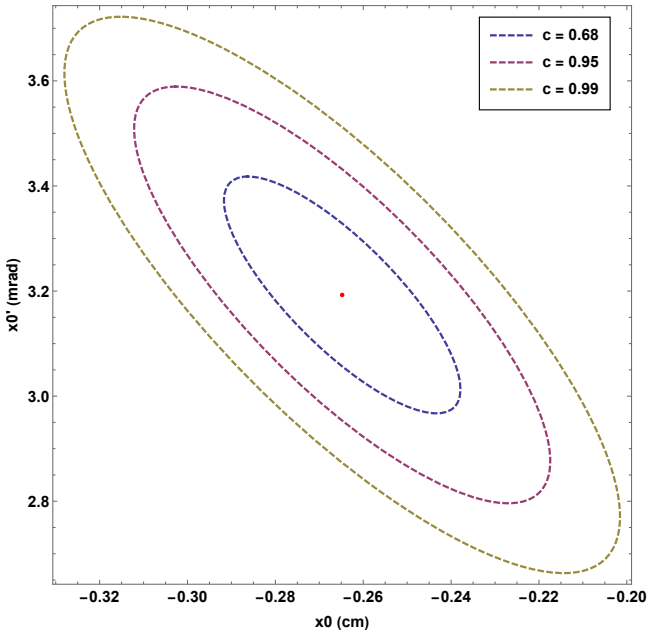

Figure 47: Confidence ellipse of x_0 and x_0', three levels are shown for a confidence interval of 68%, 95% and 99%.

Table 13: Experimental results of the quadrupole variation method, the voltages listed here are the voltages given to the horizontal plates of the quadrupoles, positive voltages indicate focusing in the horizontal direction, while negative indicate defocusing. The position is the horizontal position, given with respect to the center of the beam profile monitor.

Voltage Q1 (V)	Voltage Q2 (V)	Voltage Q3 (V)	Voltage Q4 (V)	Voltage Q5 (V)	Position (mm)
0	0	0	0	0	1.01
0	0	0	0	−170	0.95
0	0	0	0	430	0.97
0	0	0	−70	0	0.92
0	0	264	0	0	1.41
0	1147	0	0	0	3.97
129	0	0	0	0	1.20
−390	1146	−1185	470	−170	2.14
−390	1146	−1185	470	−470	2.27
−390	1146	−1185	670	−170	2.10
−390	1146	−1185	270	−170	2.09
−390	1146	−1385	470	−170	1.87
−390	1046	−1185	470	−170	1.77
−590	1146	−1185	470	−170	1.83

7 Conclusion

An algorithm was developed for automatic alignment of the beam centroid with the reference trajectory using steering and bending magnets in the system. The system is described using a first order description of the ion optics. The algorithm is based on a state-space representation of the system and uses a discrete control strategy. Measurements of the beam conditions can be done using the quadrupole variation method. Under ideal conditions, the algorithm has been shown to converge in one step. In the case that the estimated system parameters deviate slightly from the real system parameters, the control algorithm will still be stable but will converge at a slower rate.

Positional misalignment of quadrupoles used in the quadrupole variation method will result in a steady state error of the beam position and angle. The magnitude of the error depends on the beamline geometry, the gradients used during measurements, and the magnitude of the misalignments. If the misalignments are known it is possible to compensate for their effect. A method for measuring the displacement of the quadrupoles using the beam and the beam profile monitors was introduced. It was shown that it is possible to measure the displacements with reasonable accuracy if the uncertainty in the beam centroid position measured on the beam profile monitors is equal or smaller than the displacements themselves.

Misalignment effects of the steering magnets and combined function magnets were also considered. It has been shown that misalignment of these elements has the same effect on the system dynamics as a different initial beam centroid position and angle. Therefore it does not affect the steady state solution or the convergence rate of the algorithm.

When quadrupole misalignments are present, it is not possible to align the beam centroid with the reference trajectory everywhere in the system. For these cases, an objective function was defined, which can be minimized to find the initial beam conditions which yield the smallest average distance from the beam centroid to the quadrupole axis. To minimize the objective function, the misalignments of the quadrupoles need to be known. Since the misalignments are currently unknown the algorithms were tested under the assumption that all quadrupole misalignments are zero. For the steering magnets which steer the beam in the x-coordinate this assumption led to satisfactory performance. For the steering magnets for the y-coordinate this assumption resulted in poor performance due to two consecutive defocusing quadrupoles. However, it was also shown that the performance can be improved by using a specific set of measurements involving the misalignments. The same analysis was done for the bending magnets, where it was shown that the largest source of error originated from the unknown beam centroid and position at the entrance of the bending magnet.

Initial investigations into automatically controlling the beam size using the quadrupoles were also done. It was shown that having a beam waist at a specific location in the beamline is an insufficient criterion to find the optimal quadrupole gradient settings for a section of the beamline containing three or more quadrupoles. To create this algorithm in the future it might be necessary to do a simultaneous optimization of the entire beamline involving all quadrupoles and all beam monitors, instead of tuning one section at a time like for the steering and bending magnets.

Initial experiments have shown promising results for the mathematical plant description and measurements using the quadrupole variation method. Future experiments for the steering plates should

include more measurements to investigate asymmetry in the plant behaviour. This will also make the comparison to the theoretical model easier. For the quadrupole variation method, it was found that picking the correct quadrupole focusing strengths during measurements is important to decrease the correlation between and increase the precision of the calculated x_0 and x_0' values. Furthermore, it was found that if a second beam monitor is present at the location at which x_0 and x_0' are being measured, the correlation effect can be compensated by including the value of x_0 measured directly at that monitor.

To verify the performance of the algorithm it should be tested in the beamline at the AGOR facility. Once the experimental validations have taken place the algorithm can be implemented in the control system of the beamline. The algorithms that were developed should reduce the tuning time significantly. Also since the algorithm follows the same steps for every tuning procedure, the beams tuned using the algorithm should show a high degree of reproducibility.

8 Appendix

A Approximation Steering magnet

In this section a comparison is made between the real trajectory of particle traversing a steering magnet and an approximated trajectory using an instantaneous kick at the center of the magnet, Figure 48 shows a graphical comparison. We take x_0' and x_1' as angles, instead of their definition in Eq. (13). Furthermore, the convention will be used that a positive α bends the beam in the direction of negative x. This is opposite to the convention used in (91) where a positive α bend the beam to positive x. Taking this into account it is possible to use basic trigonometry to find the following exact solution for the position and angle at the exit

$$\begin{aligned} x_1 &= x_0 - \rho_0 \cos\left(x_0'\right) + \rho_0 \cos\left(x_0'\right) \cos\left(\alpha\right) + \rho_0 \sin\left(x_0'\right) \sin\left(\alpha\right) \\ x_1' &= x_0' - \alpha \end{aligned} \tag{162}$$

The approximate solution can be found using two drift matrices with length $L/2$ and the matrix equation (91), note that we take a positive α to bend the beam downwards which is the same convention as in (162)

$$\begin{aligned} x_1 &= x_0 + L\left(x_0' - \frac{\alpha}{2}\right) \\ x_1' &= x_0' - \alpha \end{aligned} \tag{163}$$

eqs. (162) and (163) show that the calculated angle using both methods is the same. To compare the calculated position, the following formula for L is derived using trigonometry and the equation for a circular segment [13]

$$L = 2\rho_0 \sin\left(\frac{\alpha}{2}\right) \cos\left(x_0' - \frac{\alpha}{2}\right) \tag{164}$$

substituting this in Eq. 163 gives

$$x_1 = x_0 + 2\rho_0 \sin\left(\frac{\alpha}{2}\right) \cos\left(x_0' - \frac{\alpha}{2}\right)\left(x_0' - \frac{\alpha}{2}\right) \tag{165}$$

this can be simplified using the following small-angle approximations

$$\begin{aligned} \sin\frac{\alpha}{2} &\approx \frac{\alpha}{2} \\ \cos\left(x_0' - \frac{\alpha}{2}\right) &\approx 1 \end{aligned} \tag{166}$$

which gives for the instantaneous kick approximation

$$x_1 = x_0 + \alpha\rho_0 x_0' - \frac{\alpha^2\rho_0}{2}. \tag{167}$$

Next Eq. (162), which is the exact derivation, is also simplified using the following small angle approximations

$$\begin{aligned} \cos\left(x_0'\right) &\approx 1 \\ \cos\left(\alpha\right) &\approx 1 - \frac{\alpha^2}{2} \\ \sin\left(x_0'\right) &\approx x_0' \\ \sin\left(\alpha\right) &\approx \alpha \end{aligned} \tag{168}$$

which gives

$$x_1 = x_0 + \alpha\rho_0 x_0' - \frac{\alpha^2\rho_0}{2} \tag{169}$$

The approximate and exact equations are now equal which means that in the case that the small-angle approximations are valid the simplified equation can be used. Since for the steering magnet, α and x_0' will be in the order of mrad the approximation will always hold.

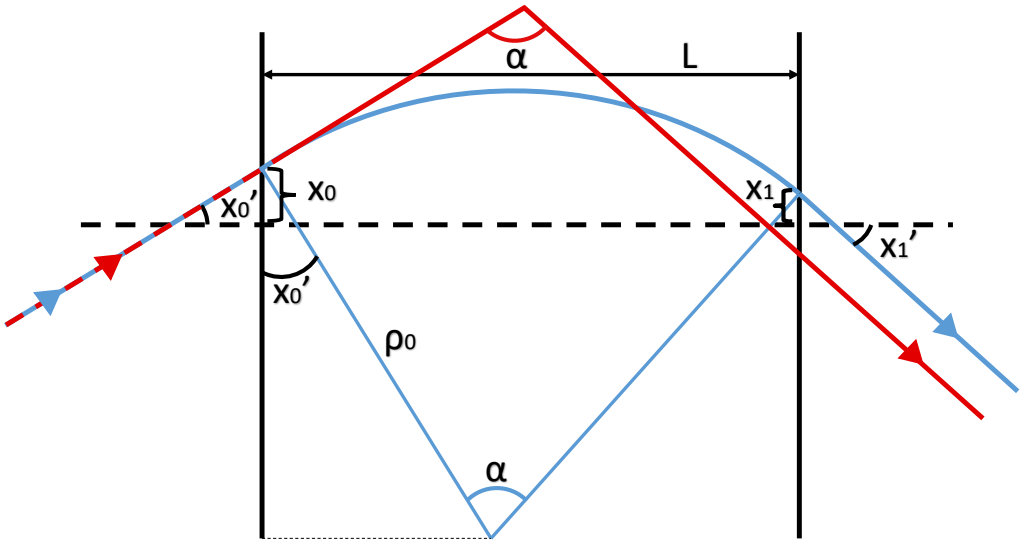

Figure 48: Comparison of the trajectory of an individual particle through a steering magnet (blue) and the approximated trajectory using an instantaneous kick (red) using a hard edge model of the magnet.

B Bending Magnet Derivation

To simplify the derivation it is assumed that x'_0 and x'_1 are defined as angles, instead of the definition in Eq. (13), which is allowed in a linear approximation. The equations will be derived according to Figure 49. We first define our coordinate system with the origin in the center of the magnet with incorrect settings, given by C1 in the figure. The vector containing spatial coordinates of the described particle will be denoted with an arrow over top to avoid confusion with the $\boldsymbol{x}$ vector as defined in Eq. (16). The spatial coordinates of the described particle in C1 when entering the magnet are given by $\overrightarrow{\boldsymbol{x}_0}$

$$\overrightarrow{\boldsymbol{x}_0}(C1) = \begin{pmatrix} -\rho \sin x'_0 \\ \rho \cos x'_0 \end{pmatrix} \tag{170}$$

To find the spatial coordinates in C1 of the described particle at the exit of the magnet $\overrightarrow{\boldsymbol{x}_0}(C1)$ is rotated by the angle α, this position is denoted by $\overrightarrow{\boldsymbol{x}_1}(C1)$

$$\overrightarrow{\boldsymbol{x}_1}(C1) = \begin{pmatrix} \cos\alpha & \sin\alpha \\ -\sin\alpha & \cos\alpha \end{pmatrix} \begin{bmatrix} -\rho \sin x'_0 \\ \rho \cos x'_0 \end{bmatrix} = \begin{bmatrix} -\rho\cos(\alpha)\sin(x'_0) + \rho\cos(x'_0)\sin(\alpha) \\ \rho\cos(x'_0)\cos(\alpha) + \rho\sin(x'_0)\sin(\alpha) \end{bmatrix} \tag{171}$$

these coordinates need to be expressed in the reference particle coordinate system, indicated with C2, this is done by a combination of translation vector P_{tran} connecting the coordinate systems and a rotation matrix $R_{rot}(\alpha_0)$.

$$\begin{aligned} \overrightarrow{\boldsymbol{x}_1}(C2) &= R_{rot}\left(\overrightarrow{\boldsymbol{x}_1}(C1) - P_{trans}\right) \\ &= \begin{pmatrix} \cos\alpha_0 & -\sin\alpha_0 \\ \sin\alpha_0 & \cos\alpha_0 \end{pmatrix} \left(\begin{pmatrix} -\rho\cos(\alpha)\sin(x'_0) + \rho\cos(x'_0)\sin(\alpha) \\ \rho\cos(x'_0)\cos(\alpha) + \rho\sin(x'_0)\sin(\alpha) \end{pmatrix} \right. \\ &\qquad \left. - \begin{pmatrix} -\rho\sin(x'_0) + \rho_0\sin(\alpha_0) \\ -\rho_0 - x_0 + \rho\cos(x'_0) + \rho_0\cos(\alpha_0) \end{pmatrix} \right) \\ &= \begin{pmatrix} -\sin(\alpha_0)[\rho_0 + x_0 - \rho\cos(x'_0) + \rho\cos(x'_0)\cos(\alpha) - \rho_0\cos(\alpha_0) + \rho\sin(x'_0)\sin(\alpha)] \\ \qquad + \cos(\alpha_0)(\rho\sin(x'_0) - \rho\cos(\alpha)\sin(x'_0) + \rho\cos(x'_0)\sin(\alpha) - \rho_0\sin(\alpha_0)) \\ \cos(\alpha_0)[\rho_0 + x_0 - \rho\cos(x'_0) + \rho\cos(x'_0)\cos(\alpha) - \rho_0\cos(\alpha_0) + \rho\sin(x'_0)\sin(\alpha)] \\ \qquad + \sin(\alpha_0)[\rho\sin(x'_0) - \rho\cos(\alpha)\sin(x'_0) + \rho\cos(x'_0)\sin(\alpha) - \rho_0\sin(\alpha_0)] \end{pmatrix} \end{aligned} \tag{172}$$

which can be simplified using trigonometric identities

$$\overrightarrow{\boldsymbol{x}_1}(C2) = \begin{pmatrix} -(\rho_0 + x_0)\sin(\alpha_0) + \rho(\sin(x'_0 + \alpha_0) - \sin(x'_0 - \alpha + \alpha_0)) \\ -\rho_0 + (\rho_0 + x_0)\cos(\alpha_0) - \rho\cos(x'_0 + \alpha_0) + \rho\cos(x'_0 - \alpha + \alpha_0) \end{pmatrix} \tag{173}$$

α can be derived by the fact that at the exit of the magnet the first entry of $\overrightarrow{\boldsymbol{x}_1}(C2)$ should be zero

$$\alpha = x_0' + \alpha_0 - \arcsin\left(\frac{-\rho_0 \sin(\alpha_0) - x_0 \sin(\alpha_0) + \rho \sin(x_0' + \alpha_0)}{\rho}\right) \tag{174}$$

By summing the angles at the exit the following equation for x_1' can be derived

$$\begin{aligned} x_1' &= x_0' + \alpha_0 - \alpha \\ x_1' &= \arcsin\left(\frac{-\rho_0 \sin(\alpha_0) - x_0 \sin(\alpha_0) + \rho \sin(x_0' + \alpha_0)}{\rho}\right) \end{aligned} \tag{175}$$

Using small-angle approximations for x_1' and x_0' allows the equation to be further simplified

$$\begin{aligned} x_1' &= \arcsin\left(\frac{-\rho_0 \sin(\alpha_0) - x_0 \sin(\alpha_0) + \rho \sin(x_0' + \alpha_0)}{\rho}\right) \\ \sin x_1' &= \frac{-\rho_0 \sin(\alpha_0) - x_0 \sin(\alpha_0) + \rho \sin(x_0' + \alpha_0)}{\rho} \\ x_1' &\approx \frac{-\rho_0 \sin(\alpha_0)}{\rho} - \frac{x_0 \sin(\alpha_0)}{\rho} + \sin\left(x_0' + \alpha_0\right) \\ &= \frac{-\rho_0 \sin(\alpha_0)}{\rho} - \frac{x_0 \sin(\alpha_0)}{\rho} + \sin x_0' \cos\alpha_0 + \cos x_0' \sin\alpha_0 \\ &\approx \frac{-\rho_0 \sin(\alpha_0)}{\rho} - \frac{x_0 \sin(\alpha_0)}{\rho} + x_0' \cos\alpha + \sin\alpha_0 \\ &= -\frac{\sin\alpha_0}{\rho} x_0 + \cos(\alpha_0) x_0' + \sin\alpha_0 \frac{\rho - \rho_0}{\rho} \end{aligned} \tag{176}$$

Next x_1 is derived which is the second component of $\boldsymbol{x}_1(C2)$, again small-angle approximations are used

$$\begin{aligned} x_1 &= -\rho_0 + (\rho_0 + x_0)\cos(\alpha_0) - \rho\cos\left(x_0' + \alpha_0\right) + \rho\cos\left(x_0' - \alpha + \alpha_0\right) \\ x_1 &= -\rho_0 + \rho_0\cos(\alpha_0) + x_0\cos(\alpha_0) - \rho\left(\cos(x_0')\cos(\alpha_0) - \sin(x_0')\sin(\alpha_0)\right) + \rho\cos(x_1') \\ x_1 &\approx -\rho_0 + \rho_0\cos(\alpha_0) + x_0\cos(\alpha_0) - \rho\left(\cos(\alpha_0) - x_0'\sin(\alpha_0)\right) + \rho \\ &= \cos(\alpha_0)x_0 + \rho\sin(\alpha_0)x_0' + (1 - \cos\alpha_0)\frac{\rho - \rho_0}{\rho} \end{aligned} \tag{177}$$

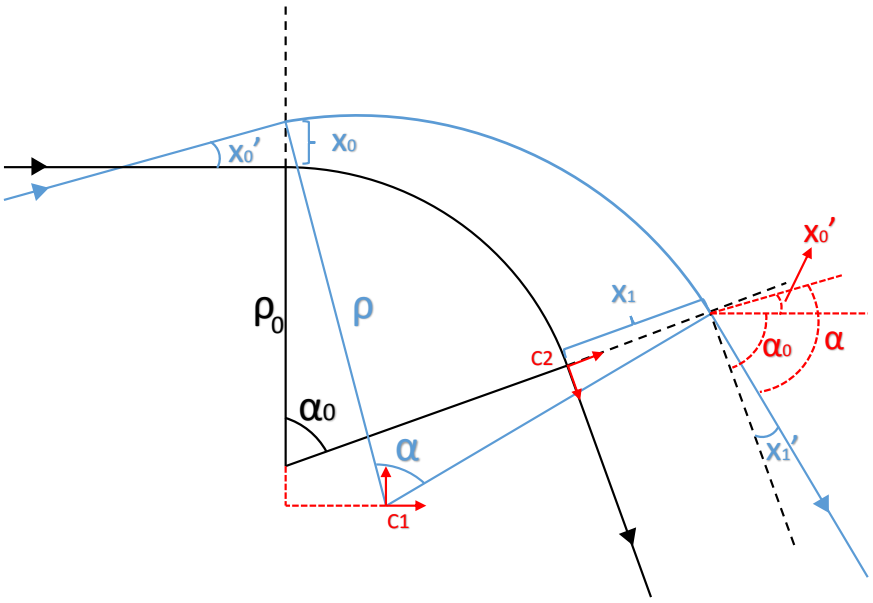

Figure 49: Image used for derivation of misaligned bending magnet equations.

C Approximation Combined Function Magnet

In this section the convention will be used that a positive α bend the beam to the negative x-direction, this is opposite to the convention in Eqs. (95) and (96) where a positive α bend the beam into the positve x-direction. The equation for a combined function magnet is derived, the exact solution is given by Eq. (56).

$$\begin{aligned} x_1 &= x_0 \cos\sqrt{1-n}\alpha + x_0' \frac{\rho_0 \sin\sqrt{1-n}\alpha}{\sqrt{1-n}} \\ x_1' &= x_0 \frac{\sqrt{1-n}\sin\sqrt{1-n}\alpha}{\rho_0} + x_0' \cos\sqrt{1-n}\alpha \end{aligned} \tag{178}$$

these values are for a coordinate system that follows the reference trajectory that is bent by the dipole component of the field. To derive the equations for correcting the beam centroid they should be expressed in the coordinate system of a particle that follows a straight line, which is illustrated in Figure 50. Also in the transfer matrix it is assumed that the central axis of the quadrupole component follows the reference trajectory, while the central axis of the quadrupoles in the beamline follow a straigh line. However, since the bending angle is very small, the error due to this effect is very small. To transform the equation to the correct coordinate system they are rotated with an angle α and

translated, we again denote the positional vector with an arrow over top, the position of a described particle entering the magnet in coordinate system C2, ($\overrightarrow{\boldsymbol{x}_1}(C2)$), is given by

$$\begin{aligned}\overrightarrow{\boldsymbol{x}_1}(C2) &= R_{rot}\overrightarrow{\boldsymbol{x}_1}(C1) - P_{trans} \\ &= \begin{pmatrix}\cos\alpha & \sin\alpha \\ -\sin\alpha & \cos\alpha\end{pmatrix}\begin{bmatrix}0 \\ x_0\cos\sqrt{1-n}\alpha + x_0'\frac{\rho_0\sin\sqrt{1-n}\alpha}{\sqrt{1-n}}\end{bmatrix} - \begin{bmatrix}0 \\ -2\rho_0\sin^2\frac{\alpha}{2}\end{bmatrix} \\ &= \begin{bmatrix}\sin(\alpha)\left(x_0\cos(\sqrt{1-n}\alpha) + x_0'\frac{\rho_0\sin\sqrt{1-n}\alpha}{\sqrt{1-n}}\right) \\ \cos(\alpha)\left(x_0\cos\left(\sqrt{1-n}\alpha\right) + x_0'\frac{\rho_0\sin\sqrt{1-n}\alpha}{\sqrt{1-n}}\right) - 2\rho_0\sin^2\frac{\alpha}{2}\end{bmatrix}\end{aligned} \tag{179}$$

where $\overrightarrow{\boldsymbol{x}_1}(C1)$ is the positional vector of particle entering the magnet expressed in coordinate system (C2). The first component of $\overrightarrow{\boldsymbol{x}_1}(C1)$ gives the z coordinate in coordinate system C_2, thus can be ignored, the second component gives the x_1 value, which will be simplified. To get remove n the following substitution is used

$$n = k\rho_0^2 \tag{180}$$

where k is the same parameter as in Eq. (46), this yields

$$x_1 = \cos(\alpha)\left(x_0\cos\left(\sqrt{1-k\rho_0^2}\alpha\right) + x_0'\frac{\rho_0\sin\sqrt{1-k\rho_0^2}\alpha}{\sqrt{1-k\rho_0^2}}\right) - 2\rho_0\sin^2\frac{\alpha}{2} \tag{181}$$

by using the linear approximation the following simplification can be made

$$\sqrt{1-k\rho_0^2}\alpha = \sqrt{\alpha^2 - k\alpha^2\rho^2} = \sqrt{\alpha^2 - kL^2} \approx \sqrt{-k}L \tag{182}$$

using the fact that the magnet length L is approximately equal to

$$L = 2\rho_0\sin\left(\frac{\alpha}{2}\right)\cos(\alpha) \approx \alpha\rho_0 \tag{183}$$

using these results in Eq. (181) gives

$$\begin{aligned}x_1 &= \cos(\alpha)\left(x_0\cos\left(\sqrt{-k}L\right) + x_0'\frac{\rho_0\sin\sqrt{-k}L}{\frac{1}{\alpha}\sqrt{-k}L}\right) - 2\rho_0\sin^2\frac{\alpha}{2} \\ &= \cos(\alpha)\left(x_0\cos\left(\sqrt{-k}L\right) + x_0'\frac{\sin\sqrt{-k}L}{\sqrt{-k}}\right) - 2\rho_0\sin^2\frac{\alpha}{2}\end{aligned} \tag{184}$$

Using the small angle approximations $\cos(\alpha) = 1$ and $sin\alpha/2 = \alpha/2$

$$x_1 = x_0 \cos\left(\sqrt{-k}L\right) + x_0' \frac{\sin\sqrt{-k}L}{\sqrt{-k}} - \rho_0 \alpha \sin\frac{\alpha}{2} \tag{185}$$

which using Eqs. (51) and (180) can be written as

$$x_1 = x_0 \cos\left(\sqrt{-k}L\right) + x_0' \frac{\sin\sqrt{-k}L}{\sqrt{-k}} - \alpha \frac{\sqrt{n}\sin\frac{\sqrt{-k}L}{2\sqrt{n}}}{\sqrt{-k}} \tag{186}$$

if $\alpha\sqrt{n}/2 \ll 1$, then this can be simplified using $\sin\frac{\sqrt{k}L}{2\sqrt{n}} \approx \sin\frac{\sqrt{k}L}{2}/\sqrt{n}$

$$x_1 = x_0 \cos\left(\sqrt{-k}L\right) + x_0' \frac{\sin\sqrt{-k}L}{\sqrt{-k}} - \alpha \frac{\sin\frac{\sqrt{-k}L}{2}}{\sqrt{-k}} \tag{187}$$

which is the same as Eq. (95).

The angle deviation x_1' in coordinate system C2 is equal to x_1' in coordinate system C1, given in Eq. (178), minus the rotation angle α

$$\begin{aligned} x_1'(C_2) &= x_1'(C_1) - \alpha \\ &= -\alpha - x_0 \frac{\sqrt{1-n}\sin\sqrt{1-n}\alpha}{\rho_0} + x_0' \cos\sqrt{1-n}\alpha \end{aligned} \tag{188}$$

similarly to the position equations, this can be simplfied using Eqs. (180) and (182)

$$x_1' = -\alpha - x_0\sqrt{-k}\sin\sqrt{-k}L + x_0' \cos\sqrt{-k}L \tag{189}$$

this is equal to Eq. (95) under the small angle approximation $\cos\sqrt{k}L/2 = \cos\sqrt{n}\alpha/2 \approx 1$

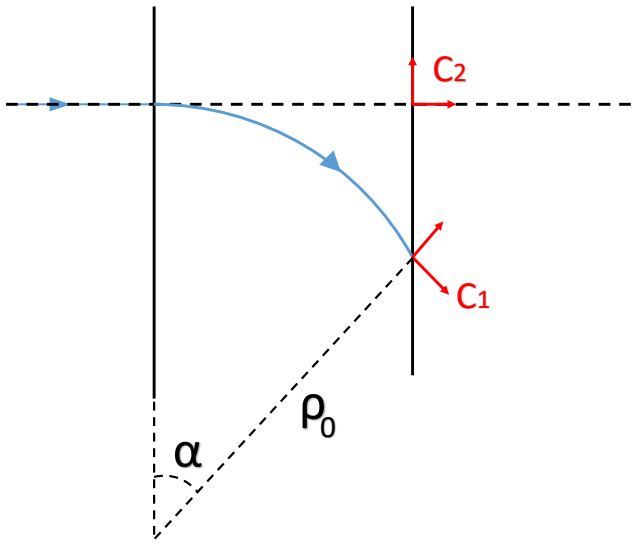

Figure 50: Coordinate system of bent reference trajectory (C_1) and coordinate system of straight reference trajectory (C_2). The reference trajectory is indicated by the blue line.

For a focusing magnet with $n > 1$, the equations from the transfer matrix in Eq. (57) are

$$\begin{aligned} x_1 &= x_0 \cosh\sqrt{|1-n|}\alpha + x_0' \frac{\rho_0 \sinh\sqrt{|1-n|}\alpha}{\sqrt{|1-n|}} \\ x_1' &= x_0 \frac{\sqrt{|1-n|}\sinh\sqrt{|1-n|}\alpha}{\rho_0} + x_0' \cosh\sqrt{|1-n|}\alpha \end{aligned} \tag{190}$$

the value of x_1 in the straight coordinate system is obtained using the same transformation as for Eq. (179)

$$x_1 = \cos\alpha \left(x_0 \cosh\left(\alpha\sqrt{|1-n|}\right) + \frac{x_0'\rho_0 \sinh\alpha\sqrt{|1-n|}}{\sqrt{|1-n|}} \right) - 2\rho_0 \sin^2\frac{\alpha}{2} \tag{191}$$

since the quadrupole is de-focussing in the x-direction, n is equal to

$$n = k\rho_0^2 \tag{192}$$

which is always positive, substituting this gives

$$x_1 = \cos\alpha \left(x_0 \cosh\left(\alpha\sqrt{|1-k\rho_0^2|}\right) + \frac{x_0'\rho_0 \sinh\alpha\sqrt{|1-k\rho_0^2|}}{\sqrt{|1-k\rho_0^2|}} \right) - 2\rho_0 \sin^2\frac{\alpha}{2} \tag{193}$$

which can be simplified using $\alpha \ll 1$

$$\alpha\sqrt{|1-k\rho_0^2|} = \sqrt{|\alpha^2 - k\alpha^2\rho_0^2|} \approx \sqrt{|0-kL^2|} = \sqrt{k}L \tag{194}$$

substituting this gives

$$\begin{aligned} x_1 &= \cos\alpha\left(x_0\cosh\left(\sqrt{k}L\right) + \frac{x_0'\rho_0\sinh\sqrt{k}L}{\frac{1}{\alpha}\sqrt{k}L}\right) - 2\rho_0\sin^2\frac{\alpha}{2} \\ x_1 &= \cos\alpha\left(x_0\cosh\left(\sqrt{k}L\right) + \frac{x_0'\sinh\sqrt{k}L}{\sqrt{k}}\right) - 2\rho_0\sin^2\frac{\alpha}{2} \end{aligned} \tag{195}$$

using the small angle approximations $\cos\alpha \approx 1$ and $\sin\alpha/2 \approx \alpha/2$

$$x_1 = x_0\cosh\left(\sqrt{k}L\right) + \frac{x_0'\sinh\sqrt{k}L}{\sqrt{k}} - \alpha\rho_0\sin\frac{\alpha}{2} \tag{196}$$

which using Eqs. (51) and (180) can be written as

$$x_1 = x_0\cosh\left(\sqrt{k}L\right) + \frac{x_0'\sinh\sqrt{k}L}{\sqrt{k}} - \alpha\frac{\sqrt{n}\sin\frac{\sqrt{-k}L}{2\sqrt{n}}}{\sqrt{-k}} \tag{197}$$

if $\alpha\sqrt{n}/2 \ll 1$, then this can be simplified using $\sin\frac{\sqrt{k}L}{2\sqrt{n}} \approx \sin\frac{\sqrt{k}L}{2}/\sqrt{n}$

$$x_1 = x_0\cosh\left(\sqrt{k}L\right) + \frac{x_0'\sinh\sqrt{k}L}{\sqrt{k}} - \alpha\frac{\sin\frac{\sqrt{k}L}{2}}{\sqrt{k}} \tag{198}$$

using the fact that for $\theta \ll 1, \sin\theta \approx \sinh\theta$

$$x_1 = x_0\cosh\left(\sqrt{k}L\right) + \frac{x_0'\sinh\sqrt{k}L}{\sqrt{k}} - \alpha\frac{\sinh\frac{\sqrt{k}L}{2}}{\sqrt{k}} \tag{199}$$

which holds for $\sqrt{n}\alpha/2 \ll 1$.

For the angle deviation x_1' it is again equal to x_1' in coordinate system C_1, given in Eq. (190), minus the rotation angle α

$$x_1' = -\alpha + x_0\frac{\sqrt{|1-n|}\sinh\alpha\sqrt{|1-n|}}{\rho_0} + x_0'\cosh\alpha\sqrt{|1-n|} \tag{200}$$

which can be simplified similar to the position equations

$$x_1' = -\alpha + x_0\sqrt{k}\sinh\sqrt{k}L + x_0'\cosh\sqrt{k}L \tag{201}$$

which is equal to (96) under the assumption that $\cosh\sqrt{k}L/2 = \cosh\sqrt{n}\alpha/2 \approx 1$

D Derivation of the Effect of a Misaligned Steering Magnet

The derivations in this section is taken from the examples given in [9] of a misaligned bending magnet and quadrupole and adapted for the case of a steering magnet.

An image of a misaligned bending magnet can be seen in Figure 51. As seen in the image, two coordinate systems are defined at both the entrance and exit face of the magnet, these are the coordinate systems of the reference trajectory and the misaligned magnet. The goal is to express the particle vector described in the misaligned coordinate systems in terms of the coordinates in the reference coordinate systems. Starting with the coordinate systems at the entrance face of the magnet the following equation is proposed

$$\boldsymbol{x_f}(0) = \boldsymbol{x}(0) - A_0\boldsymbol{m} + B_0\boldsymbol{x}(0) \tag{202}$$

where $\boldsymbol{x_f}(0)$ and $\boldsymbol{x}(0)$ are the particle vectors described in the misaligned and reference coordinate systems at the entrance face of the magnet, A_0 and B_0 are matrices which need to be derived and $\boldsymbol{m}$ is the misalignment vector given by

$$\boldsymbol{m} = \begin{pmatrix} \delta x \\ \theta x \\ \delta y \\ \theta y \\ \delta z \\ \theta z \end{pmatrix} \tag{203}$$

where δx, δy, δz are the displacements of the magnet in the x, y, and z direction and θx, θy, and θz are the rotations about the x, y, and z axes respectively. All rotations are defined to be positive when rotating in the clockwise direction, looking in the positive direction of the axis. The origin of the rotation axes is the reference trajectory position at the entrance face of the magnet.

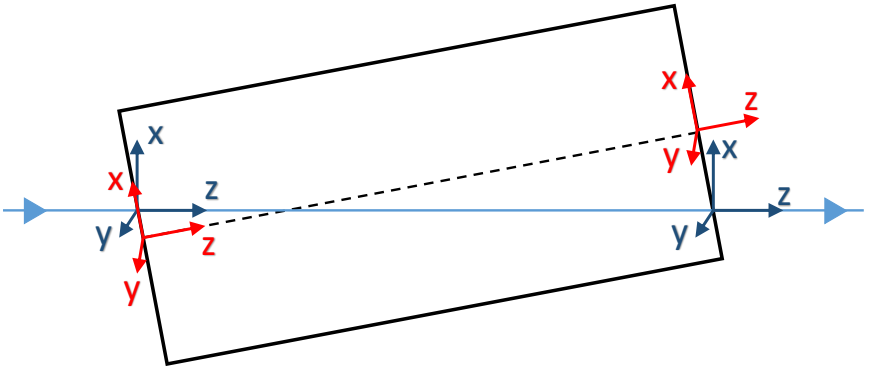

Figure 51: Figure of a misaligned steering magnet, the reference trajectory and coordinate system is indicated in blue, the local coordinate system of the misaligned magnet is indicated in red, image adapted from [9].

First, the effect of rotation of the magnet is considered, the rotation matrices around the x, y, and z axes are given by

$$R_x = \begin{pmatrix} 1 & 0 & 0 \\ 0 & \cos\theta x & \sin\theta x \\ 0 & -\sin\theta x & \cos\theta x \end{pmatrix}, \quad R_y = \begin{pmatrix} \cos\theta y & 0 & -\sin\theta y \\ 0 & 1 & 0 \\ \sin\theta y & 0 & \cos\theta y \end{pmatrix}, \quad R_z = \begin{pmatrix} \cos\theta z & \sin\theta z & 0 \\ -\sin\theta z & \cos\theta z & 0 \\ 0 & 0 & 1 \end{pmatrix} \tag{204}$$

where R_x, R_y, and R_z are the rotation matrices that describe the rotation of a point around the x, y, and z axes. The total effect of the rotations can be found by multiplying these matrices with each other. To simplify the results, the small-angle approximations $\sin\theta = \theta$ and $\cos\theta = 1$ are used, furthermore since the rotation angles are small only first-order effects are included, note that under these assumptions the order of rotation does not matter. The total rotation matrix R_{rot} is then given by

$$R_{rot} = R_x R_y R_z = \begin{pmatrix} 1 & \theta z & -\theta y \\ -\theta z & 1 & \theta x \\ \theta y & -\theta x & 1 \end{pmatrix} \tag{205}$$

using this rotation matrix the contribution of the rotational misalignment to the misaligned coordinates is given by

$$\begin{pmatrix} x_{fr} \\ y_{fr} \\ z_{fr} \end{pmatrix} = \begin{pmatrix} 1 & \theta z & -\theta y \\ -\theta z & 1 & \theta x \\ \theta y & -\theta x & 1 \end{pmatrix} \begin{pmatrix} x \\ y \\ z \end{pmatrix} \tag{206}$$

where the subscript fr indicates the contribution to x_f by the rotational part of the misalignment. The translations of the magnet δx, δy, and δz change the coordinates by the amount of displacement. Furthermore a displacement in z will act as a drift space contributing to x_f and y_f via x' and y'. The contributions of the displacement to the misaligned coordinates, indicates by the subscript fd is given by

$$\begin{aligned} x_{fd} &= -\delta x + x'\delta z \\ y_{fd} &= -\delta y + y'\delta z \\ z_{fd} &= 0 \\ l_f &= l - \delta z \\ \delta_f &= \delta \end{aligned} \tag{207}$$

in first order approximation the total effect of the misalignment can be found by summing Eqs. (206) and (207).

$$\begin{aligned} x_f &= x - \delta x + x'\delta z + y\theta z - z\theta y \\ y_f &= y - \delta y + y'\delta z - x\theta z + z\theta x \\ z_f &= z + x\theta y - y\theta x \\ l_f &= l - \delta z \\ \delta_f &= \delta \end{aligned} \tag{208}$$

the equations for the particle angles in the misaligned coordinate system can be found using the equations above

$$\begin{aligned} x'_f &= \frac{\partial x_f}{\partial z_f} = \frac{\partial x_f}{\partial z}\frac{\partial z}{\partial z_f} = \left(\frac{\partial x}{\partial z} - \theta y + \frac{\partial y}{\partial z}\theta z\right)\frac{\partial z}{\partial z_f} \\ y'_f &= \frac{\partial y_f}{\partial z_f} = \frac{\partial y_f}{\partial z}\frac{\partial z}{\partial z_f} = \left(\frac{\partial y}{\partial z} - \theta x + \frac{\partial x}{\partial z}\theta z\right)\frac{\partial z}{\partial z_f} \\ z'_f &= \frac{\partial z}{\partial z_f} = 1 - \frac{\partial y}{\partial z_f}\theta x - \frac{\partial x}{\partial z_f}\theta y \approx 1 \end{aligned} \tag{209}$$

where the last approximation can be made because the partial derivatives and rotation angles are both small quantities. Combining Eqs. (208) and (209), using the definitions $\partial x/\partial z = x'$, $\partial y/\partial z = y'$ and the fact that at the entrance face $z = 0$, the equations simplify to

$$\begin{aligned} x_f &= x - \delta x + x'\delta z + y\theta z \\ x'_f &= x' - \theta y + y'\theta z \\ y_f &= y - \delta y + y'\delta z - x\theta z \\ y'_f &= y' + \theta x - x'\theta z \\ l_f &= l - \delta z \\ \delta_f &= \delta \end{aligned} \tag{210}$$

comparing this result to Eq. (202) the matrices A_0 and B_0 can be obtained

$$A_0 = \begin{pmatrix} 1 & 0 & 0 & 0 & 0 & 0 \\ 0 & 0 & 0 & 1 & 0 & 0 \\ 0 & 0 & 1 & 0 & 0 & 0 \\ 0 & -1 & 0 & 0 & 0 & 0 \\ 0 & 0 & 0 & 0 & 1 & 0 \\ 0 & 0 & 0 & 0 & 0 & 0 \end{pmatrix}, \qquad B_0 = \begin{pmatrix} 0 & \delta z & \theta z & 0 & 0 & 0 \\ 0 & 0 & 0 & \theta z & 0 & 0 \\ -\theta z & 0 & 0 & \delta z & 0 & 0 \\ 0 & -\theta z & 0 & 0 & 0 & 0 \\ 0 & 0 & 0 & 0 & 0 & 0 \\ 0 & 0 & 0 & 0 & 0 & 0 \end{pmatrix}. \tag{211}$$

Next, the coordinate transformation at the exit face is derived, the following equation is proposed

$$\boldsymbol{x_f}(1) = \boldsymbol{x}(1) - A_0\overline{\boldsymbol{m}} + B_1\boldsymbol{x}(1) \tag{212}$$

where $\boldsymbol{x_f}(1)$ and $\boldsymbol{x}(1)$ are the particle vectors described in the misaligned and reference coordinate systems at the exit face of the magnet, $\overline{\boldsymbol{m}}$ is the misalignment vector described in the reference coordinate system at the exit face, and B_1 is equal to B_0, where the components of $\boldsymbol{m}$ are substituted by the components of $\overline{\boldsymbol{m}}$. The goal is to express $\overline{\boldsymbol{m}}$ in terms of $\boldsymbol{m}$, first the vector $\overline{\boldsymbol{m}}$ is split up into a rotational $\overline{\boldsymbol{m}}_{\boldsymbol{\theta}}$ and translational $\overline{\boldsymbol{m}}_{\boldsymbol{x}}$ part

$$\overline{\boldsymbol{m}}_{\boldsymbol{\theta}} = \begin{pmatrix} \overline{\theta}x \\ \overline{\theta}y \\ \overline{\theta}z \end{pmatrix}, \qquad \overline{\boldsymbol{m}}_{\boldsymbol{x}} = \begin{pmatrix} \overline{\delta}x \\ \overline{\delta}y \\ \overline{\delta}z \end{pmatrix} \tag{213}$$

the misalignment vector at the entrance face is also split into $\boldsymbol{m}_{\boldsymbol{\theta}}$ and $\boldsymbol{m}_{\boldsymbol{x}}$. To derive the transformation, a rotation matrix O is defined which describes the rotation of points from the reference coordinate system at the entrance face to the reference coordinate system at the exit face. Furthermore, a vector P is proposed, which is the vector pointing from the origin of the reference coordinate system at the entrance face to the origin of the reference coordinate system at the exit face. To simplify the derivation the separate contributions of $\boldsymbol{m}_{\boldsymbol{x}}$ and $\boldsymbol{m}_{\boldsymbol{\theta}}$ to $\overline{\boldsymbol{m}}_{\boldsymbol{x}}$ and $\overline{\boldsymbol{m}}_{\boldsymbol{\theta}}$ are given, the total contribution can then be found by summing the obtained results.

The contribution of $\boldsymbol{m}_{\boldsymbol{x}}$ to $\overline{\boldsymbol{m}}_{\boldsymbol{x}}$ is given by the rotation matrix

$$\boldsymbol{m_{fx}} = O\boldsymbol{m_x} \tag{214}$$

the contribution of $\boldsymbol{m_x}$ to $\overline{\boldsymbol{m}}_{\boldsymbol{\theta}}$ is zero, since parallel translations do not affect angles.

Next the contribution of $\boldsymbol{m_\theta}$ to $\overline{\boldsymbol{m}}_{\boldsymbol{\theta}}$ is given. The displacement of a point, at a certain distance from a pivot point, due to a rotation is given by the cross product of the rotation vector and displacement vector, this product then needs to be multiplied by O to account for the rotation of coordinate systems from the entrance to the exit face.

$$\boldsymbol{m_{fx}} = O(\boldsymbol{m_\theta} \times \boldsymbol{P}) \tag{215}$$

Similar to Eq. (214) the contribution of $\boldsymbol{m_\theta}$ to $\overline{\boldsymbol{m}}_{\boldsymbol{\theta}}$ is given by

$$\overline{\boldsymbol{m}}_{\boldsymbol{\theta}} = O\boldsymbol{m_\theta} \tag{216}$$

In total all the contributions can be summed to obtain

$$\begin{aligned} \overline{\boldsymbol{m}}_{\boldsymbol{x}} &= O\boldsymbol{m_x} + O(\boldsymbol{m_\theta} \times \boldsymbol{P}) \\ \overline{\boldsymbol{m}}_{\boldsymbol{\theta}} &= O\boldsymbol{m_\theta}. \end{aligned} \tag{217}$$

For a steering magnet, the rotation matrix O and displacement vector P are equal to

$$O = \begin{pmatrix} 1 & 0 & 0 \\ 0 & 1 & 0 \\ 0 & 0 & 1 \end{pmatrix}, \qquad P = \begin{pmatrix} 0 \\ 0 \\ L \end{pmatrix} \tag{218}$$

where L is the length of the steering magnet. Using these equations Eq. (217) can be written as

$$\begin{pmatrix} \overline{\delta}x \\ \overline{\theta}x \\ \overline{\delta}y \\ \overline{\theta}y \\ \overline{\delta}z \\ \overline{\theta}z \end{pmatrix} = \begin{pmatrix} \delta x + L\theta y \\ \theta x \\ \delta y - L\theta x \\ \theta y \\ \delta z \\ \theta z \end{pmatrix} \tag{219}$$

Using this in Eq. (212) gives,

$$\begin{aligned} \boldsymbol{x_f}(1) &= \boldsymbol{x}(1) - A_0\bar{\boldsymbol{m}} + B_1\boldsymbol{x}(1) \\ \boldsymbol{x_f}(1) &= \boldsymbol{x}(1) - A_1\boldsymbol{m} + B_1\boldsymbol{x}(1) \end{aligned} \tag{220}$$

where

$$
\begin{aligned}
A_1 &= \begin{pmatrix} 1 & 0 & 0 & L & 0 & 0 \\ 0 & 0 & 0 & 1 & 0 & 0 \\ 0 & -L & 1 & 0 & 0 & 0 \\ 0 & -1 & 0 & 0 & 0 & 0 \\ 0 & 0 & 0 & 0 & 1 & 0 \\ 0 & 0 & 0 & 0 & 0 & 0 \end{pmatrix} \\
B_1 &= \begin{pmatrix} 0 & \overline{\delta}z & \overline{\theta}z & 0 & 0 & 0 \\ 0 & 0 & 0 & \overline{\theta}z & 0 & 0 \\ -\overline{\theta}z & 0 & 0 & \overline{\delta}z & 0 & 0 \\ 0 & -\overline{\theta}z & 0 & 0 & 0 & 0 \\ 0 & 0 & 0 & 0 & 0 & 0 \\ 0 & 0 & 0 & 0 & 0 & 0 \end{pmatrix} = \begin{pmatrix} 0 & \delta z & \theta z & 0 & 0 & 0 \\ 0 & 0 & 0 & \theta z & 0 & 0 \\ -\theta z & 0 & 0 & \delta z & 0 & 0 \\ 0 & -\theta z & 0 & 0 & 0 & 0 \\ 0 & 0 & 0 & 0 & 0 & 0 \\ 0 & 0 & 0 & 0 & 0 & 0 \end{pmatrix} = B_0
\end{aligned}
\tag{221}
$$

Now that the coordinate transforms are found, it is possible to write out the misalignment equations. In the misaligned coordinate system, the equation describing a particle travelling through a steering magnet is given by

$$\boldsymbol{x_f}(1) = R\boldsymbol{x_f}(0) + b \tag{222}$$

where R and b depend on the geometry and bending angle of the steering magnet. Substituting in Eqs. (202) and (220) gives

$$\boldsymbol{x}(1) - A_1\boldsymbol{m} + B_1\boldsymbol{x}(1) = R\left(\boldsymbol{x}(0) - A_0\boldsymbol{m} + B_0\boldsymbol{x}(0)\right) + b \tag{223}$$

solving this for $\boldsymbol{x}(1)$ and discarding all higher-order terms gives

$$\boldsymbol{x}(1) = R\boldsymbol{x}(0) + \left(A_1 - RA_0\right)\boldsymbol{m} + (RB_0 - B_1R)\boldsymbol{x}(0) + \left(B_1 + I_3\right)b \tag{224}$$

where I_3 is the 3x3 identity matrix.

E Matrices for Combined Function Magnets

The control loop which is given in Section 4.2 is explained using matrices B and C, and the disturbance vector $\mathbf{y_0}$, which correspond to a pair of steering magnets. In the beamline combined function magnets are used in addition to steering magnets to align the beam centroid, which changes B, C and $\mathbf{y_0}$. Below the description of B, C and $\mathbf{y_0}$ are given for the magnets which are used in the beamline.

E.1 Steering Magnets y-coordinate

The magnets, $S_{x,y}$ and S_y, which are used to align the beam in the y-coordinates are both combined function magnets. The matrices B and C, and the disturbance vector $\mathbf{y_0}$ for the combined function magnets can be derived by using Eqs. 95, 96 and the transfer matrix for a drift space. A image showing pair of combined function magnets and the relevant dimensions is given in Figure 52. To allow for consistent notation with the steering magnets for the x-coordinate all of the equations will be given in terms of the x-coordinate. The analogous expressions for the y direction can be obtained by switching out the variables from x to y. During regular operation $S_{x,y}$ is always focusing in the x-coordinate, while S_y is defocusing in x. For completeness sake all possible focusing combinations are given here. To simplify the equations the following substitutions are made

- If $S_{x,y}$ is focusing in x

$$C_1 = \cos\left(\sqrt{k_1}L_{q1}\right), S_1 = \sin\left(\sqrt{k_1}L_{q1}\right)$$
$$D_1 = \cos\left(\frac{\sqrt{k_1}L_{q1}}{2}\right), T_1 = \sin\left(\frac{\sqrt{k_1}L_{q1}}{2}\right)$$

  - and S_y is focusing in x

$$\sigma_1 = -1,\ \sigma_2 = +1,\ \sigma_3 = -1$$

- If $S_{x,y}$ is defocusing in x

$$C_1 = \cosh\left(\sqrt{k_1}L_{q1}\right), S_1 = \sinh\left(\sqrt{k_1}L_{q1}\right)$$
$$D_1 = \cosh\left(\frac{\sqrt{k_1}L_{q1}}{2}\right), T_1 = \sinh\left(\frac{\sqrt{k_1}L_{q1}}{2}\right)$$

  - and S_y is defocusing in x

$$\sigma_1 = +1,\ \sigma_2 = +1,\ \sigma_3 = +1$$

- If S_y is focusing in x

$$C_2 = \cos\left(\sqrt{k_2}L_{q2}\right), S_2 = \sin\left(\sqrt{k_2}L_{q2}\right)$$
$$D_2 = \cos\left(\frac{\sqrt{k_2}L_{q2}}{2}\right), T_2 = \sin\left(\frac{\sqrt{k_2}L_{q2}}{2}\right),$$

  - and $S_{x,y}$ is defocusing in x

$$\sigma_1 = +1,\ \sigma_2 = -1,\ \sigma_3 = -1$$

- If S_y is defocusing in x

$$C_2 = \cosh\left(\sqrt{k_2}L_{q2}\right), S_2 = \sinh\left(\sqrt{k_2}L_{q2}\right)$$
$$D_2 = \cosh\left(\frac{\sqrt{k_2}L_{q2}}{2}\right), T_2 = \sinh\left(\frac{\sqrt{k_2}L_{q2}}{2}\right),$$

  - and $S_{x,y}$ is focusing in x

$$\sigma_1 = -1,\ \sigma_2 = -1,\ \sigma_3 = +1$$

(225)

where k_1, k_2, L_{q1} and L_{q2} are the quadrupole focusing strengths, as defined in Eq. (46), and effective lengths of $S_{x,y}$ and S_y respectively. Using these variables the B matrix is given by

$$B = \frac{p}{\mu_0}\begin{pmatrix} \frac{g_1}{L_{q1}n_1}B_{11} & \frac{g_1}{L_{q1}n_1}B_{12} \\ \frac{g_2}{L_{q2}n_2}B_{21} & \frac{g_2}{L_{q2}n_2}B_{22} \end{pmatrix}$$

with

$$\begin{aligned}
B_{1,1} &= \frac{D_2\sqrt{k_1}\sqrt{k_2}}{D_2\sqrt{k_2}T_1 + D_1\sqrt{k_1}\left(D_2\sqrt{k_2}L_1 + T_2\right)}, \\
B_{1,2} &= -\frac{\sqrt{k_1}\left(D_2\sqrt{k_2}L_2 + T_2\right)}{D_2\sqrt{k_2}T_1 + D_1\sqrt{k_1}\left(D_2\sqrt{k_1}L_1 + T_2\right)}, \\
B_{2,1} &= -\frac{D_1C_2\sqrt{k_1}\sqrt{k_2} + \sigma_3k_2S_2\left(D_1\sqrt{k_1}L_1 + T_1\right)}{D_2\sqrt{k_2}T_1 + D_1\sqrt{k_1}\left(D_2\sqrt{k_2}L_1 + T_2\right)}, \\
B_{2,2} &= \frac{C_2\sqrt{k_2}T_1 + \sigma_3k_2L_2T_1S_2 + D_1\sqrt{k_1}\left(C_2\sqrt{k_2}\left(L_1 + L_2\right) + S_2 + \sigma_3k_2L_1L_2S_2\right)}{D_2\sqrt{k_2}T_1 + D_1\sqrt{k_1}\left(D_2\sqrt{k_2}L_1 + T_2\right)},
\end{aligned} \tag{226}$$

where μ_0 is the permeability of free space, p is the particle momentum divided by its charge, L_1 is the distance between the first and second combined function magnet, L_2 is the distance between the second combined function magnet and the location at which y_1 and y_1' are measured, g_1, g_2, n_1, and n_2 are the gap sizes and the number of coil windings of $S_{x,y}$ and S_y respectively. The matrix C is given by

$$C = \frac{\mu_0}{p}\begin{pmatrix} \frac{L_{q1}n_1}{g_1}C_{11} & \frac{L_{q2}n_2}{g_2}C_{12} \\ \frac{L_{q1}n_1}{g_1}C_{21} & \frac{L_{q2}n_2}{g_2}C_{22} \end{pmatrix}$$

with

$$\begin{aligned}
C_{1,1} &= \frac{T_1\left(C_2 + \sigma_3\sqrt{k_2}L_2S_2\right)}{\sqrt{k_1}} + \frac{D_1\left(\sqrt{k_2}\left(L_1 + L_2\right)C_2 + \left(1 + \sigma_3k_2L_1L_2\right)S_2\right)}{\sqrt{k_2}}, \\
C_{1,2} &= L_2D_2 + \frac{T_2}{\sqrt{k_2}}, \\
C_{2,1} &= \sigma_3\frac{\sqrt{k_2}T_1S_2}{\sqrt{k_1}} + D_1\left(C_2 + \sigma_3\sqrt{k_2}L_1S_2\right), \\
C_{2,2} &= D_2,
\end{aligned} \tag{227}$$

it can be checked that $B = C^{-1}$, which was the requirement for fastest convergence of the control system. The disturbance vector $\mathbf{y_0}$ is given by

$$\mathbf{y_0} = \begin{pmatrix} y_{01} \\ y_{02} \end{pmatrix}$$

with

$$\begin{aligned} y_{01} &= \frac{S_1\left(\sqrt{k_2}\left(\sigma_1 k_1\left(L_1+L_2\right)x_0 + x_0'\right)C_2 + \left(k_1\left(\sigma_1+\sigma_2 k_2 L_1 L_2\right)x_0 + \sigma_3 k_2 L_2 x_0'\right)S_2\right)}{\sqrt{k_1}\sqrt{k_2}} \\ &\quad \frac{\sqrt{k_1}C_1\left(\sqrt{k_2}\left(x_0+\left(L_1+L_2\right)x_0'\right)C_2 + \left(x_0' + \sigma_3 k_2 L_2\left(x_0 + L_1 x_0'\right)\right)S_2\right)}{\sqrt{k_1}\sqrt{k_2}} \\ y_{02} &= \frac{S_1\left(\sigma_1 k_1 x_0 C_2 + \sqrt{k_2}\left(\sigma_2 k_1 L_1 x_0 + \sigma_3 x_0'\right)S_2\right)}{\sqrt{k_1}} + C_1\left(x_0' C_2 + \sigma_3\sqrt{k_2}\left(x_0 + L_1 x_0'\right)S_2\right) \end{aligned} \tag{228}$$

where x_0 and x_0' are the position and angle of the beam centroid at the start of $S_{x,y}$

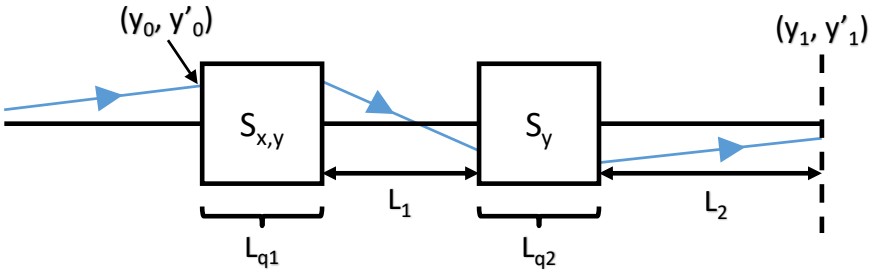

Figure 52: Pair of combined function magnets which can be used to correct for position and angle in the y-direction. The reference trajectory is indicated in black, while the described particle trajectory is given in blue.

E.2 Steering Magnets x-coordinate

To correct the angle and position of the beam centroid in the x-direction the combined function magnet $S_{x,y}$ and the regular steering magnet S_x are used. In between these magnets the combined function magnet S_y is located, as illustrated in Figure 53. During regular operation $S_{x,y}$ is focusing in x and S_y is defocusing in x.

Using the simplifications from Eq. (225), where the definitions of k_1, k_2, L_{q1} and L_{q2} remain the same, the matrix B can be written as

$$B = \frac{p}{\mu_0}\begin{pmatrix} \frac{g_1}{L_{q1}n_1}B_{11} & \frac{g_1}{L_{q1}n_1}B_{12} \\ \frac{g_2}{L_{s2}n_2}B_{21} & \frac{g_2}{L_{s2}n_2}B_{22} \end{pmatrix}$$

with

$$\begin{aligned}
B_{1,1} &= \frac{\sqrt{k_1}\sqrt{k_2}}{C_2\sqrt{k_2}T_1 + \sigma_3 k_2 L_2 T_1 S_2 + D_1\sqrt{k_1}\left(C_2\sqrt{k_2}\,(L_1+L_2) + S_2 + \sigma_3 k_2 L_1 L_2 S_2\right)}, \\
B_{1,2} &= \frac{-\sqrt{k_1}\sqrt{k_2}}{C_2\sqrt{k_2}T_1 + \sigma_3 k_2 L_2 T_1 S_2 + D_1\sqrt{k_1}\left(C_2\sqrt{k_2}\,(L_1+L_2) + S_2 + \sigma_3 k_2 L_1 L_2 S_2\right)}, \\
B_{2,1} &= \frac{D_1 C_2\sqrt{k_1}\sqrt{k_2} + \sigma_3 k_2\left(D_1\sqrt{k_1}L_1 + T_1\right)S_2}{-C_2\sqrt{k_2}T_1 - \sigma_3 k_2 L_2 T_1 S_2 - D_1\sqrt{k_1}\left(C_2\sqrt{k_2}\,(L_1+L_2) + S_2 + \sigma_3 k_2 L_1 L_2 S_2\right)}, \\
B_{2,2} &= \frac{C_2\sqrt{k_2}T_1 + \sigma_3 k_2 (L_2+L_3) T_1 S_2 + D_1\sqrt{k_1}\left(C_2\sqrt{k_2}(L_1+L_2+L_3) + S_2 + \sigma_3 k_2 L_1 (L_2+L_3) S_2\right)}{C_2\sqrt{k_2}T_1 + \sigma_3 k_2 L_2 T_1 S_2 + D_1\sqrt{k_1}\left(C_2\sqrt{k_2}(L_1+L_2) + S_2 + \sigma_3 k_2 L_1 L_2 S_2\right)}
\end{aligned} \tag{229}$$

where L_{s2} is the length of S_x, L_1 is the distance between $S_{x,y}$ and S_y, L_2 is the distance between S_y and the center of S_x, g_1, g_2, n_1, and n_2 are the gap sizes and the number of coil windings of $S_{x,y}$ and S_x respectively.

The matrix C is given by

$$C = \frac{\mu_0}{p}\begin{pmatrix} \frac{L_{q1}n_1}{g_1}C_{11} & \frac{L_{s2}n_2}{g_2}C_{12} \\ \frac{L_{q1}n_1}{g_1}C_{21} & \frac{L_{s2}n_2}{g_2}C_{22} \end{pmatrix}$$

with

$$\begin{aligned}
C_{1,1} &= \frac{T_1\left(C_2 + \sigma_3\sqrt{k_2}(L_2+L_3)S_2\right)}{\sqrt{k_1}} + \frac{D_1\left(\sqrt{k_2}(L_1+L_2+L_3)C_2 + (1+\sigma_3 k_2 L_1 (L_2+L_3))S_2\right)}{\sqrt{k_2}}, \\
C_{1,2} &= L_3, \\
C_{2,1} &= \sigma_3\frac{\sqrt{k_2}T_1 S_2}{\sqrt{k_1}} + D_1\left(C_2 + \sigma_3\sqrt{k_2}L_1 S_2\right), \\
C_{2,2} &= 1,
\end{aligned} \tag{230}$$

where L_3 is the distance between the center of S_x and the position at which x_1 and x_1' are measured. It can be checked that $B = C^{-1}$, which was the requirement for fastest convergence of the control system. The disturbance vector $\mathbf{y_0}$ is given by

$$\mathrm{y}_0 = \begin{pmatrix} y_{01} \\ y_{02} \end{pmatrix}$$

with

$$\begin{aligned} y_{01} = & \frac{\sqrt{k_2} C_2 \left(\sqrt{k_1}\left(x_0 + \left(L_1 + L_2 + L_3\right) x_0'\right) C_1 + \left(\sigma_1 k_1 \left(L_1 + L_2 + L_3\right) x_0 + x_0'\right) S_1\right)}{\sqrt{k_1}\sqrt{k_2}} + \\ & \frac{S_2 \left(\sqrt{k_1}\left(x_0' + \sigma_3 k_2 \left(L_2 + L_3\right)\left(x_0 + L_1 x_0'\right)\right) C_1 + \left(k_1 \left(\sigma_1 + \sigma_2 k_2 L_1 \left(L_2 + L_3\right)\right) x_0 + \sigma_3 k_2 \left(L_2 + L_3\right) x_0'\right) S_1\right)}{\sqrt{k_1}\sqrt{k_2}} \\ y_{02} = & \frac{S_1 \left(\sigma_1 k_1 x_0 C_2 + \sqrt{k_2}\left(\sigma_2 k_1 L_1 x_0 + \sigma_3 x_0'\right) S_2\right)}{\sqrt{k_1}} + C_1 \left(x_0' C_2 + \sigma_3 \sqrt{k_2}\left(x_0 + L_1 x_0'\right) S_2\right) \end{aligned} \tag{231}$$

where x_0 and x_0' are the position and angle of the beam centroid at the start of $S_{x,y}$.

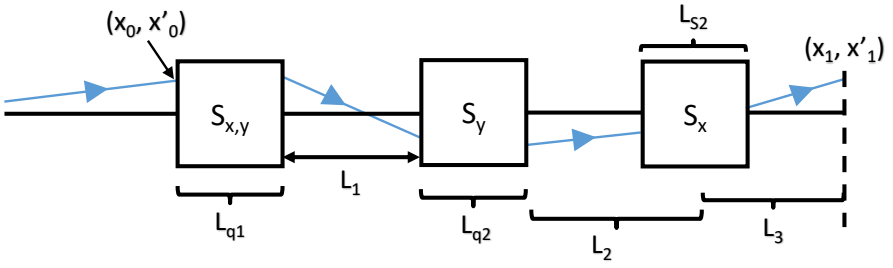

Figure 53: Steering magnets used to correct the beam in the x-coordinate.

References

[1] F. Hinterberger, *Physik der Teilchenbeschleuniger und Ionenoptik*. Berlin: Springer-Verlag, 2 ed., 2008.

[2] K. Wille, *The Physics of Particle Accelerators*. Oxford: Oxford University Press, 2001.

[3] J. T. Tanabe, "Iron dominated electromagnets: Design, fabrication, assembly and measurements," *Iron Dominated Electromagnets: Design, Fabrication, Assembly and Measurements*, no. June, pp. 1–335, 2005.

[4] J. Rossbach and P. Schmüser, "Basic Course on Accelerator Optics," in *CAS - CERN Accelerator School: 5th General accelerator physics course*, ch. 2, Jyvskyla: CERN, 1 ed., 1994.

[5] S. Skelton, *Multi-quadrupole scan for emittance determination at PITZ*. University of St. Andrews, Scotland, 2007.

[6] R. Stephens and J. Ward, *Applied Mechanics*. London: The Macmillan Press LTD, 3 ed., 1972.

[7] E. N. Bodine, "Discrete difference equations." `https://qubeshub.org/resources/469/download/DifferenceEquations.pdf`, 2014. Accessed on: Apr. 6, 2021.

[8] M. Vassilaki, J. C. Hennet, and G. Bitsorls, "Feedback control of linear discrete-time systems under state and control constraints," *International Journal of Control*, vol. 47, no. 6, pp. 1727–1735, 1988.

[9] K. L. Brown, D. C. Carey, F. C. Iselin, and F. Rothacker, *TRANSPORT: a computer program for designing charged-particle beam transport systems; 2nd ed.* CERN Yellow Reports: Monographs, Geneva: CERN, 1973. Also publ. as SLAC and FERMILAB.

[10] I. Farrance and R. Frenkel, "Uncertainty of measurement: A review of the rules for calculating Uncertainty components through functional relationships," *Clinical Biochemist Reviews*, vol. 33, no. 2, pp. 49–75, 2012.

[11] C. P. Niculescu and L.-E. Persson, *Convex Functions and Their Applications: A Contemporary Approach*. Cham: Springer International Publishing, 2 ed., 2018.

[12] M. L. Johnson, "Parameter correlations while curve fitting," *Methods in Enzymology*, vol. 321, no. February 2000, pp. 424–446, 2000.

[13] E. W. Weisstein, *Circular Segment*. MathWorld–A Wolfram Web Resource, n.d., Accessed on: Feb. 1, 2021. [Online]. Available: `https://mathworld.wolfram.com/CircularSegment.html`.